Drainage structures and transit-time distributions in conduit-dominated and fissured karst aquifer systems

Zur Erlangung des akademischen Grades einer

DOKTORIN DER NATURWISSENSCHAFTEN

von der Fakultät für

Bauingenieur-, Geo- und Umweltwissenschaften

des Karlsruher Instituts für Technologie (KIT)

genehmigte

DISSERTATION

von

Dipl.-Geol. Ute Lauber

aus Dachau

Tag der mündlichen

Prüfung: 21.11.2014

Referent: Prof. Dr. Nico Goldscheider

Korreferent: Prof. Dr. Tim Bechtel

Karlsruhe 2014

Abstract

Karst aquifers are widely distributed across the world and are important groundwater resources. Solutionally-enlarged conduits embedded in fissured rock matrix result in a highly heterogeneous underground drainage pattern that makes karst aquifers difficult to characterize. To ensure sustainable protection and management of karst water resources, hydrogeologic knowledge of karst systems is required. However, the quantitative characterization of groundwater flow in karst systems remains a major challenge. Specific investigating techniques and approaches are needed to account for the complexity of drainage. This thesis emphasizes the identification of drainage structures and the quantification of related transit-time distributions and hydraulic parameters. To account for the strong heterogeneities of different types of catchment areas, three diverse karst aquifer systems are investigated: a conduit-dominated karst system, a fissured karst system and an aquifer system that comprises a karst and a porous-media (alluvial/rockfall) aquifer. For a detailed hydrogeologic assessment of the different catchment areas, adapted methods applied include a combination of artificial tracer tests, natural tracer analysis, and discharge analysis.

The first two parts of this thesis describe a conduit-dominated karst system, the catchment area of the Blautopf (Swabian Alb, Germany). This highly karstified plateau comprises a well-developed conduit system with two accessible and active caves. To resolve the internal structure of karst drainage and to obtain hydraulic parameters for the conduit system, combined tracer tests with two injections in the cave streams and two injections on the land surface were conducted in the catchment area. By using field fluorimeters, it was possible to record breakthrough curves directly in the cave system. The approach enabled verification of the hierarchical structure of the conduit network and identification of sub-catchment areas of the cave streams. High-resolution spatial and temporal information about conduit flow was determined by analyzing the breakthrough curves with an advection-dispersion model. Flow parameters were highly variable, showing a substantial decrease of flow velocities from the epiphreatic to the phreatic section of this well-developed conduit system.

To characterize drainage of the fissured karst system, hydrogeologic investigations were conducted in the steep Wetterstein Mountains (Bavarian Alps, Germany). Because of steady tectonic uplift of the area and strong gravitational erosion, small-scale karst structures dominate the catchment. A combination of artificial and natural tracers was useful to resolve drainage structures and related transit times. Predominantly associated with zones of tectonic weakness, underground drainage crosses topographic catchment divides, follows cross-formational flow paths, and contributes to deep drainage systems underneath alpine valleys. Artificial tracer tests defined a fast-flow component with transit times of a few days in karst conduits and open fissures, which is highly dependent on hydrologic flow conditions. Using stable isotopes (^{18}O) as a natural tracer, an intermediate-flow component with a mean transit time of a few months was

associated with well-drained fissures and fractures. Both tracer methods also document a slow-flow component with mean transit times greater than one year that is attributable to slow flow and storage in a poorly-drained fissured network. The results enabled the first evaluation of groundwater resources in this alpine karst area.

The last part of this thesis describes a complex aquifer system comprising a karst and a porous-media (alluvial/rockfall) aquifer in the Reintal valley (Bavarian Alps, Germany). The hydrogeologic importance of alluvial/rockfall aquifers, which are often found in high-alpine valleys, is examined regarding effects on discharge and groundwater storage within the karstic catchment area. By conducting tracer tests and investigating discharge characteristics in the valley it was possible to demonstrate that the presence of the alluvial/rockfall aquifer delays and dampens sharp discharge peaks that are related to the karst conduit system. The sediments in the valley store groundwater and provide a continuous discharge source during periods of low flow. In this way, the alluvial/rockfall aquifer system in the high-alpine valley influences discharge of the karstic catchment area and play an important role in flood attenuation and the maintenance of baseflow.

In conclusion, the integration of unique approaches provided new information on karst aquifer heterogeneity and dynamics of karst systems. This understanding of relevant flow parameters for the three different systems is crucial for the development of numerical models, for the prediction of effects of potential contamination, and for estimates about availability of groundwater resources in the future.

Kurzfassung

Karstgrundwasserleiter sind auf der Erde weit verbreitet und beinhalten einige der wichtigsten Grundwasservorkommen. Lösungserweiterte Karströhren, die in einer geklüfteten Gesteinsmatrix eingebettet sind, führen zu einer sehr heterogenen unterirdischen Entwässerung der Karstsysteme und erschweren die Erschließung der Grundwasservorkommen. Um einen nachhaltigen Schutz und Bewirtschaftung der Karstwasserressourcen zu gewährleisten, ist eine detaillierte hydrogeologische Kenntnis der Karstsysteme erforderlich. Dabei ist die quantitative Charakterisierung von Karstsystemen nach wie vor eine große Herausforderung, die spezielle Untersuchungsmethoden und Ansätze erfordert, um die Komplexität zu berücksichtigen. Besonderer Fokus dieser Arbeit liegt in der Identifizierung von Entwässerungsstrukturen und Quantifizierung der Verteilung der unterirdischen Fließzeiten und der hydraulischen Parameter. Um die Heterogenität verschiedener Einzugsgebiete zu berücksichtigen, werden in dieser Studie drei unterschiedliche Karstsysteme untersucht: ein röhrendominiertes Karstsystem, ein kluftdominiertes Karstsystem und ein Aquifersystem, das einen Karst- und einen Porengrundwasserleiter beinhaltet. Zur detaillierten hydrogeologischen Erkundung der Einzugsgebiete wurden geeignete Untersuchungsmethoden ausgewählt, die eine Kombination aus Markierungsversuchen mit künstlichen Tracern, Auswertung natürlicher Tracer und Auswertung von Abflussganglinien an den Quellen beinhalten.

In den ersten beiden Teilen dieser Arbeit wird ein röhrendominiertes Karstsystem beschrieben, das Quelleinzugsgebiet des Blautopfs (Schwäbische Alb). Das stark verkarstete Plateau beinhaltet ein gut ausgebildetes Karströhrensystem mit zwei zugänglichen und aktiven Höhlen. Um die interne Struktur der Karstentwässerung aufzulösen und hydraulische Parameter für das Röhrensystem zu erhalten, wurden die ersten kombinierten Markierungsversuche mit zwei Eingaben in die Höhlenflüsse und zwei weiteren Eingaben auf der Landoberfläche im Einzugsgebiet durchgeführt. Mithilfe von Feldfluorimetern konnten die Durchgangskurven direkt im Höhlensystem beobachtet werden. Damit konnten die hierarchische Struktur des Karstnetzwerks nachgewiesen und die zwei Teileinzugsgebiete der beiden Höhlenflüsse zu lokalisiert werden. Um räumlich und zeitlich hoch aufgelöste Informationen zu den hydraulischen Parametern zu erhalten, wurden alle Durchgangskurven mit einem Advektion-Dispersion-Modell analysiert. Innerhalb des gut entwickelten Röhrensystems wurde eine starke Variabilität der hydraulischen Parameter beobachtet. Die Fließgeschwindigkeiten nehmen vom epiphreatischen zum phreatischen Bereich hin deutlich ab.

Um die Entwässerung eines kluftdominierten Karstsystems zu charakterisieren, wurden im dritten Teil hydrogeologische Untersuchungen im hochalpinen Wettersteingebirge durchgeführt (Bayerische Alpen). Aufgrund der anhaltenden tektonischen Hebung des Gebietes und der damit verbundenen starken Erosion dominieren kleinräumige Karststrukturen im Einzugsgebiet.

Eine Kombination aus künstlichen und natürlichen Tracern ermöglichte es, Entwässerungsstukturen und Verweilzeiten zu charakterisieren. Die Entwässerung erfolgt überwiegend entlang tektonischer Schwächezonen, unabhängig von den topographischen Einzugsgebieten und unter tief eingeschnittenen Tälern und durch stratigraphische Einheiten hindurch. Künstliche Tracer ermöglichten den Nachweis einer raschen Entwässerungskomponente mit Fließzeiten von wenigen Tagen, die entlang von Karströhren und größeren Klüften vorherrscht und stark von den Abflussverhältnissen abhängig ist. Die Auswertung von stabilen Isotopen (^{18}O) ermöglichte den Nachweis einer intermediären Fließkomponente mit mittleren Verweilzeiten von wenigen Monaten, die entlang des gut vernetzten Kluftsystems dominiert. Beide Methoden deuten auf eine langsame Fließkomponente mit Verweilzeiten von mehr als einem Jahr hin, die auf langsame Grundwasserströmung und -speicherung im schlechter vernetzten Kluftsystem zurückzuführen ist. Die Untersuchungen ermöglichten eine erste Abschätzung der vorhandenen Wassermengen im alpinen Karstgebiet.

Abschließend befasst sich die Studie mit einem komplexen Aquifersystem im Reintal, das aus einem Karst- und einem Porengrundwasserleiten aufgebaut wird (Bayerische Alpen). Ziel dieser Studie war es, die hydrogeologische Bedeutung einer komplex aufgebauten Abfolge aus alluvialen Sedimenten und Bergsturzmassen, die häufig in hochalpinen Tälern auftreten, hinsichtlich der Auswirkungen auf das Abflussverhalten und der Grundwasserspeicherung im verkarsteten Einzugsgebiet zu untersuchen. Mit Hilfe von Markierungsversuchen und der Auswertung von Abflussganglinien konnte gezeigt werden, dass die alpinen Porengrundwasserleiter eine Verzögerung und Dämpfung der Abflussspitzen des Karstsystems hervorrufen. Die Sedimente im Tal können Grundwasser speichern und einen kontinuierlichen Abfluss während Perioden mit Niedrigwasserabflüssen gewährleisten. Dadurch haben die alpinen Porengrundwasserleiter einen bedeutenden Einfluss auf das Abflussregime und nehmen eine wichtige Rolle in der Dämpfung von Hochwasserereignissen und der Erhaltung des Basisabflusses im Karstgebieten ein.

Durch die Kombination verschiedener Methoden wurde es möglich, neue Informationen über die Heterogenität und die Dynamik von Karstsystemen zu erhalten. Das Verständnis relevanter, hydraulischer Parameter der drei unterschiedlichen Systeme ist entscheidend für die Erstellung von numerischen Modellen, die Prognose von Auswirkungen möglicher Schadstoffe im System und die Abschätzungen der Verfügbarkeit der Grundwasserressourcen in der Zukunft.

Contents

Chapter 1

Introduction

1.1 General motivation

Groundwater in karst aquifer systems is an important freshwater resource providing drinking water for about one quarter of the world's population (Ford and Williams 2007). Karst aquifers are characterized by a highly permeable drainage network that arises by dissolution of soluble bedrock. In Europe, such soluble carbonate rocks are widely distributed and cover approximately 35% of the land surface (COST 65 1995). Accordingly, karst resources supply up to 50% of drinking-water supply in some European countries. Large cities like Vienna, Grenoble and Rome depend on karst water.

Heterogeneity and anisotropy related to the diverse distribution of solutionally-enlarged conduits in fissured carbonate rock are challenges to understanding karst aquifers (Worthington and Ford 2009). Groundwater flow is governed by discrete and fast drainage through the conduit network resulting in a great variability of spring discharge and groundwater that is highly vulnerable with respect to contamination. In contrast, diffuse infiltration and slow percolation through the fissured rock matrix enable groundwater storage, natural attenuation of contamination and the maintenance of baseflow. Depending on the degree of karst development, karst aquifers show a wide variety of fissured- to conduit-dominated drainage systems (Bakalowicz 2005; Ford and Williams 2007). Furthermore, discharge dynamics in karst aquifer systems are highly variable depending on hydrologic flow conditions. Considering all of these aspects, there is considerable variability and complexity of underground drainage in karstic catchment areas.

Sustainable use and protection of groundwater resources in karst aquifer systems requires comprehensive knowledge about underground drainage. A detailed characterization of karst aquifer systems is necessary to understand drainage properties, to define realistic hydraulic and geometric parameters, and to support numerical models (Geyer et al. 2013). A quantitative description of karst drainage is challenging because numerous classical investigation techniques fail

to identify flow and transport characteristics in the strongly heterogeneous flow field. Furthermore, it is not possible to scale-up flow parameters in karst systems, a method which is often appropriate in comparatively homogenous porous-media systems. Specific methods are necessary to characterize karst underground drainage systems adequately and to provide reliable predictions about possible effects of contamination and the availability of groundwater resources in the future (Goldscheider and Drew 2007). Facing climate change, population growth, and increasing water demand, detailed information about karst water resources is needed (Hartmann et al. 2014). Alpine (karst) water resources in particular are of great hydrologic importance and are especially sensitive to climatic change because of their snow dominated flow regime (Viviroli and Weingartner 2004). Understanding the key parameters of karst aquifer systems is critical to evaluate impacts of future climate scenarios. Detailed knowledge about drainage structures and related transit-times can help to draw reliable conclusions about natural retention zones, and available water resources, and is important for future water management in karst areas.

1.2 Objectives and approaches

The aim of this study is to contribute to a better understanding of karst aquifer systems regarding their heterogeneity of underground drainage. The thesis focuses on the identification of underground drainage structures and the quantification of flow parameters and drainage properties in different types of karst aquifer system. Selected catchment areas of three diverse karst aquifer systems (a conduit-dominated system, a fissured karst system, and a system comprised of a karst and porous-media aquifer) were investigated to address the following research questions:

- What is the relation between geologic and tectonic structures and underground drainage? Are well-developed flow paths present and what is the structure of the karst drainage network?

- What are the transit times in the conduit-dominated system? What are the flow velocities and flow properties in the epiphreatic and phreatic zones of the aquifer and how vulnerable is the system to contamination?

- What is the transit-time distribution in the fissured karst system? What are the properties of different drainage systems and how vulnerable are the karst water resources with respect to water quantity and quality?

- What are the characteristics of drainage through the (thick) unsaturated zone? Do retardation and storage processes occur?

- What is the role of a porous-media aquifer (alluvial/rockfall deposits) as a natural retention zone in a karstic catchment area? Can alluvial/rockfall aquifers influence the progradation and intensity of flood waves related to fast discharge from the karst conduit system after precipitation events?

Underground drainage in karst aquifer systems can vary substantially depending on the degree of karstification and the characteristics of the conduit and fissured network. To address this range of variability, this thesis provides detailed insights into three different karst aquifer systems (Fig. 1.1). The catchment area of the Blautopf at the Schwabian Alb is an example of a highly karstified, conduit-dominated system. The karst plateau has been exposed since the Oligocene and is characterized by intense karstification. The high-alpine Wetterstein Mountains in the Bavarian Alps is an example of a less karstified, fissured karst system. Steady tectonic uplift of the western part of the Alps since the Miocene and mechanical weathering has resulted in the dominance of small-scale karst structures. The third example is the Reintal valley in the Wetterstein Mountains, a karstic catchment area comprising a karst and an alluvial/rockfall aquifer.

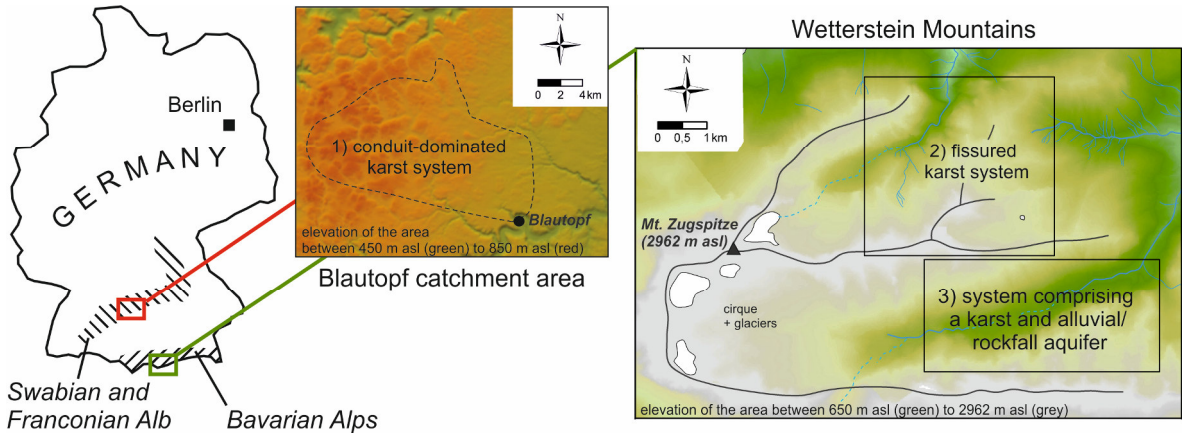

Figure 1.1: Overview over the three different karst aquifer systems: the conduit-dominated system, the fissured karst system and the aquifer system comprising a karst and porous-media (alluvial/rockfall) aquifer.

To address the specific research questions for each catchment area, different approaches have been applied, i.e., artificial tracer tests, use of natural tracers, and discharge and hydrograph analysis. Each of these methods provides different types of information, and thus, specific adjustments and combinations of the approaches were applied for each catchment area. The methodical approach included the following research questions:

- Can tracer tests conducted in active caves help to determine the internal structure of karst drainage? Is the method suitable for the spatial resolution of flow parameters in the vadose, epiphreatic and phreatic zone?

- Is the combined use of artificial and natural tracers (^{18}O) suitable to develop a conceptual model of drainage in a fissured karst system? Can the obtained transit-time distribution help to estimate water amount and availability?

- Which methods can be applied to describe the role of a porous-media (alluvial/rockfall) aquifer in a karstic catchment area? Which parameters are suitable to quantify the effects on discharge characteristics?

- Which methods are suitable for areas, that are difficult to access, e.g., caves or steep alpine areas? Are long-term data records necessary and if yes, which data sources could be used?

1.3 Structure of the thesis

The present work is a cumulative PhD thesis and consists of an introduction to karst hydrogeology and the methods used (chapter 2), four studies focused on different aspects regarding drainage of karst aquifer systems (chapters 3, 4, 5 and 6), a summary (chapter 7), and a section with overall conclusions of the thesis (chapter 8). The studies in chapters 3, 4, and 5 have been published in peer-reviewed journals and the manuscript in chapter 6 is in final phase of the review process.

The aim of chapter 2 is to provide a general overview of karst hydrogeology and the related terminology and methods. A conceptual model of karst aquifer systems is introduced to describe their general structure and characteristics. The strong heterogeneity of karst systems can best be assessed by a combination of different methods, which are discussed in chapter 2. The four

studies (chapters 3, 4, 5 and 6) focus on different karst aquifer systems to identify drainage structures and to characterize the heterogeneity of the individual systems, i.e. the variability of transit times and flow velocities. Depending on the hydrogeological setting of each catchment area, adapted field and evaluating methods are applied.

In chapter 3, new insights into the structure of karst drainage in the active cave system of Blautopf spring, Germany, are presented. The focus of this chapter is on the hydrogeologic setting of a conduit-dominated karst system. The strong karstification of the system and the presence of accessible active caves in the catchment allowed for application of a rarely used experimental design for tracer tests: the injection and monitoring of tracer inside the cave system. Comparison with previous tracer tests was aimed at defining the variability of transit times and the dilution of tracer under variable flow conditions.

Chapter 4 provides further information, including a quantitative evaluation, of the results from the tracer test of chapter 3. Spatially resolved information on karst conduit flow from in-cave dye-tracing is obtained by analyzing all breakthrough curves with an analytical advection-dispersion model, implemented in the program CXTFIT (Toride et al. 1999). This evaluation is used to define mean flow velocities and further hydraulic parameters, e.g., dispersion and dispersivity, for individual sections of the cave, i.e. the epiphreatic and phreatic zones.

In chapter 5, artificial and natural tracers are used to assess drainage structures and transit-time distribution for a fissured karst system in the Wetterstein Mountains. Because of steady tectonic uplift of the high-alpine area, mechanical weathering dominates, and this has limited the evolution of large karst structures. The drainage system is dominated by smaller karst structures and through the strongly fissured limestone. Tracer tests with fluorescent dyes were conducted to investigate underground drainage and to estimate transit times along karst structures and the fissured rock matrix. Observed breakthrough curves were evaluated by using a multi-dispersion-model, implemented in the program TRACI95 (Käss 2004). Additionally, stable isotopes, ^{2}H and ^{18}O, were analyzed and evaluated with the program FLOWPC (Maloszewski et al. 1983).

The aim of chapter 6 is to look beyond the boundaries of a karst aquifer and characterize an aquifer system comprising a karst aquifer and a porous-media (alluvial/rockfall) aquifer in the Wetterstein Mountains. Discharge from a karst spring completely infiltrates into postglacial

alluvial/rockfall deposits. Tracer tests and hydrograph analyses were conducted to quantify the role of the alluvial/rockfall aquifer and its natural storage properties with regard to flood attenuation and maintenance of baseflow in the karst area. Flow velocities in the system were determined based on the tracer tests. Discharge peaks at the karst spring and the discharge peak downstream from the alluvial/rockfall aquifer were evaluated quantitatively using the discharge ratio, recession coefficients, and the lag time between the two signals.

Chapter 7 summarizes the results of the individual studies and chapter 8 provides the overall conclusions of the thesis and an outlook with suggestions for future investigations.

Chapter 2

Overview of karst hydrogeology and applied methods

2.1 Conceptual model of karst aquifer systems

Karst groundwater systems have a special role in hydrogeology because of their complex and heterogeneous drainage. In contrast with porous-media aquifers that have comparatively homogenous porosity and permeability, karst aquifers are characterized by triple porosity and strong anisotropy (Fig. 2.1). While the primary porosity of the rock matrix is negligible in old limestone formations, the secondary porosity along a fissured network and the tertiary porosity related to a solutionally-enlarged conduit network have a great influence on groundwater recharge, flow, and storage (Ford and Williams 2007).

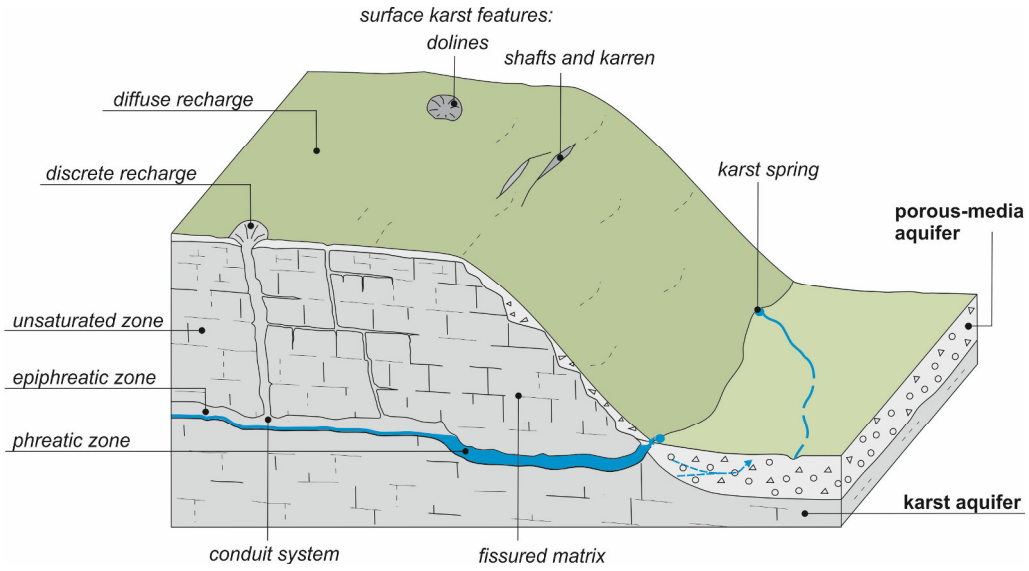

Figure 2.1: Schematic sketch of a karst aquifer system comprising a karst and a porous-media aquifer. The karst aquifer is characterized by a strong heterogeneity and duality (discrete/diffuse) of recharge, flow and storage. Water flows in vadose (unsaturated), epiphreatic and phreatic zones of the aquifer to the spring. In the valley, there is interaction between the karst and the porous-media aquifer.

Karst aquifers evolve in fissured limestones, as water percolates along bedding planes, joints, and faults. The secondary porosity arising from rock folding and faulting comprises a variety

of individual fissures that differ by their extension and aperture width. Depending on the hierarchy of fissures and their interconnection, all intermediate stages between a poorly-drained fissured network and a well-drained fissured network coexist in karst aquifers (Kiraly 2003; Worthington and Ford 2009). Chemical dissolution of CO_2-containing water circulating through the soluble limestone creates tertiary porosity (Fig. 2.1). Depending on the initial aperture width of fissures, preferential flow paths evolve by progressive dissolution of limestone and result in the enlargement of prominent fissures. Because of the positive feedback between increasing flow and dissolution, the rapid evolution of conduits results in a reorientation of the flow field towards the fast-draining structures (Gabrovsek et al. 2004; Worthington and Ford 2009). Thus, the conduit network is embedded in, and interacting with, a dense network of fissures at different scales and hydraulic connectivity, forming a complex hierarchical drainage network. While the hierarchical structure can be approximated from numerical modeling, it is challenging to determine the structure of drainage in real-world karst systems. Such internal structure has been documented only in rare cases, largely because of the poor accessibility of caves (Hauns et al. 2001; Meiman et al. 2001; Jeannin 2001). On a geologic time scale, karst development is a very rapid process that may require only a few thousand years (Gabrovsek et al. 2004; Dreybrodt et al. 2010). Depending on the geomorphologic and hydrogeologic evolution, karst aquifers can be found at different stages of karst development, varying from non-karstic aquifers to fissured-dominated systems to well-developed karst systems with a large conduit network.

The heterogeneous and anisotropic structure of karst systems strongly affects underground drainage and transit-time distribution. Hydraulically high-conductive conduits and a fissured network with a substantially lower hydraulic conductivity result in the duality of recharge, flow, and storage (Kiraly 2003). While discrete recharge occurs through surface karst features like karren, dolines, and poljes, diffuse recharge into the fissured network dominates in large parts of the catchment area (Fig. 2.1). Similarly, drainage through the aquifer is controlled by discrete flow in the karst conduit network and diffuse flow in the fissured network. In the conduit-system, transit times determined by tracer tests are generally in the range of hours to a few days (Massei et al. 2006; Geyer et al. 2007; Göppert and Goldscheider 2008). Fast and turbulent flow in the conduits results in a large variability of discharge at springs after precipitation events (Bonacci 1993; Winston and Criss 2004). Storage of water in the conduits is often limited

(Smart and Hobbs 1986), and potential contaminants are transported without substantial retardation through the system (Göppert and Goldscheider 2008). Because of natural flushing of contaminants through the conduit system, groundwater quality is often affected by bacterial contamination shortly after precipitation events (Mahler et al. 2000; Pronk et al. 2006). In contrast, slow percolation and accordingly long transit times have been found to occur in fissures and fractures of the system. Transit times determined by using natural tracers for the fissured network are generally in the range of several months to several years (Maloszewski et al. 2002; Worthington 2007; Einsiedl et al. 2009). Because of slow and diffuse water movement, storage of water and retardation and natural attenuation of potential contaminants is enabled in the fissured system, especially in the unsaturated zone (Pronk et al. 2009; Mudarra and Andreo 2011). Storage possibilities in the fissured network and a slow release of water provide baseflow in periods with low precipitation and low-flow conditions. In summary, the presence and development of drainage structures have a great influence on transit times and affect water quantity and quality. Transit times and other flow parameters can vary by orders of magnitude between the dominating drainage structures (Worthington 2007), detailed knowledge of which is needed for improved management of karst water resources. Additionally, karst drainage systems are dynamic systems that can exhibit a high variability of transit times depending on hydrologic flow conditions (Göppert and Goldscheider 2008; Perrin and Luetscher 2008; Morales et al. 2010). Tracer tests conducted under high-flow conditions demonstrate that transit times can be by a factor of 5 to 10 shorter than under low-flow conditions. The fast transport of the tracer can be linked with sharp breakthrough curves and high maximum concentrations (Göppert and Goldscheider 2008). Depending on water pressure gradients in the conduits and interconnection of the drainage structures, hydraulic exchange of water between the matrix and conduits may occur and can induce water storage in the fissured matrix or release of stored water (Massei et al. 2006; Bailly-Comte et al. 2010; Mudarra et al. 2014). As numerous factors influence the transit-time distribution, detailed investigations and different methodical approaches are needed to estimate available water resources and their vulnerability with respect to water quantity and quality.

Groundwater flow in karst systems is influenced by flow properties of the vadose (unsaturated), epiphreatic (partially water saturated) and phreatic (fully water saturated) zones of the aquifer. Depending on the aperture width of flow structures in the unsaturated zone, drainage occurs by

gravitational percolation or pressurized flow (Perrin et al. 2003; Pronk et al. 2009). In small fissures, stored water can only be mobilized by a pressure pulse mechanism after recharge events, and drainage is characterized by vadose seepage (Pronk et al. 2009). In larger flow structures, water seeps under the influence of gravity through the unsaturated zone resulting in fast drainage through vertical conduits, shafts and caves. At and below groundwater level, water follows the hydraulic gradient to the lowest outlet of the system, flowing in epiphreatic and phreatic passages (Fig. 2.1). In this case, the karst structures predominantly show a horizontal orientation (Kiraly 2003). While flow in epiphreatic conduits is comparable to flow mechanisms of surface water passing as a kinematic wave, drainage through phreatic conduits can be described as pressurized flow controlled by the hydraulic pressure (Jeannin 2001; Ford and Williams 2007; Reimann et al. 2011). In summary, the different flow mechanisms result in a wide range of hydraulic parameters in karst systems that make the aquifers difficult to assess.

So far, only a few studies have focused on the hydrogeology of karstic catchment areas that are characterized by a complex karst and porous-media (alluvial/rockfall) aquifer system (Sinreich et al. 2002; Wassmer et al. 2004; Bichler et al. 2012). Porous-media aquifers in deep incised valleys in karstic catchment areas often are hydraulically in contact with the karst aquifer (Fig. 2.1). Discharge from karst springs and surface streams can infiltrate into the porous-media aquifer, and springs that are hidden under sediments may directly contribute to groundwater flow in the porous-media aquifer (Massei et al. 2002; Pilli et al. 2012). Concentrated and fast drainage through the karst aquifer results in a great discharge variability in the karstic catchment area. In contrast, underground drainage in porous-media aquifers is generally characterized by lower flow velocities, comparable long transit times, and a high storage capacity. Discharge characteristics of a karstic catchment area comprising a connected karst and porous-media aquifer are likely to be influenced by discharge properties of the overall catchment. In this way, the rapid discharge response of a karst spring might be damped at the outlet of the overall catchment area because of the hydraulic interaction between the karst and porous-media aquifer.

2.2 Applied methods

Conventional hydrogeologic investigating methods reach their limits when applied to karst aquifer systems. The heterogeneous structure of karst systems requires special investigating techniques to account for drainage characteristics in different flow compartments. While artificial tracer tests are often applied to assess the conduit system (Goldscheider et al. 2008), the use of natural tracers (Maloszewski et al. 2002; Mudarra et al. 2014) and monitoring of spring discharge (Geyer et al. 2008) provide information about the fissured matrix and storage processes in the whole karst system. The selection and application of individual methods is based on information about the geologic and tectonic setting, hydrology, geomorphology, speleology, previous work and available data integrated into an initial conceptual model of each karst system. Different combinations of methods were used to assess drainage properties of the selected karst aquifer systems. This thesis examines whether the adjusted methods are suitable to address the research questions in the individual catchment areas (Chapter 1.2) and if the combination of methods is appropriate to describe the aquifer systems quantitatively. This chapter gives an overview of the basic concepts of the applied methods and the techniques for evaluating the obtained data.

2.2.1 Artificial tracer tests

Tracer tests are a powerful tool in karst hydrogeology to investigate groundwater flow in fast-draining conduit systems. To trace groundwater movement, artificial tracers are injected into the aquifer and the spread of the tracer plume is monitored at surrounding sampling points. In this way, tracer tests deliver specific information about point-to-point connections and catchment areas of springs, underground drainage pattern and flow paths, and transit-time distributions and flow velocities in karst systems (Käss 2004; Goldscheider and Drew 2007). In conjunction with detailed geologic and hydrologic information, the underground drainage of a karst aquifer system can be characterized.

Fluorescent dye tracers are often used as artificial tracers because their solubility, chemical stability and low adsorption properties facilitate dilution and transport in groundwater. Uranine is an almost ideal tracer as, in comparison with other dyes, it has the lowest adsorption properties and the lowest detection limit – 0.005 µg/L (Käss 2004; Goldscheider and Drew 2007). The tracers sulforhodamine G, eosine, sodium naphthionate and tinopal are often used as additional

dyes when conducting multi-tracer tests with several tracer injections. Because of their characteristic fluorescent wavelength, the dye tracers are clearly detectable in water samples. High-precision analytical laboratory results are obtained using a fluorescent spectrometer (Perkin Elmer, LS50B / LS55) and the syncho-scan method. Field fluorimeters (Albillia, GGUN-FL 43, 334 and 335) can be used for continuous detection, providing high temporal resolution of tracer concentrations. Cumulative and qualitative detection of tracers is possible with charcoal bags.

Most tracer tests are conducted with tracer injections on the land surface and the tracer is flushed into the karst system using natural seeping water, e.g., meltwater, or artificial irrigation, e.g., water tanks (Fig. 2.2). Under these conditions, the tracer seeps gravitationally through the unsaturated zone of the aquifer and follows the hydraulic gradient through the saturated zone to the sampling point. Results of hydraulic parameters characterize groundwater drainage along the whole flow path and allow estimates for flow velocities (v) and transit times (t) in the conduit system. The shape of the observed breakthrough curve (BTC), i.e., the peak and the tailing, provide information about the flow path (Field and Nash 1997; Massei et al. 2006). While almost symmetrical BTCs are indicative of well-developed conduits, highly asymmetrical and right-skewed BTCs indicate retardation and storage processes in the unsaturated zone as a result of interaction between the karst conduits and the fissured rock matrix.

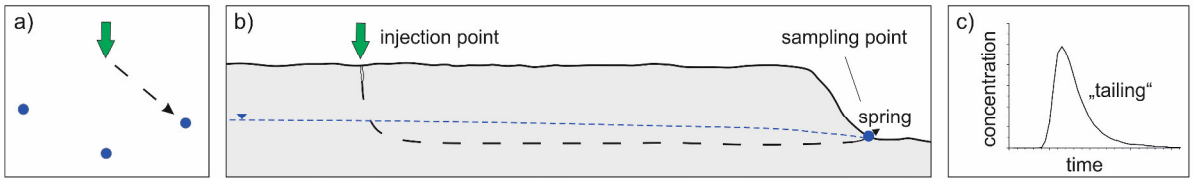

Figure 2.2: a) Point-to-point connection between injection point and sampling points, b) schematic profile between the injection point and sampling point at the land surface, and c) observed breakthrough curve at the spring.

A specific tracing technique is possible where active karst conduits are accessible (Goldscheider et al. 2008). In contrast to classical applications, tracer tests with injection and monitoring in active caves have been used to determine variable flow parameters for different zones of the aquifer, i.e., vadose, epiphreatic and phreatic zone (Fig. 2.3) (Hauns et al. 2001). It has been shown by Meiman et al. (2001) that tracer tests can contribute to resolving the internal structure of the karst drainage network and to identify sub-catchment areas. Because of the logistical challenges of working in caves and the often high associated effort and costs, in-cave tracer

tests are not common (Perrin et al. 2007; Goldscheider et al. 2008). However, in collaboration with committed cave researchers, in-cave tracer tests offer a unique opportunity to observe undisturbed groundwater flow in karst systems.

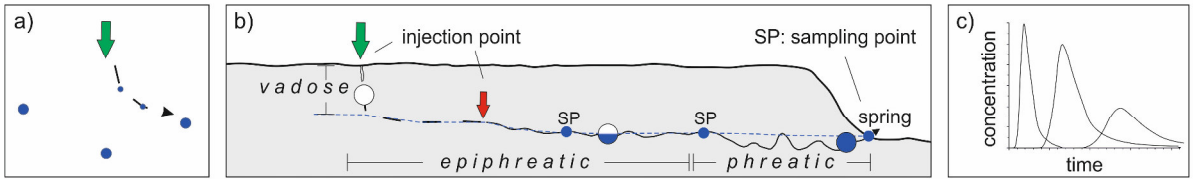

Figure 2.3: In-cave tracer tests make it possible to obtain a) spatially resolved information about the flow path from injection point to the spring, b) spatially resolved information about conduit flow in the epiphreatic and phreatic zones of the aquifer and c) temporally resolved information can be obtained by analyzing breakthrough curves at all sampling points.

Hydrologic flow conditions can affect groundwater flow in karst areas. It has been shown by Göppert and Goldscheider (2008) and Pronk et al. (2007, 2009) that transit times and dilution of the tracer are highly variable under high-flow and low-flow conditions. Furthermore, underground drainage divides and catchment areas can shift depending on water levels in the system (Ravbar et al. 2011). Therefore, tracer tests conducted under different flow conditions can provide insight into different flow parameters across the temporal variations of underground drainage.

For a quantitative evaluation of tracer tests and the determination of transport parameters, such as longitudinal dispersion coefficient (D), BTCs can be modeled by different advection-dispersion models (ADM) (Field and Pinsky 2000; Geyer et al. 2007; Massei et al. 2006; Morales et al. 2007; Goldscheider et al. 2008). The models account for one-dimensional flow that is controlled by advective and dispersive transport processes in the direction of groundwater flow (Eq. 2.1). To solve the general transport equation, simplifying assumptions are necessary, such as homogenous flow, a uniform and unidirectional flow field that is constant in time and space, and constant flow parameters along the flow path (van Genuchten et al. 2012). An inverse modeling tool of the ADM provides best estimates of the two flow parameters (v, D) by fitting a modeled BTC to observed values.

$$\frac{\delta c}{\delta t} = D\frac{\delta^2 c}{\delta x^2} - v\frac{\delta c}{\delta x} \qquad (2.1)$$

For the evaluation of nearly symmetric to slightly skewed BTCs, the advection-dispersion model implemented in the program CXTFIT (Toride et al. 1999) is used to obtain flow parameters of the karst conduit system. As highly asymmetric and right-skewed BTCs are characterized by a strong interaction between conduits and the rock matrix, the application of a multi-dispersion model, as implemented in TRACI95 (Käss 2004), is required to obtain flow parameters for the fast drainage of the conduits and the intermediate drainage at the margins of the conduit system.

2.2.2 Use of natural tracers

While tracer tests with artificial tracers are widely used to investigate flow properties of preferential flow paths in the conduit system, natural tracers can be used to determine drainage properties in the slowly draining fissured network. In general, hydrochemical compounds or environmental isotopes, such as stable water isotopes, are described as natural tracers. Because of water-rock interaction along the underground flow path or mixing processes of water in the aquifer, the original input-signal in precipitation is transferred to an output-signal at the measuring point (e.g., springs, wells). Analysis of natural tracers in precipitation (the input signal) and a discharging spring (the output signal) can be used to estimate residence time of the water, to identify sources and mixing of water and to calculate water volumes in the aquifer (Dewalle et al. 1997; Rodgers et al. 2005; Maloszewski and Zuber 2002; Einsiedl 2005). In contrast to artificial tracer tests, where only preferential and discrete flow paths are considered, natural tracers can be used to quantify diffuse flow through the aquifer and to characterize long-term properties of aquifer systems that play an important role in water storage and baseflow maintenance.

In this study, the stable isotopes ^{2}H and ^{18}O are used to investigate underground drainage processes. Because of the differences in physical and chemical properties, heavier isotopic molecules have lower mobility and higher binding energies, resulting in the fractionation of isotopes during condensation and precipitation. The isotopic composition of precipitation is strongly affected by temperature. Annual temperature variability results in a seasonally distinctive isotopic signal in precipitation that can be used as an input signal into the aquifer (Clark and Fritz 1997; Mook 2006). In catchment areas with high differences in elevation, there is also a relative

enrichment in heavy isotopes originating from the temperature decrease with increasing altitude. Isotopic values for ^{2}H and ^{18}O are expresses as delta values, relative to a standard, Vienna Standard Mean Ocean Water (VSMOW). High-precision detection of stable isotopes is possible by laser adsorption spectroscopy (LWIA, Liquid Water Isotope Analyzer, Los Gatos Research).

Depending on the drainage structure of the aquifer system, the input-signal in precipitation is dispersed in time and results in a damped output signal at the springs (Fig. 2.4). The annual variability ($\delta^{18}O$) in precipitation and the springs can be modeled by a sine wave curve to determine the annual mean value y_0, the amplitude A, and the phase shift θ (Eq. 2.2) (Dewalle et al. 1997; Rodgers et al. 2005).

$$\delta^{18}O = y_0 + A[\cos(ct - \theta)] \qquad (2.2)$$

Additional necessary parameters needed are the radial frequency c of annual fluctuations (0.017214 rad/d), and the time t in days after the beginning of sampling. In general, groundwater has a mean isotopic composition that is equal to the weighted annual mean of the isotopic composition of precipitation. Therefore, the annual mean value at a spring gives information about the mean elevation of the recharge area. The dampening of the signal and the phase shift enable estimates of the mean transit time of the natural tracer (Trček and Zojer 2009).

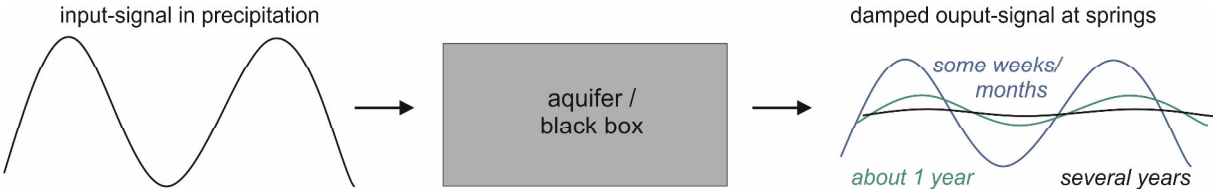

Figure 2.4: The isotopic input signal in precipitation, showing a distinctive seasonal variability, is transferred in a dampened output-signal at the karst springs and provides estimates of the mean transit time of the tracer in the aquifer system.

For quantitative evaluation, a lumped-parameter model implemented in the software FLOWPC (Maloszewski et al. 1983) can be applied. The relatively simple structure of the model provides a best estimate of the mean transit time (τ) of the natural tracer using only a few input parameters. The software fits the input-signal in precipitation ($\delta^{18}O_{IN}$) with the damped output signal at a spring ($\delta^{18}O_{OUT}$) by calculating predefined impulse-response functions ($g(\tau)$) (Eq. 2.3).

$$\delta^{18}O_{out} = \int_0^{\infty} \delta^{18}O_{in}(t-\tau)g(\tau)d\tau \qquad (2.3)$$

For model simplification, the exponential transfer function can be used assuming that there are numerous individual flow paths in the fissured aquifer, but that mixing of groundwater occurs only shortly before the outlet of the system (Maloszewski and Zuber 2002). Applying the exponential model, there is only one unknown fitting parameter, the mean transit time (τ). The best fit between the measured and modeled values gives an estimate of the mean transit time based on the natural tracer. The exponential transfer function further calculates a distribution of transit times and demonstrates the wide range of transit times (Maloszewski et al. 2002).

2.2.3 Discharge and hydrograph analysis

Discharge dynamics at karst springs provide important information about the drainage system (Smart and Hobbs 1986; Kiraly 2003). Spring-flow response, i.e., discharge through time, following individual recharge events can be used to resolve internal characteristics of the karst aquifer and to identify flow processes and underground storage properties in the catchment area (Bonacci 1993; Geyer et al. 2013). While well-developed flow paths lead to a fast response in spring discharge after precipitation events, a strong interaction between conduits and matrix at high water levels favors groundwater storage in the aquifer and results in a delayed and less-distinctive discharge peak (Kiraly 2003). The potential for groundwater storage during high-flow periods plays an important role in flood-buffering during high-flow events and the maintenance of baseflow during low-flow periods. Seasonal fluctuations of annual hydrographs can indicate recharge and depletion periods in the aquifer system.

To characterize discharge characteristics quantitatively, individual discharge peaks after precipitation events are analyzed in this thesis. A first assessment of parameters includes the determination of initial discharge (Q_i), the amount and time of peak discharge (Q_p), and the quantification of the precipitation event regarding amount and time (Fig. 2.5). For further analyses, the discharge response (R_D) is used, here defined as the ratio between peak discharge (Q_p) and the maximum precipitation intensity (P_{peak}), a unit conversion factor (f_c) and the size of the catchment area (A) (Eq. 2.4, Blume et al. 2007).

$$R_D = \frac{Q_P}{P_{peak} \cdot f_c \cdot A} \qquad (2.4)$$

The discharge ratio (Q_p/Q_i) characterizes the ratio between peak discharge and initial discharge, and a lag time (t) is introduced to quantify the time difference between the input signal, which is generally the maximum precipitation, and the output signal at the spring. In this study, the definition of input and output signal was modified, because discharge from the karst spring completely infiltrates into the porous-media aquifer. The discharge peak from the karst aquifer is used as the decisive input signal, while the discharge of the porous-media aquifer system is used as the output signal. Because of the underground flow path through porous media, the sharp discharge peak of the karst spring is transferred to a delayed discharge peak downgradient from the porous-media aquifer. This modified technique is used to describe the aquifer system comprising karst and porous-media aquifers in detail and to quantify discharge properties of the whole catchment area.

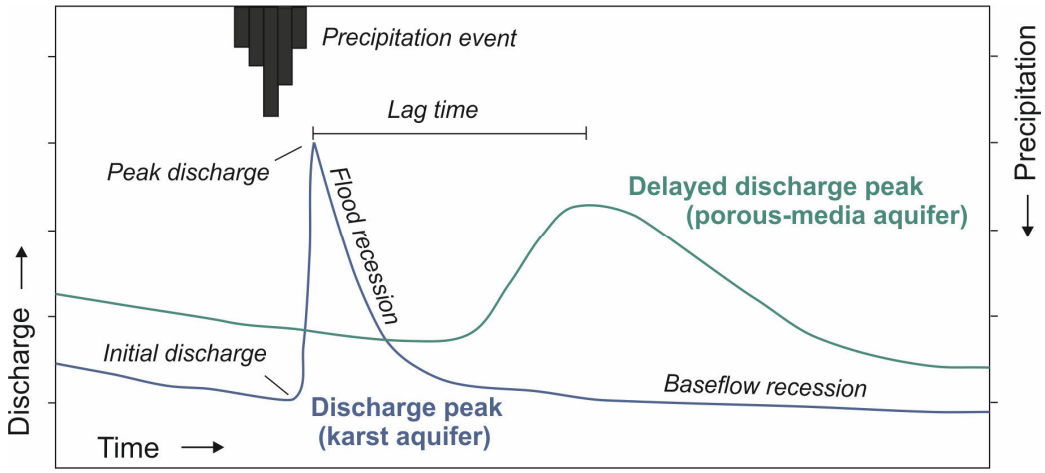

Figure 2.5: Schematic model of spring hydrographs. The precipitation event results in a sharp discharge peak at the karst spring. Discharge from the karst spring infiltrates into the porous-media aquifer and serves as the input signal for the delayed peak downgradient from the porous-media aquifer.

A quantitative analysis of the recession curve, i.e., the decline of spring discharge after a recharge event, is useful to determine dominant drainage structures. Based on the principles of linear reservoir behavior, changes in the gradient of the recession slope can reveal the presence of different drainage structures releasing water from the system (Bonacci 1993). The recession coefficient α, specified in the unit d^{-1}, is widely used to characterize relatively homogenous

porous-media systems as well as highly heterogeneous karstic systems. Of particular importance are the flood recession, defined as the steep slope segment, and the baseflow recession defined as the gently-sloped segment of the falling limb (Fig. 2.5) (Kovács and Perrochet 2008). The flood recession characterizes properties of the fast-draining network and results from fast infiltration and groundwater flow in conduits with high hydraulic conductivity. The baseflow recession is related to slow depletion of the aquifer after a recharge event and represents low-flow characteristics and the storage properties of the drainage system with low hydraulic conductivity (Bailly-Comte et al. 2010). As the recession curve is strongly influenced by the intensity, duration, and frequency of recharge events, a long time-series enables a more profound description of the system (Ford and Williams 2007).

For the quantitative evaluation of recharge-response characteristics, individual discharge peaks were modeled by an impulse-response function. Along the underground flow path, the sharp input signal is dispersed in time leading to a wide and damped output signal (Q_t) that can be described by a lognormal response function (Eq. 2.5, Long and Mahler 2013).

$$Q_t = Q_i + \frac{A_{out}}{t\omega\sqrt{2\pi}} e^{-\frac{\left[ln\frac{t}{t_m}\right]^2}{2\omega^2}} \qquad (2.5)$$

Fitted parameters are the initial discharge Q_i, a scaling coefficient A_{out} that quantifies the area under the discharge curve, and the mean transit time t_m and its variance ω. As described above, the discharge signal at the karst spring serves as input signal in this study, while discharge downstream of the porous-media aquifer was used as the output signal. The analyses were used to determine the distribution of underground transit times along the underground flow path through the porous sediments that influence the overall discharge characteristics of the karstic catchment area.

Chapter 3

Neue Erkenntnisse zur Struktur der Karstentwässerung im aktiven Höhlensystem des Blautopfs

Reproduced from: Lauber, U., Ufrecht, W., Goldscheider, N. (2013): Neue Erkenntnisse zur Struktur der Karstentwässerung im aktiven Höhlensystem des Blautopfs. – Grundwasser, 18, 247-257, doi: 10.1007/s00767-013-0239-z.

Kurzfassung

Der Blautopf, eine der größten Karstquellen Deutschlands, entwässert ein 165 km^2 großes Einzugsgebiet auf der Schwäbischen Alb. Dort befinden sich zwei große, aktive Karsthöhlen: das Blauhöhlensystem (10 km) und die Hessenhauhöhle (3,5 km). Aufgrund deren schwerer Zugänglichkeit war über die interne Entwässerungsstruktur dieses Karstsystems bisher nichts bekannt. Im Frühjahr 2012 wurde der erste Markierungsversuch mit Tracereingaben direkt in die beiden Höhlenflüsse durchgeführt, um die Verbindung zwischen den Höhlen zu lokalisieren. Durch zwei weitere Eingaben an der Geländeoberfläche sollte die Anbindung des Einzugsgebiets an die Höhlen erkundet werden. Mittels Feldfluorimetern wurden die Tracer-Durchgangskurven im Höhlensystem beobachtet. So konnte ein dendritischer Aufbau der unterirdischen Entwässerung nachgewiesen und für beide Höhlenflüsse eigene Teileinzugsgebiete abgegrenzt werden, die jeweils etwa 50% zur Gesamtschüttung beitragen. Neue geologisch-tektonische Befunde ermöglichten eine verbesserte hydrogeologische Modellvorstellung. Demnach liegt ein komplexes Karstsystem mit zwei Grundwasserstockwerken und hydraulischer Kontinuität durch eine bisher als weitgehend trennend geltende Mergelformation hindurch vor.

Abstract

The Blautopf ("blue pot"), one of Germany's largest karst springs, drains a catchment area of 165 km² in the Swabian Alb. There are two large, active caves: the Blue Cave System (10 km) and the Hessenhau Cave (3.5 km). Because of the difficult accessibility, the internal drainage structure had previously been unknown. The first tracer injections directly into cave streams were conducted in 2012 to localize connections between the two caves. Two surface injections in remote parts of the catchment were aimed at investigating drainage towards the caves. Field fluorometers allowed tracer monitoring in the caves. This demonstrated the dendritic structure of the drainage network and identified two sub-catchments that each contribute about 50% to the total discharge. New geologic-tectonic findings allowed an improved conceptual model, according to which the karst system consists of two aquifers with hydraulic continuity across a marl aquitard previously considered as impervious.

3.1 Einleitung

Eine der bekanntesten und wasserreichsten Karstquellen Deutschlands ist der Blautopf am südlichen Rand der Schwäbischen Alb (MQ: 2,3 m^3/s, HHQ: 32,6 m^3/s; Villinger 1978). Zahlreiche Sagen und Legenden handeln von der Quelle, die aufgrund der Tiefe des Quelltopfes lange Zeit als bodenlos galt. Die blaue Färbung wurde früher durch ein Fass Tinte erklärt, das täglich ins Wasser geschüttet wird. Im 17. Jahrhundert wurde die Herkunft des Quellwassers erstmals durch den ortsansässigen Pfarrer Mayer (1681) erforscht. Seine einfachen Markierungsversuche mit Spreu und Sägemehl führten zum Nachweis der hydraulischen Verbindung zwischen einer Versickerungsstelle auf der Albhochfläche und dem Blautopf. Seit 1952 wurden im Einzugsgebiet des Blautopfs über 65 Markierungsversuche durchgeführt, meist mit Fluoreszenztracern (Villinger und Ufrecht 1989; Selg und Schwarz 2009). Auf der wasserarmen Karsthochfläche der Schwäbischen Alb sollten damit vorrangig Fragen der Abwasserversickerung und der Nutzung von Karstquellen zur Trinkwasserversorgung beantwortet werden.

Hinter dem Blautopf verbirgt sich – wie lange Zeit vermutet – ein weitreichendes Höhlensystem, dessen einziger natürlicher Zugang über den Quelltopf selbst besteht (Abb. 3.1). Erste Tauchgänge fanden seit 1957 statt; kurz darauf erfolgte die Vermessung der ersten 130 m stromaufwärts des Höhleneingangs, der sich am Grund des 21 m tiefen Quelltopfs befindet. Zwischen

1961 und 2004 erkundete Jochen Hasenmayer u.a. mit einem von ihm gebauten U-Boot die Höhle über eine Länge von mehr als einem Kilometer. Aufbauend auf seinen Arbeiten wird das Höhlensystem seit 1997 durch die Arbeitsgemeinschaft (Arge) Blautopf erforscht und vermessen (Kücha und Jantschke 2009; Arge Blautopf 2011). Nach einer Tauchstrecke von 1.200 m beginnt ab dem Mörikedom ein über dem Wasserspiegel liegender Höhlenteil. Entlang riesiger Hallen und Gänge, teils auch enger Versturzzonen setzt sich das Höhlensystem weiter ins Quelleinzugsgebiet fort; stellenweise wird der unterirdische Fluss (Ur-Blau) angetroffen. Seit 2010 ermöglicht eine Forschungsbohrung einen trockenen Zugang in das Höhlensystem.

Parallel zur Erforschung des Blauhöhlensystems wurden seit 2006 Grabungen an der nahegelegenen Hessenhaudoline durchgeführt (Bohnert 2009). In einer Tiefe von 130 m erreichten die Höhlenforscher der Arge Blaukarst einen unterirdischen Fluss (Nord-Blau), der im Norden und Süden an Siphonen unter die Höhlendecke abtaucht. Schlechte Wasserqualität, starke Biofilmbildungen und intensiver Geruch ließen auf hydraulische Verbindungen zur rund 7 km entfernten Kläranlage Laichingen schließen. Dort war über Jahre hinweg – wie auf der Schwäbischen Alb üblich – das geklärte Abwasser in einer Karstspalte, dem Krempenschacht, versickert worden (Villinger und Ufrecht 1989).

Von oberflächennahen, ungespannten Karstsystemen ist bekannt, dass sie in der Regel dendritisch aufgebaut sind (Palmer 1991; Gabrovsek et al. 2004; Worthington und Ford 2009; Dreybrodt et al. 2010). Aufgrund der Lage beider Höhlensysteme in direkter Nähe zum Blautopf wurde eine hydraulische Verbindung vermutet, konnte aber bislang nicht nachgewiesen werden. Im Rahmen der vorliegenden Studie sollte diese Verbindung mit Hilfe von Fluoreszenztracern erkundet und lokalisiert werden. Im Gegensatz zu den zahlreichen vorangegangenen Tracerversuchen, bei denen Eingabe und Beprobung jeweils an der Geländeoberfläche bzw. am Blautopf erfolgten, lag der Fokus 2012 erstmals auf Tracereingaben und Monitoring direkt in den Höhlen. Solche Markierungsversuche mit räumlich und zeitlich hochaufgelösten Durchgangskurven in aktiven Höhlensystemen liefern detaillierte Informationen über Entwässerungsstrukturen, unterirdische Fließgeschwindigkeiten und hydraulische Parameter des Karstaquifers (Goldscheider et al. 2008). Aufgrund der oft schweren Zugänglichkeit aktiver, wasserführender Karströhren (Conduits) können solche Versuche nur in seltenen Fällen durchgeführt werden (Hauns et al. 2001; Göppert und Goldscheider 2008). Begünstigt durch den künstlichen Zugang war es 2012 erstmals möglich, Markierungsversuche im aktiven Höhlensystem des Blautopfs,

also im Blauhöhlensystem und in der Hessenhauhöhle, durchzuführen. Das Versuchsprogramm war wie folgt aufgebaut (Abb. 3.1):

- Zwei Tracer wurden direkt in die beiden Höhlenflüsse eingegeben, um die unterirdischen Fließwege im epiphreatischen bis phreatischen Höhlensystem bis zum Blautopf verfolgen zu können: lokaler Versuch.

- Zwei weitere Tracer wurden in oberstromiger Verlängerung der Höhlensysteme in die vadose Zone eingegeben, um entlang unterirdischer Messpunkte in beiden Höhlensystemen die Fließwege bis zum Blautopf zu lokalisieren: regionaler Versuch.

Neben der hydraulischen Verbindung der Höhlensysteme sollten auch Teileinzugsgebiete der einzelnen Höhlensysteme abgegrenzt werden, um so die bestehende hydrogeologische Modellvorstellung des Quelleinzugsgebiets zu verfeinern (Selg und Schwarz 2009; Bartenbach et al. 2009; Bartenbach und Ufrecht 2009; Ufrecht 2009; Geyer et al. 2011). Dazu erfolgten die Tracereingaben in Zainingen am Nordwestrand des Einzugsgebiets und in Laichingen im östlichen Teil.

3.2 Untersuchungsgebiet

Das Untersuchungsgebiet befindet sich auf der mittleren Schwäbischen Alb, die das 165 km^2 große Einzugsgebiet des Blautopfs beinhaltet (Abb. 3.1). Es wird aus einer 400 m mächtigen Folge von Kalksteinen im Wechsel mit Mergelkalk- und Mergelserien des Oberjuras aufgebaut. Mindestens ab der Unteren Felsenkalk-Formation sind die Schichten von Schwammriffen durchzogen (Schwamm- oder Massenkalkfazies), die Bankung der Gesteine nimmt hier zugunsten einer massigen Gesteinsausbildung ab (Abb. 3.2).

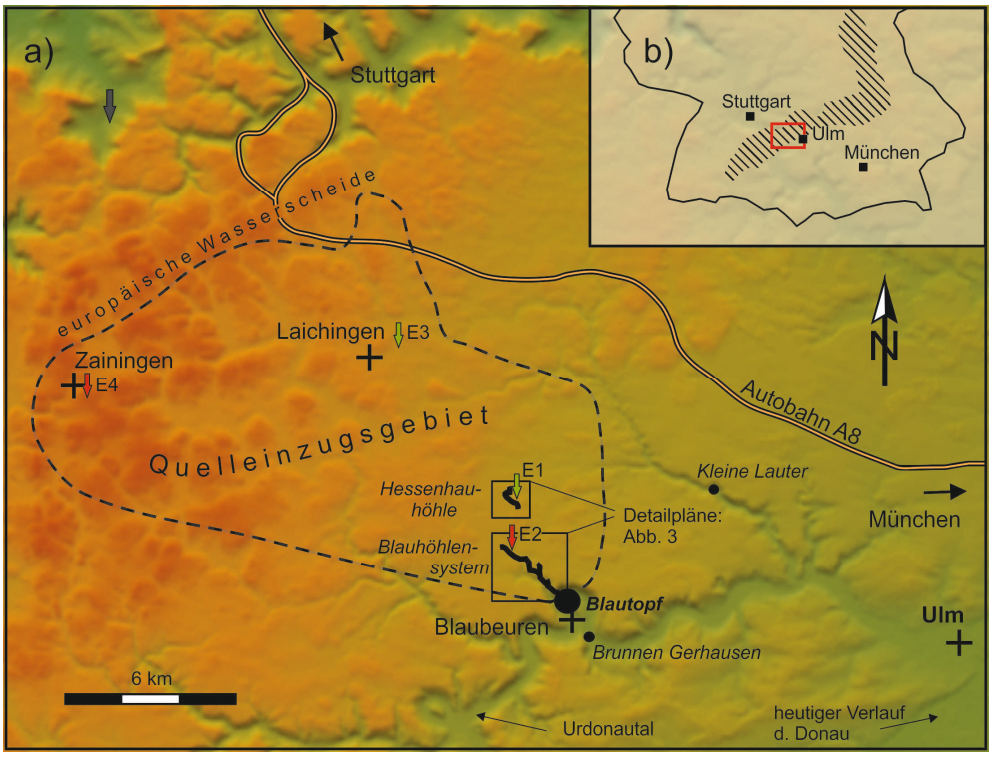

Abbildung 3.1: a) Einzugsgebiet des Blautopfs mit Eingabestellen E1-E4 (Pfeile) in beiden Höhlen (lokaler Versuch), und im entfernteren Quelleinzugsgebiet (regionaler Versuch); hinterlegt mit digitalem Höhenmodell, Höhen zwischen 450 m (grün) und 850 m ü. NN (braun), Daten: Landesvermessungsamt Baden-Württemberg; b) Karstgebiete der Schwäbischen und Fränkischen Alb (schraffiert) und Lage des Untersuchungsgebiets.

Die wechselnde Lithologie bedingt eine hydrostratigraphische Gliederung in zwei Grundwasserstockwerke (unten: Wohlgeschichtete Kalk-Formation, oben: Untere und Obere Felsenkalk-Formation) die jeweils von geringdurchlässigen Gesteinen unterlagert werden (Impressamergel- und Lacunosamergel-Formation). Beide Stockwerke unterliegen der Verkarstung, allerdings sind die Wohlgeschichteten Kalke nur im exponierten Bereich nahe der Oberjura-Schichtstufe, dem Albtrauf, stark verkarstet. Mit dem Einfallen der Schichten nach Süden verringert sich die Verkarstung dieser Formation, die im Bereich des Blautopfs etwa 100 m unter dem Vorflutniveau liegt. In der klassischen Vorstellung trennen die 35 bis 55 m mächtigen Lacunosamergel die beiden Karstgrundwasserstockwerke, wobei jedoch potenziell vertikale Wegsamkeiten an Störungen bestehen. Neuere Befunde lassen vermuten, dass die aus höheren Schichten bekannte Schwammfazies stratigraphisch tiefer und damit bis in die Lacunosamergel hineinreicht. Dadurch ist die Gesteinsfolge stärker geklüftet, in exponierter Position auch verkarstet und folglich besser vertikal durchlässig (Selg und Schwarz 2009; Bartenbach und

Ufrecht 2009; Regierungspräsidium Tübingen 2009), sodass die vertikale Stockwerksgliederung ganz aufgehoben sein kann. Im südlichen Teil des Blautopf-Einzugsgebiets, wo die Schichten deutlich nach Süden abtauchen und unter dem Urdonautal liegen, dürfte die hydraulische Trennwirkung wieder weitgehend intakt sein.

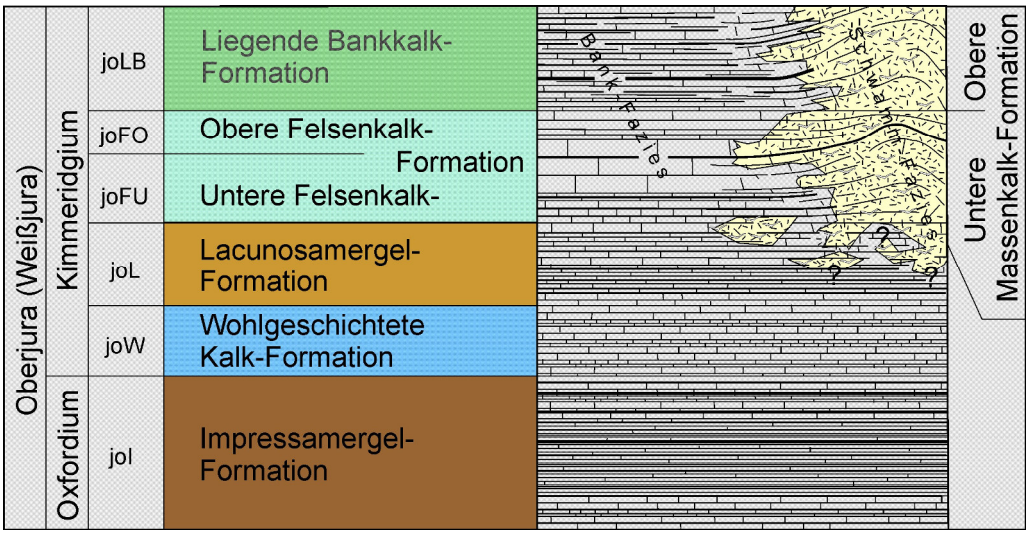

Abbildung 3.2: Stratigraphie des unteren und mittleren Oberjuras mit Verbreitung der Schwamm-Fazies im Gebiet der mittleren Schwäbischen Alb.

Seit der Kreide wurde das Gebiet durch mehrere Verkarstungsphasen geprägt. Zunächst kam es während der Kreide und dem Alttertiär in einer Phase tektonischer Ruhe unter dem vorherrschenden tropischen Klima vorwiegend zu einem flächigen Gesteinsabtrag. Eine tiefgründige Verkarstung setzte erst im Obermiozän infolge der tektonischen Hebung ein. Sie führte zur Bildung zahlreicher Dolinen, Höhlen und Trockentäler (Ufrecht 2011). Die Entwicklung der Karsthydrographie und die Ausbildung horizontaler Höhlenabschnitte (Höhlenniveaus) sind dabei von der Eintiefungsgeschichte der Fließgewässer abhängig, die als regionale Vorfluter wirken. Diese Zusammenhänge sind im Gebiet der mittleren Alb mit dem Einzugsgebiet des Blautopfs und dem am Südrand des Karstgebiets verlaufenden Tal der Urdonau gut untersucht (Ufrecht 2009, 2011). Ab dem Pliozän, v.a. aber während des Pleistozäns hat sich die Urdonau bis zu 200 m tief in die Massenkalke des Oberjuras eingetieft und dadurch das Potenzial für eine tiefgründige Verkarstung geschaffen.

Die ober- und unterirdischen Karstformen wurden durch Höhlenforscher gut dokumentiert. Im Umfeld des Blautopf-Einzugsgebiets sind über 150 Vertikal- und Horizontalhöhlen erforscht

und vermessen worden. Herausragende Objekte sind das knapp über 10 km lange Blauhöhlensystem und die 3,5 km lange Hessenhauhöhle (Abb. 3.3).

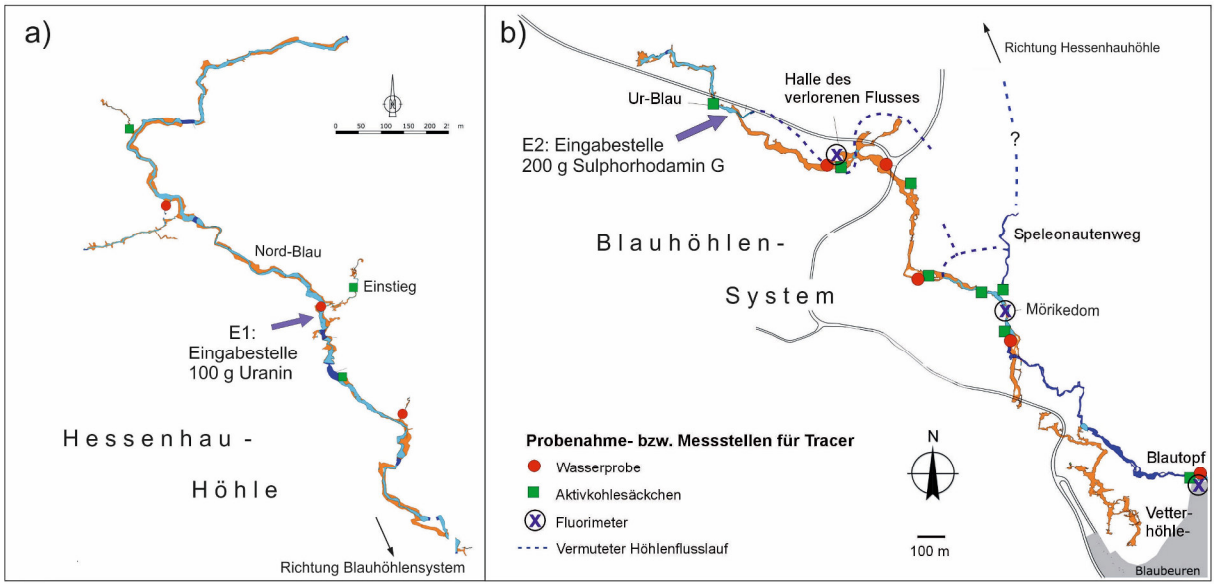

Abbildung 3.3: a) Grundrissplan der Hessenhauhöhle mit Probenahmestellen und Messpunkten zum Nachweis der Markierungsstoffe. Vermessung: Arge Blaukarst, Zeichnung: J. Bohnert. b) Grundrissplan des Blauhöhlensystems mit Probenahmestellen und Messpunkten während der Tracerversuche. Vermessung und Plandarstellung: Arge Blautopf sowie Arge Höhle und Karst Grabenstetten, Zeichnung: H. Jantschke und F. Mammel.

3.3 Versuchsaufbau

Beim lokalen Versuch wurden am 21.04.2012 in den Höhlenfluss der Hessenhauhöhle (Nord-Blau) 100 g Uranin eingegeben (E1, Abb. 3.1 und 3.4b). Fast gleichzeitig erfolgte die Eingabe von 200 g Sulphorhodamin G in die Ur-Blau im Blauhöhlensystem (E2 in Abb. 3.1 und 3.4a). Es wurde Uranin AP (C.I. 45350; AppliChem GmbH, Deutschland) und ORCO ACID Sulphorhodamin G (C.I. 45220; Organic Dyestuffs Corp., USA) verwendet.

Beim regionalen Versuch wurden eine Woche später erneut Uranin und Sulphorhodamin G verwendet, da dies die optimale Tracer-Kombination für den Nachweis mittels Feld-Fluorimeter ist. Zum Zeitpunkt der zweiten Eingabe waren die Konzentrationen aus dem ersten Versuch bereits bis unter die Nachweisgrenze abgesunken. Am 28.04.2012 wurden in eine Karstspalte (Krempenschacht, E3) bei der Kläranlage Laichingen 1500 g Uranin eingegeben, etwa 10 km vom Blautopf entfernt (Abb. 3.1). Dort wurde früher das geklärte Abwasser der Kläranlage eingebracht. Zur Vor- und Nachspülung der Eingabe wurde über eine Woche lang 1 bis 10 L/s

Wasser eingeleitet. Am gleichen Tag erfolgte die Eingabe von 2000 g Sulphorhodamin G in eine Doline am Ortsrand von Zainingen, rund 19 km vom Blautopf entfernt (E4). Hier wurde mit insgesamt 78 m^3 Leitungswasser nachgespült. Alle Eingaben wurden impulsartig durchgeführt, die Vorlösung der Tracer erfolgte jeweils in einem Kanister mit 10 bzw. 20 L Wasser.

Da Blauhöhlensystem und Hessenhauhöhle nur mit sehr großem Aufwand begangen werden können, stützt sich der Nachweis der Tracer dort vor allem auf Feldfluorimeter-Messungen und Aktivkohlesäckchen (Abb. 3.3). Zur kontinuierlichen Messung wurden Feldfluorimeter (GGUN-FL 43, 334 und 335, Albillia, Schweiz) an zwei Stellen im Blauhöhlensystem (Halle des verlorenen Flusses und Mörikedom) und am Blautopf eingesetzt (Abb. 3.4c und d). Die Aktivkohle-Säckchen wurden alle ein bis zwei Wochen gewechselt. Zusätzlich wurden so oft wie möglich durch die Höhlenforscher Wasserproben im Höhlensystem genommen, teils sogar durch mehrtägige Untertage-Biwaks. Eine besonders intensive manuelle Beprobung fand am Blautopf statt. Stündliche Daten zur Quellschüttung wurden vom Landesamt für Umwelt (LUBW) zur Verfügung gestellt. Die Aktivkohle sowie die Wasserproben wurden mit einem Fluoreszenzspektrometer (LS 55, Perkin-Elmer) im Synchro-Scan-Verfahren analysiert.

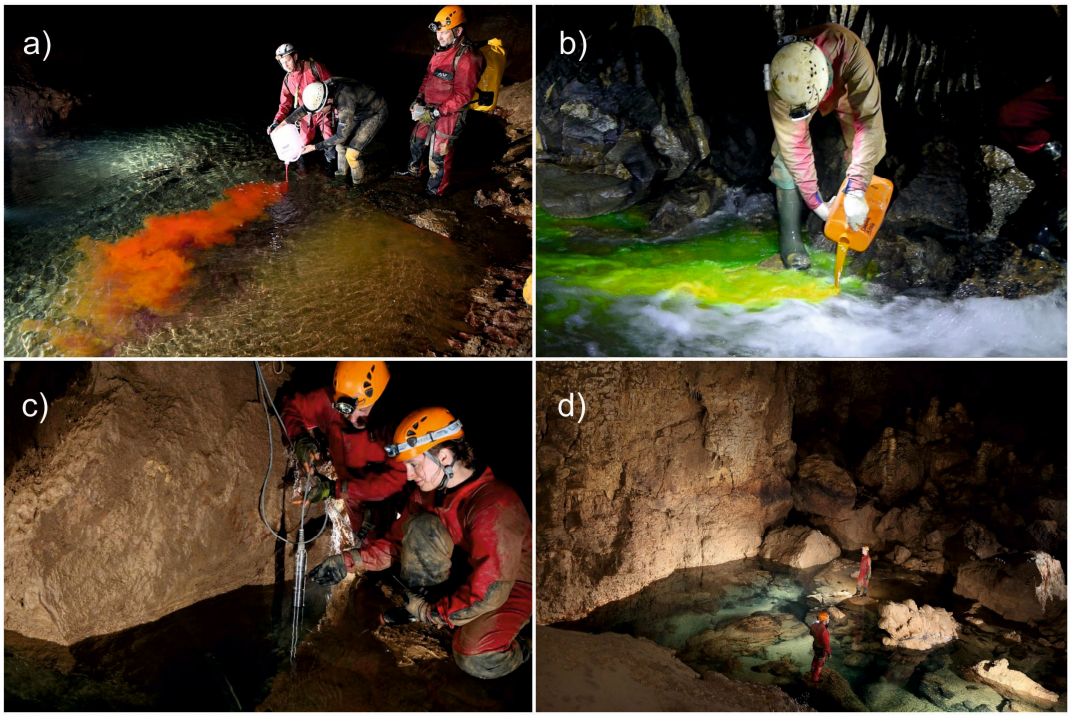

Abbildung 3.4: a) Eingabe (E2) von Sulphorhodamin G, b) Eingabe (E1) von Uranin, c) Einbau des Feldfluorimeters und d) Messstelle „Halle des verlorenen Flusses“ im Blauhöhlensystem. Aufnahmen von A. Kücha, Arge Blautopf (a, c, d) und A. Schober, Arge Blaukarst (b).

3.4 Ergebnisse und Diskussion

Im folgenden Teil wird im Wesentlichen auf die Ergebnisse der Wasserproben und Feldfluorimeter eingegangen. Dabei liegt der Fokus auf der geologischen und hydrogeologischen Interpretation, repräsentativ für die Versuchsergebnisse wird eine der zahlreichen Durchgangskurven gezeigt. Weitere Ergebnisse sind tabellarisch dargestellt (Abb. 3.5). Soweit nicht anders beschrieben wurden diese Ergebnisse durch die Aktivkohle-Analysen bestätigen.

Ein positiver Nachweis von Uranin aus der Hessenhauhöhle (E1) erfolgte im Blauhöhlensystem am Mörikedom und am Blautopf (Abb. 3.3). Die Durchgangskurven an beiden Messstellen zeigen einen deutlichen Peak und ein kurzes Tailing. Im Mörikedom trat die Maximalkonzentration von 1,9 µg/L nach 32 h auf. Am Blautopf wurde 49 h nach der Eingabe die Maximalkonzentration von 1,1 µg/L dokumentiert (Abb. 3.5b und c). Die dominierende Abstandsgeschwindigkeit zwischen Eingabestelle und Blautopf beträgt demnach 65 m/h bzw. 111 m/h unter Berücksichtigung einer Tortuosität von 1,7. Dieser Wert wurde über das Verhältnis von realer Ganglänge zu linearer Entfernung zwischen Mörikedom und Blautopf ermittelt. Während des Versuchs lag die Quellschüttung bei durchschnittlich 1320 L/s. Die Rückgewinnung von Uranin beträgt 52% und ist für eine direkte Eingabe in ein aktives Höhlengerinne vergleichsweise gering.

Die Durchgangskurven am Mörikedom und am Blautopf sind nahezu identisch und weisen jeweils nur einen Peak auf. Am Blautopf wurde eine etwas geringere Maximalkonzentration aber eine breitere Durchgangskurve als am Mörikedom gemessen, was auf Dispersion zurückgeführt werden kann. Es gibt also keinerlei Hinweise auf mehrere sich überlagernde Fließwege, die zu einem Multi-Peak-Effekt führen würden. Die Ergebnisse zeigen damit, dass nur eine einzige hydraulisch relevante Verbindung zwischen den beiden Höhlensystemen existiert – wohl in Form einer gut ausgebildeten Karströhre. Wie durch die topographischen Vermessungen der Höhlenforscher bekannt ist, existiert am Mörikedom ein phreatischer Höhlenast (Abb. 3.3b). Dieser sogenannte Speleonautenweg zweigt vom Blauhöhlensystem in Richtung Nordosten ab, also Richtung Hessenhauhöhle, konnte aber bislang nur rund 300 m verfolgt werden. Er ist Teil der markierungstechnisch nachgewiesenen Verbindung zur Hessenhauhöhle.

Das Quelleinzugsgebiet des Blautopfs gilt als annähernd natürliches Lysimeter (Armbuster und Selg 2006). Als Ursache für die vergleichsweise geringe Rückgewinnung von Uranin werden

dennoch weitere Fließwege in Betracht gezogen – tiefe Fließsysteme unter der Vorflut hindurch, Übertritte in die quartäre Talfüllung des Urdonautals und / oder Fließwege entlang alter Entwässerungsstrukturen in das Einzugsgebiet der Kleinen Lauter. Dort wurden geringe Spuren von Uranin in Aktivkohle nachgewiesen (< 0,5 µg/L im Eluat).

Der Nachweis von Sulphorhodamin G (E2) erfolgte in der Halle des verlorenen Flusses, im Mörikedom und am Blautopf (Abb. 3.3b). In der Halle des verlorenen Flusses traten die maximalen Konzentrationen nach 2 h 15 min auf und betrugen rund 50 µg/L. Im Mörikedom erfolgte der maximale Tracerdurchgang nach 15 h mit Konzentrationen von 6,0 µg/L. Am Blautopf wurde das Maximum von 4,0 µg/L nach 31 h erreicht (Abb. 3.5c). Die Entfernung zur Eingabestelle in der Ur-Blau beträgt Luftlinie 2,5 km, sodass die dominierenden Abstandsgeschwindigkeiten linear 86 m/h bzw. mit Berücksichtigung der Tortuosität 147 m/h betragen. Die Quellschüttung lag bei durchschnittlich 1240 L/s, die Rückgewinnung beträgt 79%.

Die Durchgangskurve weist ein etwas längeres Tailing auf, das vermutlich auf Verzögerungen in den zahlreichen Versturzzonen im Blauhöhlensystem zurückzuführen ist. Auch hier deutet der singuläre Peak auf einen Hauptfließweg entlang des Blauhöhlensystems von Ur-Blau über Halle des verlorenen Flusses und Mörikedom zum Blautopf hin (Abb. 3.3b). Die Rückgewinnung resultiert aus Sorptionsprozessen oder potenziell vorhandenen weiteren Fließwegen, die noch diskutiert werden.

Beim regionalen Versuch wurde das Uranin aus Laichingen (E3) sowohl in der Hessenhauhöhle als auch in der Blauhöhle am Mörikedom sowie am Blautopf nachgewiesen. Im Mörikedom setzte der Durchgang nach 134 h ein; die maximal gemessenen Konzentrationen von 11,5 µg/L wurden nach 155 h gemessen. Am Blautopf wurden erste Spuren nach 153 h gemessen; die maximalen Konzentrationen waren mit 10,3 µg/L nach 177 h erreicht (Abb. 3.5c). Die dominierende Abstandsgeschwindigkeit beträgt linear 55 m/h. Bei einer mittleren Quellschüttung von 1040 L/s wurde eine Rückgewinnung von 63% berechnet, die ebenfalls auf weitere Fließwege hindeutet. An der Quelle der Kleinen Lauter erfolgte über die Aktivkohle kein Tracernachweis.

Mit dem positiven Nachweis in der Hessenhauhöhle wurde die hydraulische Verbindung zur Kläranlage Laichingen belegt. Obwohl der Tracer durch die mindestens 100 m mächtige ungesättigte Zone gesickert ist, weist die Durchgangskurve einen annähernd symmetrischen Peak

mit kurzem Tailing auf – ähnlich wie bei der Eingabe in die Nord-Blau (E1, Abb. 3.5b). Generell wäre bei einer Eingabe an der Geländeoberfläche ein längeres Tailing zu erwarten, aufgrund des verzögerten Transports in ungesättigten Klüften und Schichtfugen. Der markierte Fließweg befindet sich jedoch im Bereich eines gut ausgebildeten Karstschachts, durch künstliches Einleiten von Wasser wurde die Wasserwegsamkeit über die Jahre hinweg wahrscheinlich zusätzlich erhöht. Entlang dieser stark verkarsteten Zone sind die Fließgeschwindigkeiten bis zum Karstgrundwasser daher offensichtlich sehr hoch, und der Einfluss der ungesättigten Zone ist entsprechend gering. Auf weiten Bereichen der Albhochfläche überwiegt dagegen die flächige und diffuse Infiltration. Sickerwässer werden dort lange in der vadosen Zone zwischengespeichert. Der Anteil dieser langsamen Abflusskomponente wurde über Wasserbilanzen und die Abflussdynamik ermittelt und liegt im Quelleinzugsgebiet des Blautopfs zwischen 90 und 95% (Selg et al. 2006; Geyer et al. 2011).

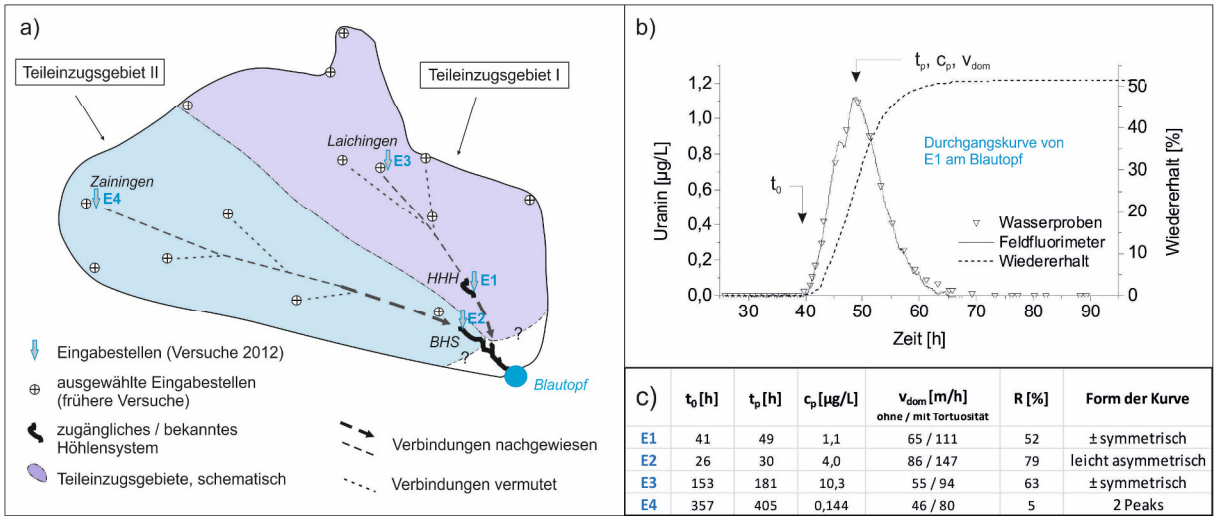

c)	t_0 [h]	t_p [h]	c_p [µg/L]	v_{dom} [m/h] ohne / mit Tortuositat	R [%]	Form der Kurve
E1	41	49	1,1	65 / 111	52	± symmetrisch
E2	26	30	4,0	86 / 147	79	leicht asymmetrisch
E3	153	181	10,3	55 / 94	63	± symmetrisch
E4	357	405	0,144	46 / 80	5	2 Peaks

Abbildung 3.5: a) Dendritischer Aufbau im Quelleinzugsgebiet des Blautopfs. Die beiden neu nachgewiesenen Teileinzugsgebiete tragen jeweils rund 50% zur Gesamtschüttung bei; HHH: Hessenhauhöhle, BHS: Blauhöhlensystem. b) Durchgangskurve von Uranin der Eingabe E1 in den Höhlenfluss (Nord-Blau) am Blautopf; c) tabellarische Übersicht der Ergebnisse von den Eingaben E1 bis E4 am Blautopf.

Das in Zainingen in die Doline eingegebene Sulphorhodamin G (E4) wurde ausschließlich im Blauhöhlensystem nachgewiesen – in der Halle des verlorenen Flusses, im Mörikedom und am Blautopf (Abb. 3.3b). Die Ergebnisse dieser Eingabe sind nur bedingt auszuwerten. Die Durchgangskurve zeigt an allen drei Messstellen zwei Peaks, und die Maximalkonzentrationen sind mit weniger als 0,2 µg/L sehr gering. Am Blautopf wurden erste Spuren des Tracers nach 355

h gemessen. Das erste Maximum von 0,15 µg/L wurde nach 405 h erreicht, das zweite Maximum nach etwa 555 h. Die dominierende Abstandsgeschwindigkeit (erster Peak) beträgt linear 46 m/h. Die Quellschüttung ist während des Versuchs auf 975 L/s zurückgegangen, die Rückgewinnung des Tracers ist sehr gering und liegt bei 5%.

Bei einem Tracerversuch 1986 in derselben Eingabestelle bei Zainingen wurde eine Durchgangskurve mit einem deutlichen Peak und einem raschen Tailing beobachtet (Villinger und Ufrecht 1989). Die Quellschüttung lag damals deutlich höher, bei 3400 L/s, und die Rückgewinnung betrug 90%. Während des aktuellen Versuchs bei insgesamt niedrigeren Abflussbedingungen kam es zwischenzeitlich zu Niederschlägen und zu einem Anstieg der Quellschüttung. Der geringe Wiedererhalt und die doppelten Peaks sind daher vermutlich auf Rückhalt und Remobilisierung in der ungesättigten Zone zurückzuführen. Daher wird nur der erste Peak in der weiteren Interpretation berücksichtigt.

Durch den regionalen Versuch wird deutlich, dass die beiden Höhlensysteme jeweils ein eigenes Teileinzugsgebiet entwässern: Teileinzugsgebiet I zeigt eine Entwässerung von Laichingen (E3) über die Hessenhauhöhle und den Mörikedom zum Blautopf (Abb. 3.5); Teileinzugsgebiet II drainiert von Zainingen (E4) über das gesamte Blauhöhlensystem zum Blautopf (Abb. 3.5a). Am Mörikedom, etwa 700 m vor dem Quellaustritt, münden die beiden Fließsysteme ineinander, erstmals belegt durch den lokalen Versuch. Ähnliche Beobachtungen mit drei bzw. vier Teileinzugsgebieten sind aus der Milandre Höhle im Schweizer Jura bekannt (Perrin et al. 2007). Das Einzugsgebiet der Höhlenflüsse der Mammoth Cave (USA) lässt sich ebenfalls in mehrere Teileinzugsgebiete untergliedern (Meiman et al. 2001).

Diese Existenz der beiden Teileinzugsgebiete wird auch durch Abflussmessungen zu Beginn der Markierungsversuche bestätigt. In der Hessenhauhöhle wurde am 14.04.2012 ein Abfluss von 770 L/s bestimmt, in der Halle des verlorenen Flusses im Blauhöhlensystem wurden 690 L/s gemessen. Die Quellschüttung lag zu diesem Zeitpunkt bei rund 1300 L/s. Demnach tragen beide Höhlenäste jeweils etwa 50% zum Gesamtabfluss des Blautopfes bei. Aus der Wasserbilanz ergibt sich im Vergleich zur Quellschüttung ein Wasserüberschuss von rund 10% in den Höhlensystemen. Diese Differenz ist zwar mit Messunsicherheiten der Abflussmessungen behaftet, allerdings existieren zum Blautopf hin vermutlich noch weitere Zuflüsse, die bei der Bilanzierung nicht berücksichtigt werden konnten.

Die Ergebnisse der Abflussmessungen und der Tracerversuche lassen in Kombination mit der Kartierung der Höhlenforscher auf den hierarchischen Aufbau des unterirdischen Entwässerungssystems schließen (Abb. 3.5a). Über Spalten und Klüfte sickert das Wasser durch die meist mehr als 100 m mächtige ungesättigte Zone, bis es die (epi-)phreatische Zone erreicht. Anschließend folgt das Wasser dem hydraulischen Gradienten zum Blautopf, wobei es entlang von netzwerkartig angeordneten, korrosiv geweiteten Trennflächen vorwiegend in der epiphreatischen Zone fließt. Mit zunehmender Wasserführung weiten sich die bevorzugten Fließwege durch verstärkte Lösungsprozesse und es kommt zur Entwicklung von Hauptästen der Entwässerung (Abb. 3.5a). Aufgrund der gemessenen Wassermengen sind für den quellnahen Bereich zwei Hauptäste nachgewiesen, die Hessenhauhöhle und das Blauhöhlensystem. In einer Entfernung von 700 m Luftlinie zum Blautopf, am Mörikedom, führen die Höhlensysteme zusammen und bilden eine einzige, große, vollständig wassererfüllte Karströhre bis zum Blautopf. Dort windet sich der Höhlenverlauf stark und erstreckt sich auf eine reale Länge von 1200 m; die Tortuosität liegt demnach bei 1,7 (Abb. 3.6a). Der Höhlenabschnitt ist phreatisch, da das Vorflutniveau des Ur-Donautals ehemals tiefer lag und durch die Verlagerung des Flusslaufes ab der Riß-Kaltzeit aufgeschottert wurde und dadurch das ausfließende Wasser rückstaut (Villinger 1987). Die Auslaufhöhe bestimmt zudem das kleine Stauwehr am Quelltopf.

Die lithostratigraphischen, strukturgeologischen, speläologischen und hydrogeologischen Informationen über das Blautopf-Einzugsgebiet bilden die Grundlage einer verbesserten Modellvorstellung, die in Abb. 3.6a in Form eines Längsschnitts präsentiert wird. Die Darstellung der Grundwasseroberfläche beruht auf einer weiträumigen und mit Unsicherheiten behafteten Interpolation von Grundwasserstandsdaten und Quellauslaufhöhen (Regierungspräsidium Tübingen 2009). Der Schnitt zeigt, dass die beiden Eingabestellen für die regionalen Markierungsversuche im Zentrum (Laichingen) bzw. Randbereich (Zainingen) eines tektonischen Hochgebiets liegen, welches das zentrale bis nördliche Blautopf-Einzugsgebiet etwa in Richtung SW-NE durchzieht (Ufrecht 2009). Große Teile des unterirdischen Abflusses müssen also diese tektonische Hochstruktur queren, um nach Süden zum Blautopf zu gelangen. Gemäß dem Verschnitt von Schichtlagerung und Grundwasseroberfläche müssen die tektonisch hoch liegenden Gebiete zunächst in den Wohlgeschichteten Kalken nach Süden entwässern, um dann etwa im zentralen Teil bis südlichen Drittel des Einzugsgebiets, wo die Schichten steiler nach Süden einfallen, wieder das Obere Karststockwerk zu erreichen. Damit muss Karstwasser, das in der

Nordhälfte des Blautopf-Einzugsgebiets neugebildet wird, zweimal die Lacunosamergel durchdringen, zuerst als Sickerwasser in der ungesättigten Zone und später als auf die Vorflut zugerichteter Karstwasserstrom über die beiden epiphreatischen bis phreatischen Höhlenflüsse. Für den Großteil des Blautopf-Einzugsgebiets bilden also erst die Impressamergel die hydrogeologisch wirksame Verkarstungsbasis.

In Anbetracht dieser hydrogeologischen Situation ist der rasche Tracerdurchgang nur durch eine starke Verkarstung bis in das tiefere Grundwasserstockwerk bzw. eine hohe Durchlässigkeit der Lacunosamergel zu erklären, vermutlich entlang von Klüften. Darüber hinaus muss die Durchlässigkeit so groß sein, dass sich keine zwei Fließsysteme entwickeln (über und unter den Lacunosamergeln) (Abb. 3.6a und b). Innerhalb der Lacunosamergel kommt es zu keinem nachweisbaren Rückhalt der Tracer, weder in vertikaler Richtung durch die ungesättigte Zone noch in horizontaler Richtung durch die epiphreatische und phreatische Zone. Auch dort scheint nur ein hydraulisch wirksamer präferentieller Fließweg zu existieren, der zu einem Tracerdurchgang mit nur einem deutlichen Peak an allen Messstellen führt (abgesehen von den nicht eindeutigen Ergebnissen aus Zainingen). Ein Abstrom in einem stark verzweigten Karstnetzwerk würde zu einer Durchgangskurve mit zahlreichen Peaks und/oder langem Tailing führen (Goldscheider et al. 2008). Die Einflüsse der ungesättigten Zone können in diesem Fall als gering betrachtet werden. Der Anteil am gesamten Fließweg ist mit 130 m bei einer Gesamtstrecke von 10 km sehr gering. Zudem ist für beide Eingabestellen eine starke Verkarstung der ungesättigten Zone erwiesen. Jahrelanges Einleiten von geklärtem Abwasser kann die Wasserwegsamkeit zusätzlich erhöht haben, u.A. durch Auswaschungen von Sedimenten aus dem Epikarst.

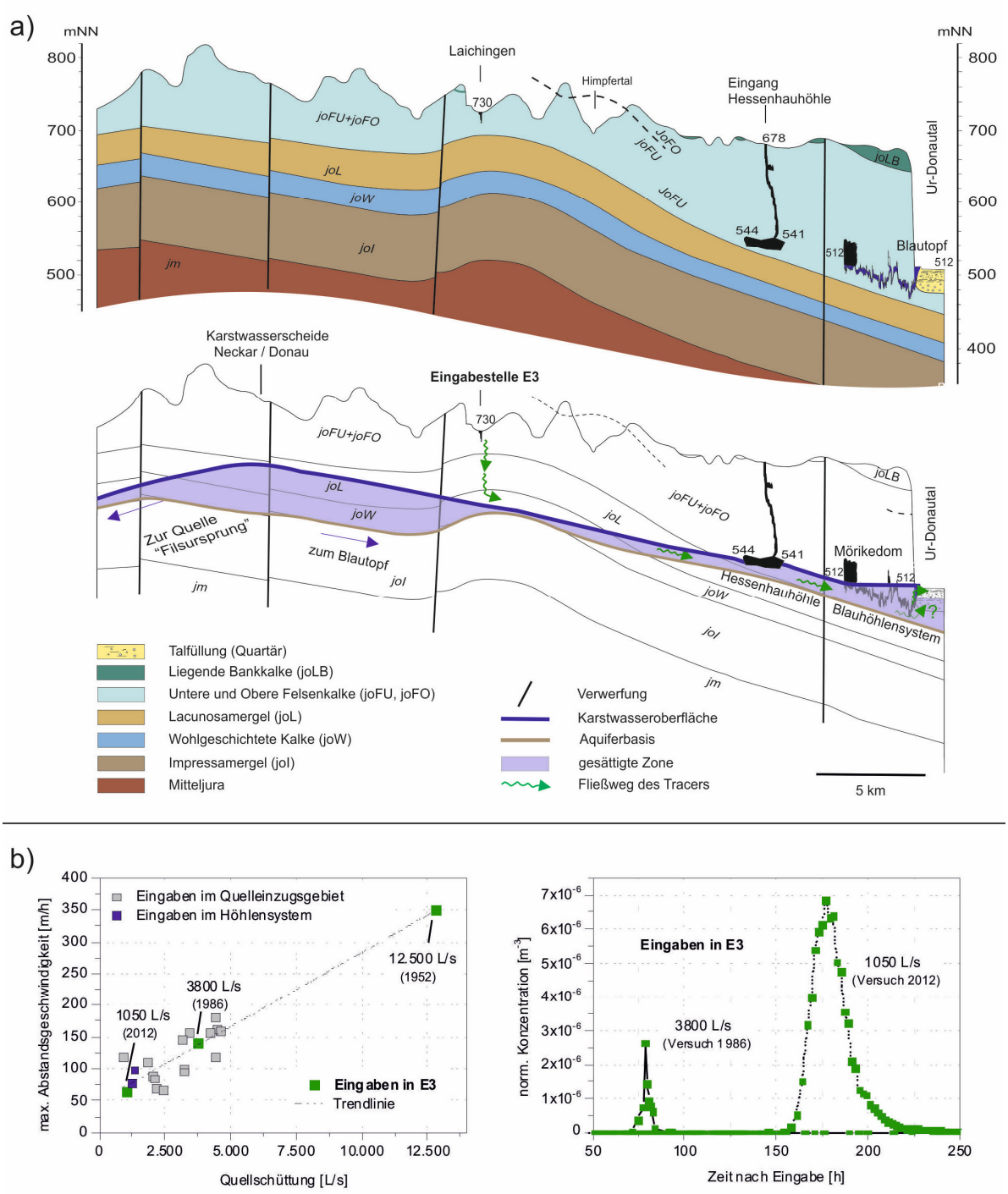

Abbildung 3.6: a) Geologischer und hydrogeologischer Längsschnitt des Blautopf-Einzugsgebiets mit neuen Erkenntnissen zur Karstentwässerung. Das Profil verläuft entlang des vermuteten Fließwegs von Eingabestelle E3 bei Laichingen über die Hessenhauhöhle zum Blauhöhlensystem und Blautopf; b) Vergleich der Ergebnisse von Eingabestelle E3 bei Laichingen (grüne Markierung): Maximale Abstandsgeschwindigkeiten (v) in Abhängigkeit von der Quellschüttung (Q), annähernd lineare Beziehung durch $Q = v \cdot A$ (A = wasserdurchflossener Querschnitt), und der Einfluss auf Fließzeit und Verdünnung des Tracers.

Mit Hilfe der Wasserbilanz kann gezeigt werden, dass Karstwasser maximal in der Menge des Bilanzfehlers von 13% der mittleren Schüttung (Armbuster und Selg 2006), das sind etwa 300 L/s, den Bilanzraum durch Unterströmen der Vorflut in den Wohlgeschichteten Kalken verlassen kann und/oder direkt am Blautopf vom Oberen Grundwasserstockwerk aus (Untere Felsenkalk-Formation) in die quartäre Talfüllung des Urdonautals übergeht. Dabei ist die Wasserbilanz auch mit Unsicherheiten behaftet, u.A. durch Verwendung des Bodenwasserhaushaltsmodells, die etwa in der gleichen Größenordnung liegen (Mttl. v. M. Selg). Auch wurde im abstromig gelegenen Brunnen Gerhausen im Probennahmezeitraum kein Uranin nachgewiesen – die potenziellen Fließzeiten des Tracers im Porengrundwasserleiter wären aber wesentlich länger. Zu einem ähnlichen Ergebnis wie die Wasserbilanz von Armbuster und Selg (2006) führen auch die Abflussmessungen im Höhlensystem, die eine Differenz von 10% zwischen den Teilabflüssen im Höhlensystem zum Gesamtabfluss am Blautopf zeigen. Auch die unterschiedliche Rückgewinnung der Tracer, die zwischen 52 und 79% liegt, ist ein Indiz für die Existenz weiterer Fließwege und einem Verlust von Wasser im Bilanzraum. Möglicherweise tritt ein Teil des Wassers aber auch entlang von „alten“ Fließwegen in das Quelleinzugsgebiet der Kleinen Lauter über. Diese sind aus der Entwicklungsgeschichte des Gebiets bekannt (Ufrecht 2009), wurden teilweise bei Markierungsversuche nachgewiesen (Villinger und Ufrecht 1989) und können u.U. je nach Abflussbedingungen reaktiviert werden.

Bei den vorangegangenen 65 Tracerversuchen im Quelleinzugsgebiet mit Eingaben an der Karstoberfläche und Beprobung am Blautopf haben 21 Versuche zu einem Durchgang am Blautopf geführt. Dabei wurden maximale Abstandsgeschwindigkeiten zwischen 67 und 350 m/h festgestellt; der Mittelwert beträgt 131 m/h (Selg und Schwarz 2009). Die dominierenden Abstandsgeschwindigkeiten liegen im Mittel bei 110 m/h, mit Schwankungen zwischen 62 und 310 m/h. Im Vergleich zu diesen Tracerversuchen wurden 2012 trotz direkter Eingabe in die Höhlenflüsse die bislang niedrigsten Abstandsgeschwindigkeiten festgestellt; die Werte lagen zwischen 47 und 73 m/h. Dabei sind die Fließgeschwindigkeiten stark von den hydrologischen Bedingungen abhängig. Zum direkten Vergleich wurden Ergebnisse von Tracereingaben in E3 bei Laichingen verwendet (Abb. 3.6b), die bei Niedrigwasser mit einer Schüttung von 1050 L/s (2012) und bei vergleichsweise hoher Schüttung mit 3800 L/s durchgeführt wurden (Villinger und Ufrecht 1989) und die Konzentrationen normiert ($C_{norm} = C/M$). Eine weitere Eingabe in Laichingen zu einem Spitzenabfluss von 12 500 L/s ist nicht auswertbar, da keine vollständige

Durchgangskurve vorliegt. Es zeigt sich, dass die Abstandsgeschwindigkeiten bei rund 3,5 mal höheren Abflüssen am Blautopf (3800 L s^{-1}) rund 3 mal höher sind als bei Niedrigwasser (1050 L/s). Ein höherer Abfluss und damit ein größeres Karstwasservolumen führen zu einer stärkeren Verdünnung des Tracers; die normierte Maximalkonzentration beträgt rund 3×10^{-6} m^{-3}. Dagegen sind die normierten Maximalkonzentrationen bei Niedrigwassern mit 7×10^{-6} m^{-3} deutlich höher (Abb. 3.6b). Dieser Unterschied um den Faktor 2,5 ist auf das geringere Wasservolumen zurückzuführen, das bei Niedrigwasser zu einer geringeren Verdünnung führt. Dies wirkt sich entsprechend auf den potenziellen Schadstoffeintrag ins Karstsystem aus. Auch aus anderen Karstgebieten sind ähnliche Zusammenhänge bekannt. Pronk et al. (2007, 2009) zeigten für das Karstsystem in Yverdon, Schweiz, dass die Fließzeiten um den Faktor 10 schwankten, während die Maximalkonzentrationen nur um den Faktor 1,5 variierten – mit höchsten Konzentrationen bei Niedrigwasser, aufgrund der geringeren Verdünnung. Von Göppert und Goldscheider (2008) wurde der gegenteilige Effekt in einem vadosen bis epiphreatischen Karstsystem beobachtet: bei Hochwasser wurden höhere Maximalkonzentrationen festgestellt, die auf höhere Abstandsgeschwindigkeiten und damit schmalere Durchgangskurven zurückgeführt werden konnten.

3.5 Zusammenfassung und Schlussfolgerungen

Im Höhlensystem des Blautopfs (Blauhöhlensystem und Hessenhauhöhle) konnten durch Tracereingaben bzw. Monitoring direkt in den schwer zugänglichen Höhlenflüssen erstmals detaillierte Informationen über die interne Entwässerungsstruktur dieses Karstsystems erhalten werden. Das Quelleinzugsgebiet des Blautopfs wird demnach aus zwei Teileinzugsgebieten aufgebaut. Das nördliche Teilgebiet entwässert zur Hessenhauhöhle, das südliche zum Blauhöhlensystem. Erst am Mörikedom, also etwa 700 m oberhalb der Quelle, münden beide Systeme ineinander. In Verbindung mit Abflussmessungen, die in den Höhlen gemacht wurden, konnte der Anteil der beiden Höhlenäste zur Gesamtschüttung des Blautopfs mit jeweils rund 50% quantifiziert werden. Die Kombination von geologischen Profilschnitten und Informationen zur Lage der Grundwasseroberfläche zeigen eine komplexe unterirdische Entwässerung. Entgegen der bisherigen Modellvorstellung müssen sowohl in den beiden Karstgrundwasserstockwerken als auch in den bislang als sehr gering durchlässig geltenden Lacunosamergeln sehr gut durchlässige Fließwege ausgebildet sein. Dies geht aus den Durchgangskurven hervor, die mit ihrem

Einzelpeak und ihrem kurzen Tailing eher mit den Durchgangskurven der Eingaben in die Höhlenflüsse zu vergleichen sind. Tracerversuche in aktiven Höhlensystemen ermöglichen es, wichtige Informationen über Fließeigenschaften in der vadosen, epiphreatischen und phreatischen Zone zu gewinnen. Im Quelleinzugsgebiet des Blautopfs wurden bei den Tracereingaben in die Höhlenflüsse die bislang niedrigsten Abstandsgeschwindigkeiten festgestellt. Dies ist einerseits darauf zurückzuführen, dass die Versuche bei Niedrigwasser durchgeführt wurden. Andererseits konnte festgestellt werden, dass der phreatische Höhlenabschnitt aufgrund des geringen hydraulischen Gradienten als Staubereich fungiert, in dem sehr geringe Abstandsgeschwindigkeiten dominieren.

Durch die Tracereingabe in den Krempenschacht bei Laichingen konnte die hydraulische Verbindung zwischen der Kläranlage und dem Blautopf nachgewiesen werden. Wie der Versuch gezeigt hat, werden potenzielle Schadstoffe über die stark verkarsteten Bereiche schnell ins Grundwasser eingetragen und je nach Abflussbedingungen im Karstsystem verdünnt. Es konnte gezeigt werden, dass die Maximalkonzentrationen bei Niedrigwasser besonders hoch sind, aufgrund der geringeren Verdünnung. Dies wirkt sich auch auf Schadstoffeinträge aus, die im Vergleich zu Hochwasserbedingungen zwar länger im System verweilen, dafür aber in höheren Konzentrationen am Blautopf wieder austreten. Tracerversuche bei unterschiedlichen Abflussbedingungen liefern somit zusätzliche Informationen über das Karstsystem, die für die Erschließung von Karstgrundwasserleitern zur Trinkwasserversorgung, aber auch zum Schutz der Karstwasserressourcen vor Schadstoffeinträgen wichtig sind.

Danksagung

Wir danken den Höhlenforschern der Arge Blautopf und Blaukarst – insbesondere den Projektleitern Andreas Kücha und Jürgen Bohnert –, den Gemeinden Zainingen und Laichingen, der Stadt Blaubeuren, der freiwilligen Feuerwehr Blaubeuren, der Landesanstalt für Umwelt, Messungen und Naturschutz Baden-Württemberg und dem Landesamt für Geologie, Rohstoffe und Bergbau Baden-Württemberg für ihre Unterstützung. Das Projekt wurde durch die Umweltstiftung Hofbräu Stuttgart finanziell unterstützt. Das Abstract wurde freundlicherweise von Tim Bechtel korrekturgelesen.

Chapter 4

Spatially resolved information on karst conduit flow from in-cave dye tracing

Reproduced from: Lauber, U., Ufrecht, W., Goldscheider, N. (2014): Spatially resolved information on karst conduit flow from in-cave dye tracing. – Hydrology and Earth System Sciences, 18, 435–445, doi: 10.5194/hess-18-435-2014.

Abstract

Artificial tracers are powerful tools for investigating karst systems. Tracers are commonly injected into sinking streams or dolines, while springs serve as monitoring sites. The obtained flow and transport parameters represent mixed information from the vadose, epiphreatic and phreatic zones (that is, the aquifer remains a black box). Accessible active caves constitute valuable but underexploited natural laboratories to gain detailed insights into the hydrologic functioning of the aquifer. Two multi-tracer tests in the catchment of a major karst spring (Blautopf, Germany) with injections and monitoring in two associated water caves aimed at obtaining spatially and temporally resolved information on groundwater flow in different compartments of the system. Two tracers were injected into the caves to characterize the hydraulic connections between them and with the spring. Two injections at the land surface, far from the spring, aimed at resolving the aquifer's internal drainage structure. Tracer breakthrough curves were monitored by field fluorimeters in caves and at the spring. Results demonstrate the dendritic drainage structure of the aquifer. It was possible to obtain relevant flow and transport parameters for different sections of this system. The highest mean flow velocities (275 m/h) were observed in the near-spring epiphreatic section (open-channel flow), while velocities in the phreatic zone

(pressurized flow) were one order of magnitude lower. Determined conduit water volumes confirm results of water balances and hydrograph analyses. In conclusion, experiments and monitoring in caves can deliver spatially resolved information on karst aquifer heterogeneity and dynamics that cannot be obtained by traditional investigative methods.

4.1 Introduction

Karst aquifers are characterized by strong heterogeneity and anisotropy related to the diverse distribution of solutionally enlarged conduits in the carbonate rock (Worthington and Ford 2009). Groundwater flow and contaminant transport in karst aquifers are difficult to predict because of the unknown configuration and geometry of the conduit network. However, the sustainable use and protection of karst groundwater resources requires detailed knowledge of the underground flow paths and spring catchment areas. Geological mapping and speleological investigations can deliver direct information about karst development and the presence of larger conduits (Goldscheider and Drew 2007). Further insights into drainage structures and dominating transit times can be achieved by observations of spring hydrographs and environmental tracers (e.g., electrical conductivity, hydrochemical components and isotopes) (Winston and Criss 2004; Ravbar et al. 2011; Mudarra and Andreo 2011). Artificial tracer tests are often used to investigate the drainage pattern of karst aquifers. In contrast to other methods, tracer tests deliver clear information on hydraulic connections, spring catchment areas, transit time distributions and linear flow velocities. Relevant conservative and reactive transport parameters, such as dispersion and retardation can be obtained by quantitative analysis and modeling of tracer breakthrough curves (BTCs) (e.g., Geyer et al. 2007; Massei et al. 2006; Morales et al. 2007; Goldscheider et al. 2008). In most cases, tracers are injected into stream sinks, dolines or other surface karst structures, while springs serve as sampling and monitoring sites. Consequently, all obtained data and parameters represent mixed information from the entire flow path between the injection and recovery sites (i.e., from the unsaturated (vadose), epiphreatic and phreatic (saturated) zones of the aquifer). However, flow velocities and transport parameters are highly variable between and within these zones.

Experiments and monitoring in caves make it possible to obtain more detailed insights into the internal structure and hydraulic functioning of karst aquifer systems (Goldscheider et al. 2008). Owing to the difficult to near-impossible access to active caves, as well as the associated cost

and dangers, this approach has not been used very often. In this sense, caves are valuable but underexploited natural laboratories for hydrologic research. Perrin et al. (2007) quantified the role of tributary mixing in chemical variability at a karst spring by means of detailed monitoring inside a cave system. Meiman et al. (2001) conducted in-cave dye-tracer tests to delineate subbasins within the Mammoth Cave aquifer. The hierarchical structure of conduit systems is known from speleological observations (Palmer 1991) and numerical simulations of speleogenesis (Gabrovsek et al. 2004; Dreybrodt et al. 2010). Tracer tests in caves can help to reveal the drainage structure of inaccessible conduit systems (e.g., Smart 1988). In-cave tracer tests have also previously been used to determine flow velocities and dispersion in openchannel cave streams at local scales (Hauns et al. 2001) and to compare the transport of solutes and colloids (Göppert and Goldscheider 2008). Tracer injections at the land surface and monitoring of water inlets in caves can help to quantify water storage, percolation and contaminant transport in the epikarst zone (Pronk et al. 2009).

In order to obtain spatially and temporally resolved information on conduit flow in karst aquifer systems, a karst catchment in southern Germany that includes two major caves and is drained by a large spring was selected as a test site for this study. This paper presents the first tracer tests that were done inside the active conduit network of this karst system, accompanied by detailed geological investigations and water balances (Lauber et al. 2013). The experimental approach consists of two in-cave dye-tracer injections and two injections at the land surface, with detailed monitoring at several sampling sites inside the caves and at the spring (Figs. 4.1 and 4.2).

There were five major goals to this study: (1) localize and quantify the hydraulic connections between the two water caves and towards the karst spring; (2) reveal and characterize the supposed hierarchical drainage structure of the aquifer system; (3) delineate subcatchments within the large overall spring catchment area; (4) obtain spatially resolved information on flow velocities and transport parameters in the vadose, epiphreatic and phreatic zones; and (5) estimate the water volume in the conduit network in comparison with results of other studies.

4.2 Field site

The Blautopf ("Blue Pot") spring is located at the southern margin of the Swabian–Franconian Alb, Germany's largest karst area (Fig. 4.1). It drains an area of 165 km^2 and has a mean discharge of 2.3 m^3/s, with variation ranging from 0.3 m^3/s in dry periods up to 32.5 m^3/s during high-flow conditions. The stratigraphy is composed of a series of Upper Jurassic limestone and marl with a total thickness of up to 400 m. The aquifer system consists of an upper and lower karst aquifer, separated and underlain by marl aquitards (Bartenbach et al. 2009; Lauber et al. 2013). The landscape is characterized by numerous dolines and dry valleys. The lowering of the main valley during the Plio-Pleistocene and the subsequent backfilling with gravel have created a deep karst system; that is, the basis of the karst aquifer is below the level of the valley and main spring (Bartenbach and Ufrecht 2009; Ufrecht 2009). Blautopf spring cannot safely be used for drinking-water supply because wastewater and agricultural runoff have adversely affected the water quality of the spring.

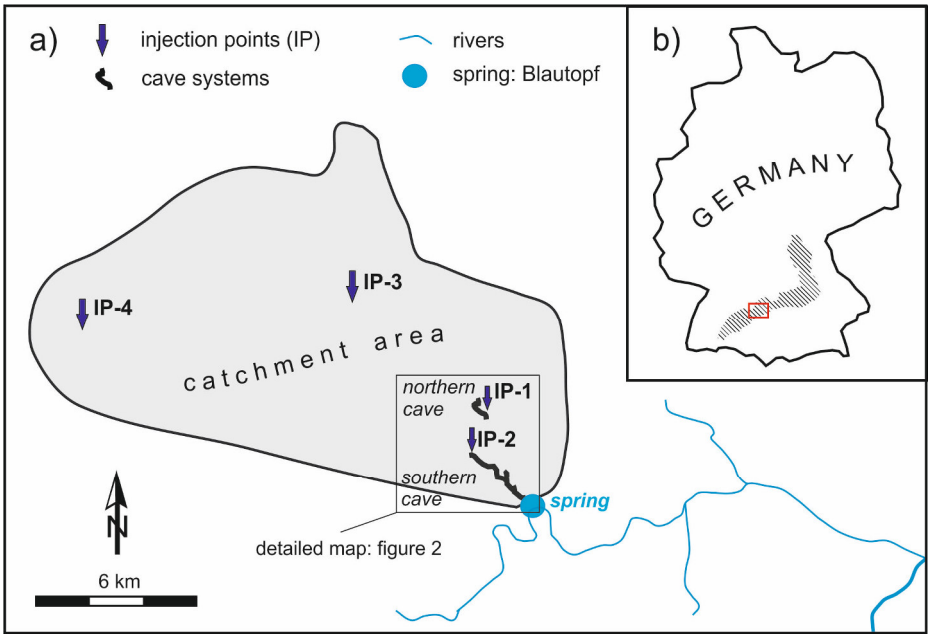

Figure 4.1: (a) Catchment area of the Blautopf spring with location of the Blue Cave system (southern cave), the Hessenhau Cave (northern cave) and the four tracer injection sites (IP-1 to IP-4). (b) Location of the test site (rectangle) within the southern German karst region of the Swabian and Franconian Alb (shaded).

Since 1975, more than 65 tracer tests have been conducted in the catchment area. All injections were done at the land surface, mostly into dolines or stream sinks (Villinger and Ufrecht 1989; Selg and Schwarz 2009). Therefore, the catchment area of the spring is well known (Armbuster

and Selg 2006). However, the internal drainage structure of this aquifer system had previously been unknown due to great difficulties in accessing existing caves. To date, more than 150 caves have been mapped in the area (Arbeitsgemeinschaft Blautopf 2011; Bohnert 2009). The most important one is the Blauhöhlensystem ("Blue Cave system", southern cave in Figs. 1 and 2). Previously, the Blautopf spring was the only entrance to the systems. Cavers had to dive 1200 m in order to access and explore the inner parts of this cave. The Blue Cave system is more than 10 km long and consists of phreatic (fully watersaturated), epiphreatic (open-channel flow) and vadose passages (Fig. 4.2). Another important cave is the 3.5 km long Hessenhauhöhle ("Hessenhau Cave", northern cave). The entrance of the cave is a vertical shaft under a doline passing into a horizontal water cave at a depth of 130 m (Fig. 4.2). This cave was presumed to drain towards the Blue Cave system and Blautopf spring; however, there is no clear evidence for this. Since 2010, a drilled shaft has permitted access to the Blue Cave system without diving, providing an easier way for scientific research to be carried out within the cave systems.

4.3 Methods

4.3.1 Tracer tests

The first two tracer injections into cave streams were done on 21 April 2012: 100 g of uranine was injected into the northern cave at IP-1, and 200 g of sulforhodamine G (sulfoG) was injected into the southern cave at IP-2 (Figs. 4.1 and 4.2). One week later, on 28 April 2012, two injections were done at the land surface, in distal parts of the catchment area. Due to the first two tracers being injected directly into the cave streams, it was possible to use the same two dye tracers again. In the conduit systems, no significant storage possibilities were to be expected under stable flow conditions. Monitoring in the active caves and at the spring demonstrated that tracer concentrations from the first experiment had dropped below the detection limit. Based on this, 1500 g of uranine was injected into a vertical karst shaft at IP-3, about 10 km away from the spring. For decades, this shaft had been used to dispose of overflow water from a sewage treatment plant. At IP-4, 19 km away from the spring (Fig. 4.1), 2000 g of sulfoG was injected into a doline. A minimum of 78 m^3 of water was used at each surface injection site to flush the tracer through the vadose zone.

In order to obtain detailed tracer breakthrough curves, a total of three field fluorimeters (GGUN-FL 43, 334 and 335; Albillia, Switzerland) were installed at sampling points in the cave system (SP-2 and 3) and at the spring (SP-4) (Fig. 2). The fluorimeters were calibrated using water from the cave system; the sampling interval during the tracer tests was 4 min. At SP-1, water samples were collected by cavers; water samples were also collected at other sites in order to check the fluorimeter results. Additionally, charcoal bags were placed at several sites in the cave system and replaced at intervals of two weeks or less. Qualitative results from the charcoal bags were obtained to better resolve the spatial flow pattern, in particular the location of the confluence between the two caves. Water samples and charcoal bags were analyzed in the KIT laboratory using a spectrofluorimeter (LS 55, Perkin Elmer).

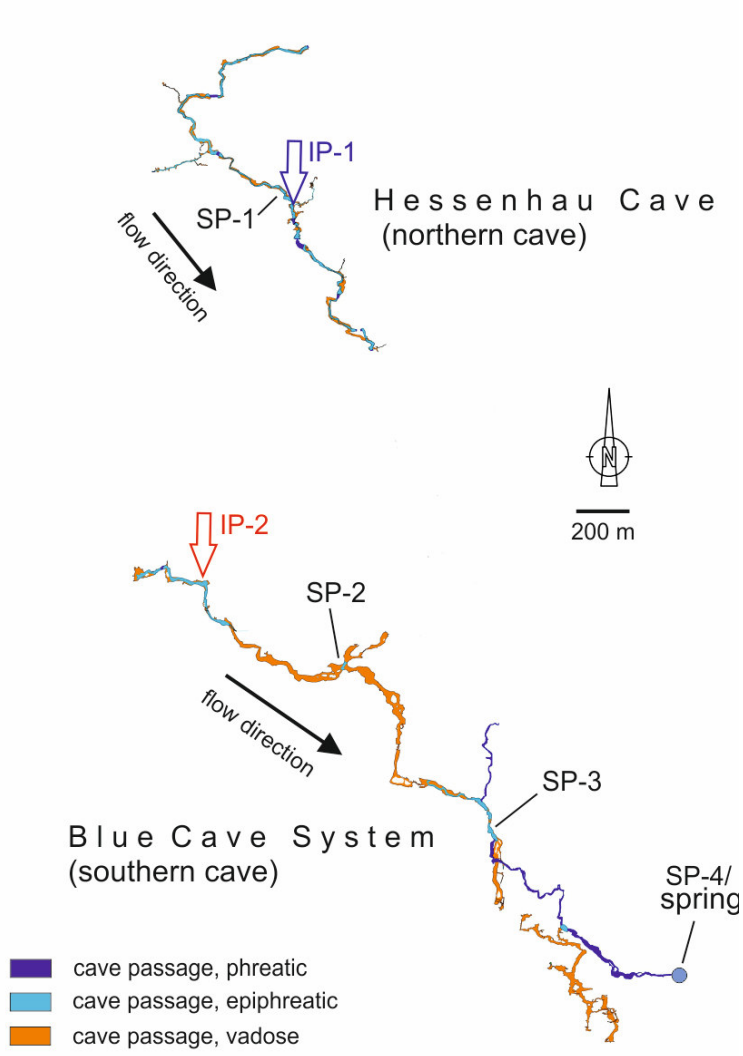

Figure 4.2: Map of the two caves with indication of phreatic, epiphreatic and vadose cave passages, injection points IP-1 and IP-2 in the cave streams, and sampling points (SP-1 to SP-4).

Discharge measurements were conducted in the two cave systems at SP-1 and SP-2 one week before the tracer tests using the salt-dilution method. The data make it possible to relate cave stream flow and spring discharge. Continuous discharge data from the spring were obtained from the regional authority for water balance calculations and for estimation of the total recovery and water volumes in the cave system.

4.3.2 Evaluation and modeling of the results

Flow velocities and dispersion/dispersivity were calculated with and without considering tortuosity ($\tau = x_\tau/x$). While the surveyed length (x_τ) of the phreatic cave passage between SP-3 and the spring is 1200 m, the linear distance (x) is only 700 m (Fig. 4.2). Thus, a tortuosity of 1.7 can be defined for this karst system. For the sake of simplicity, all velocities and dispersions mentioned in the text do not consider tortuosity. The complete results (with and without tortuosity) are provided in Table 4.1.

All breakthrough curves (BTCs) were analytically modeled with a conventional advection–dispersion model (ADM) and a two-region non-equilibrium (2RNE) model using the software CXTFIT (Toride et al. 1999). The models calculate one-dimensional flow in karst conduits, which is predominantly characterized by advection, i.e., flow velocity (v), and mechanical dispersion (D) in the direction of flow. The general advection–dispersion equation (Eq. 4.1) is solved analytically by assuming homogeneous profiles, a uniform and unidirectional flow field that is constant in time and space, and constant flow parameters (van Genuchten et al. 2012). An inverse modeling tool of the ADM provides best estimates of the two flow parameters (v, D) by fitting a modeled BTC to observed values.

$$\frac{\delta c}{\delta t} = D\frac{\delta^2 c}{\delta x^2} - v\frac{\delta c}{\delta x} \qquad (4.1)$$

The 2RNE model further accounts for exchange between mobile and immobile fluid regions in the karst system (Field and Pinsky 2000). Therefore, the advection–dispersion equation is extended by two parameters, a partitioning coefficient β between mobile and immobile fluid regions and a mass transfer coefficient ω between the two regions. Thus, a total of four parameters (v, D, β, ω) need to be fitted simultaneously, resulting in less robust (i.e., more ambiguous) estimates (van Genuchten et al. 2012). Due to the nearly symmetric shapes of the breakthrough curves and the short tailing, most of the BTCs were fitted well by both models. Therefore, the

ADM was used to obtain more robust values; the results are listed in Table 4.1 and used for discussion.

Based on the modeling, mean flow velocities and dispersion coefficients were determined between the four injection sites and the four sampling sites. In order to quantify flow velocities between individual sampling points (e.g., the section between SP-2 and SP-3 or between SP-3 and SP-4), peak transit times were used. Effects of the vadose zone were estimated by comparing parameters from surface and cave injections. Additional flow parameters for epiphreatic and phreatic zones (i.e., the partitioning coefficient and the mass transfer coefficient) were determined with the 2RNE model for selected BTCs of cave injections. Water volumes (V) of the karst conduit system were estimated by multiplying the mean discharge (Q_{mean}) and the mean transit time of the tracer (t_{mean}) (Field and Nash 1997).

4.4 Results and discussion

4.4.1 Results of the tracer injections in cave streams

All observed BTCs resulting from the two injections in cave streams (IP-1 and IP-2) show a single and nearly symmetric peak and a short tailing (Fig. 4.3). Uranine (IP-1) was detected at SP-3 and at the spring (SP-4). The first detection occurred 26 h after injection. The maximum concentration of 1.9 µg/L was reached after 32 h. At SP-4, uranine was first detected after 41 h, and the maximum of 1.1 µg/L occurred after 49 h. Spring discharge was about 1.24 m^3/s. Despite direct injection into the cave stream, total tracer recovery only reached 52% (Table 4.1). Mean flow velocities of 74 m/h and a dispersion of 734 m^2/h were calculated between IP-1 and SP-3 (without considering tortuosity). Between IP-1 and SP-4, mean flow velocities were lower, 64 m/h, with dispersion of 784 m^2/h. The flow velocities in the phreatic sections between SP-3 and SP-4 are based on peak transit times and are about 41 m/h. Uranine was not detected in the more distant and upstream part of the southern cave at SP-2.

SulfoG (IP-2) was detected at all three sampling points – SP-2, SP-3 and SP-4 – tracing the flow path through the southern cave. The first arrival at SP-2 occurred 1 h after injection; the maximum of 50 µg/L was reached after 2.3 h (Fig. 4.3). At SP-3, first detection was after 12 h, and a maximum concentration of 6 µg/L was measured after 16 h. SulfoG arrived after 26 h at the spring, where the maximum of 4.0 µg/L occurred after 29 h. During breakthrough, spring

discharge was 1.32 m^3/s, and 79% of the tracer was recovered (Table 4.1). Highest mean flow velocities, 275 m/h, were calculated for the epiphreatic section between IP-2 and SP-2, with dispersion of 4920 m^2/h. Significantly lower values for mean flow velocity (112 m/h) and dispersion (1160 m/h) were found between IP-2 and SP-3. Coefficients of determination (R^2) from modeled BTCs in the cave system are greater than 0.931, showing good curve fitting. The lowest flow velocities, 47 m/h, were measured in the phreatic section between SP-3 and the spring and are based on peak transit times. After 75 h, concentrations at the spring had decreased below detection limits (Fig. 4.3).

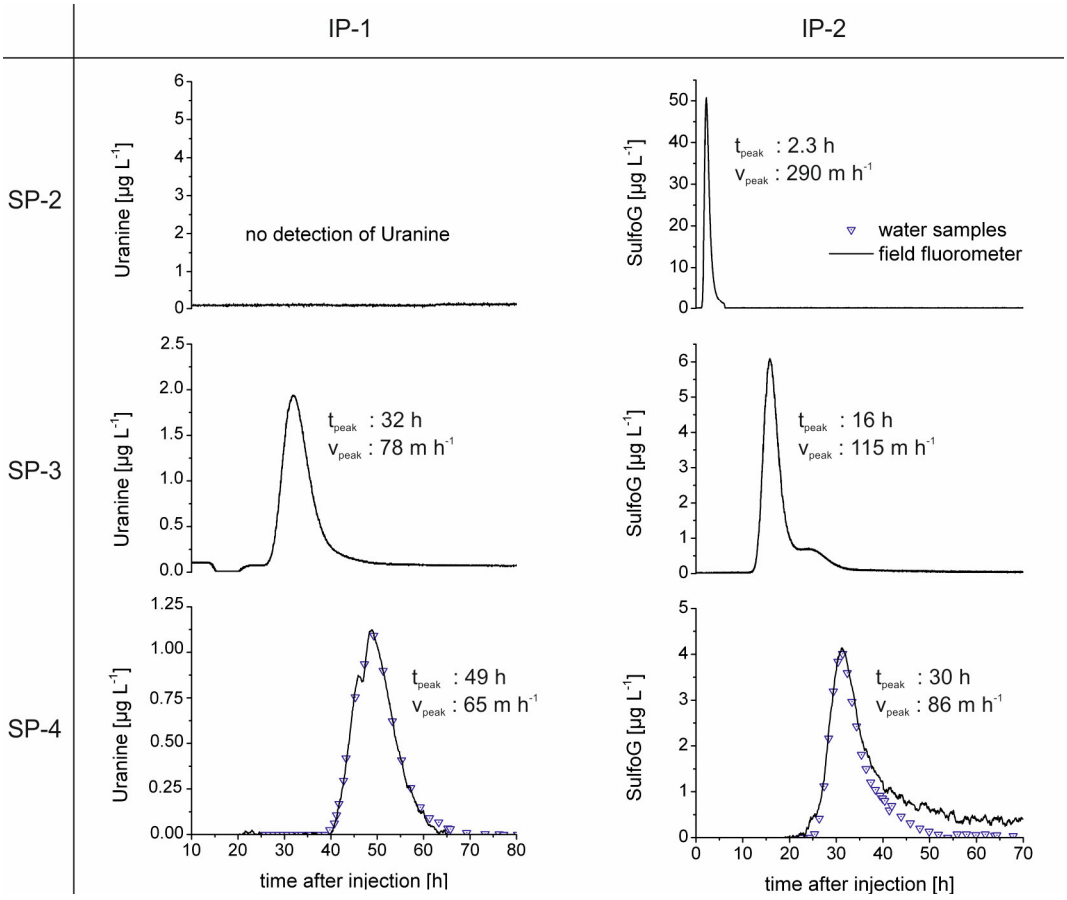

Figure 4.3: Breakthrough curves resulting from in-cave dye-tracer injection at IP-1 (uranine) and IP-2 (sulfoG) obtained at sampling points in the cave (SP-2, SP-3) and at the spring (SP-4).

4.4.2 Results of the tracer injections at the land surface

Uranine (IP-3) was detected at SP-1, SP-3 and the spring (SP-4) (Fig. 4.4). Due to poor accessibility to the northern cave, sampling at SP-1 was only temporarily feasible; as a result the

BTC is incomplete. Uranine was first detected at SP-1 after 98 h. The first arrival at SP-3 occurred after 136 h, and the maximum of 11.5 µg/L was reached after 155 h. At SP-4, first detection was after 153 h and a maximum concentration of 10.3 µg/L was measured after 177 h. Despite the injection via the unsaturated zone (into a karst shaft), the BTCs display a single peak and nearly symmetric shapes. During breakthrough, spring discharge was about 1.04 m^3/s, and a recovery of 63% was calculated (Table 4.1). Maximum flow velocity between IP-3 and SP-1 is 69 m/h. Mean flow velocity from IP-3 to SP-3 was calculated at 56 m/h, dispersion being 794 m^2/h. The ADM provides good curve fitting, with R^2 values greater than 0.973. Approaching the spring, flow velocities between SP-3 and SP-4 decline to 27 m/h and are based on peak transit times.

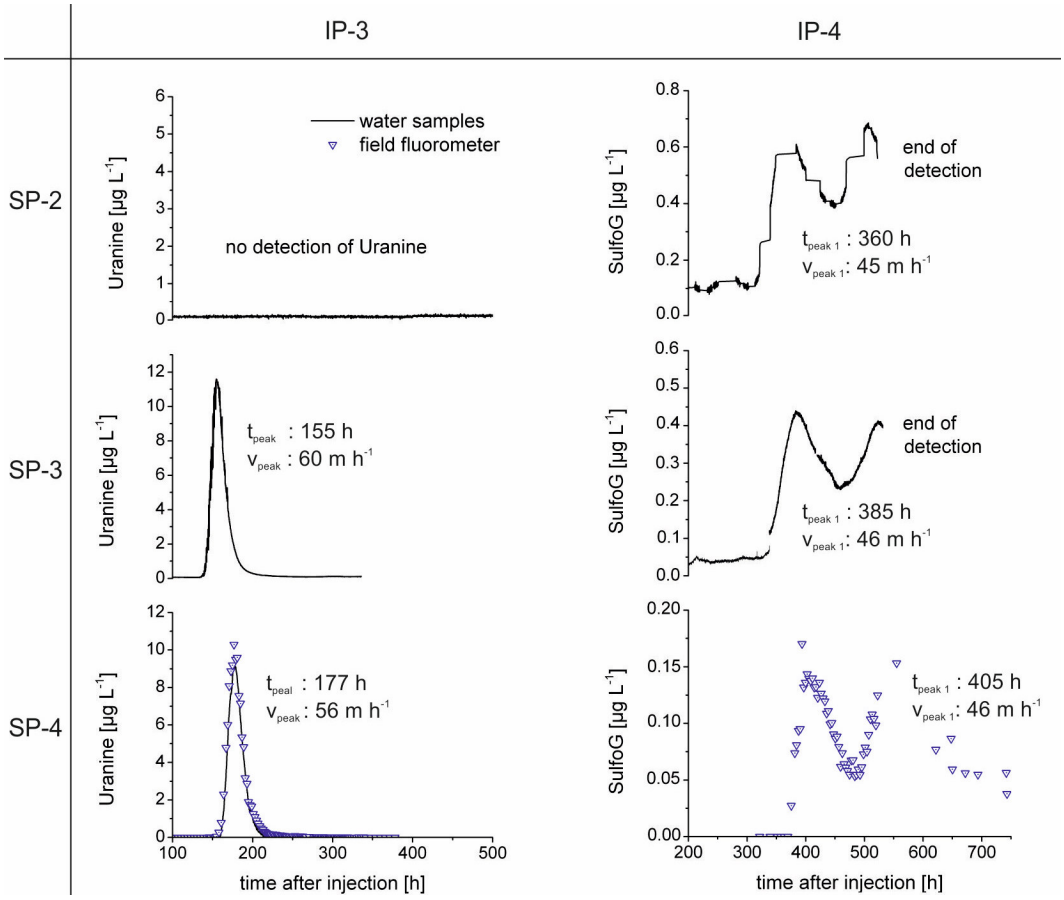

Figure 4.4: Breakthrough curves resulting from injections at the land surface, at IP-3 (uranine) and IP-4 (sulfoG), observed at sampling points in the cave (SP-2, SP-3) and at the spring (SP-4).

Table 4.1: Results of the tracer test.

Injection / Sampling	Injection Points / Tracer / Type of Injection Point		IP-1 Uranine Cave stream	IP-2 SulfoG Cave stream	IP-3 Uranine Karst shaft	IP-4 SulfoG Doline
Sampling Points	Parameter	Unit				
SP-1	Time of first detection [a]	[h]	= injection point	no detection	98.1	no detection
	Maximum velocity [a]	[m/h]			69 / 118	
SP-2	Time of first detection	[h]	no detection	1.2	no detecion	320
	Peak time	[h]		2.3		360
	Maximum concentration	[µg/L]		50		0.6
	Maximum velocity	[m/h]		578 / 983		51 / 87
	Peak velocity	[m/h]		290 / 493		45 / 77
	Mean flow velocity	[m/h]		275 / 468		-
	Dispersion	[m^2/h]		4920 / 14200		-
	Dispersivity	[m]		18 / 30		-
SP-3	Time of first detection	[h]	26.0	12.0	136	335
	Peak time	[h]	31.8	15.9	155	385
	Maximum concentration	[µg/L]	1.9	6.0	11.5	0.5
	Maximum velocity	[m/h]	96 / 163	152 / 258	68 / 115	54 / 91
	Peak velocity	[m/h]	78 / 132	115 / 195	60 / 102	46 / 79
	Mean flow velocity	[m/h]	74 / 130	112 / 191	56 / 100	45 / 74[b]
	Dispersion	[m^2/h]	734 / 2350	1160 / 3360	794 / 2290	6230/16700[b]
	Dispersivity	[m]	10 / 18	10 / 17	14 / 23	138 / 225[b]
SP-4	Time of first detection	[h]	41.0	25.6	153	357
	Peak time	[h]	48.8	29.2	177	405
	Maximum concentration	[µg/L]	1.1	4.0	10.3	0.14
	distance to spring	[km]	3.2 / 5.4	2.5 / 4.3	10 / 17	19 / 32
	Maximum velocity	[m/h]	78 / 132	98 / 167	65 / 111	53 / 91
	Peak velocity	[m/h]	65 / 111	86 / 147	56 / 96	46 / 80
	Spring discharge	[m^3/s]	1.24	1.32	1.04	0.97
	Recovery	[%]	52	79	63	5
	Mean flow velocity	[m/h]	64 / 110	74 / 133	56 / 95	45 / 76[b]
	Dispersion	[m^2/h]	784 / 2270	1120 / 3300	727 / 2100	3260 / 9240[b]
	Dispersivity	[m]	12 / 20	15 / 25	12 / 22	74 / 121[b]
	partitioning coefficient β	[-]	0.96	0.89	0.97	0.91[b]
	Mass transfer coefficient ω	[-]	0.57	0.82	0.39	1.37[b]

Note: mean flow velocity and dispersion are calculated by using ADM of the software CXTFIT (Toride et al. 1999). Coefficients of determination are greater than 0.931, except for IP-4 ($R^2 > 0.8$). Values are determined without / with respect to tortuosity. Partitioning coefficients and mass transfer coefficients are calculated by using 2RNE model of CXTFIT.
[a]: incomplete BTC
[b]: parameters are only calculated for the first peak

SulfoG from IP-4 was only detected in the southern cave. All BTCs at SP-2, SP-3 and the spring (SP-4) display two peaks with maximum concentrations between 0.1 and 0.7 µg/L (Fig. 4.4). First detection at SP-4 was 357 h after injection, and the first tracer maximum occurred after 405 h with 0.14 µg/L. Mean spring discharge was 0.97 m^3/s, and only 5% of this tracer was recovered. The results indicate that sorption processes in the vadose zone and remobilization after a rain event caused the second peak. The rainfall event caused spring discharge to increase to 1.25 m^3/s after peak 1, resulting in additional dilution of tracer. Mean flow velocity for the first peak is 45 m/h. The existence of two separate flow paths can be largely ruled out because a previous tracer test at the same injection site in 1986 exhibited a BTC with a single peak. Spring discharge at this time had been about 3.20 m^3/s with recovery of about 90% (Villinger and Ufrecht 1989). Therefore, only the first peak of the BTC of the current test injection is modeled with CXTFIT, resulting in lower values of R^2 (>0.8).

4.4.3 Structure of the drainage network

Uranine BTCs from injections IP-1 and IP-3 monitored at SP-3 demonstrate that there is a connection between the two caves (Figs. 4.2, 4.3 and 4.4). Uranine was also detected at the spring (SP-4), but not in upstream parts of the southern cave (SP-2). The high similarity and the single-peaked shapes of the BTCs observed at SP-3 and SP-4 suggest that there is only one major flow path connecting the two caves. Based on tracer detection by means of the charcoal bags placed around SP-3, it was possible to precisely identify the location of the connecting conduit; this is valuable information for the further exploration of the cave (Fig. 4.5b).

There appear to be two main branches of drainage towards the spring – the two known caves (Figs. 4.2 and 4.5). This is confirmed by discharge measurements conducted in both cave systems. In the northern cave, a channel flow of 0.77 m^3/s was determined, while a flow of about 0.69 m^3/s was measured at SP-2 in the southern cave. At that time, discharge at the spring was 1.30 m^3/s, meaning that each cave stream contributes approximately 50% of the total flow to the spring (Lauber et al. 2013).

Based on continuous tracer monitoring in the caves, it was possible to subdivide the catchment area of the Blautopf karst spring into two subcatchments contributing to the two active water caves (Fig. 4.5b). The northeastern part of the area drains via the northern cave into the spring, while the southwestern subcatchment is connected to the southern cave (IP-2). At a distance of

700 m upgradient of the spring, the two cave streams merge just ahead of SP-3 and form a single, large phreatic cave passage towards the main outlet. It has been demonstrated by numerical modeling that solutionally enlarged pathways will form such dendritic drainage structures in karst aquifers, as increasing flow and dissolution are self-enhancing processes (Gabrovsek et al. 2004; Worthington and Ford 2009; Dreybrodt et al. 2010). Although numerous flow paths exist in the epikarst and vadose zone due to discrete and diffuse infiltration, only a few preferential flow paths prevail with increasing flow distance (Fig. 4.5a). The rapid enlargement of such initial conduits results in reorientation of flow field towards these conduits and thus the formation of tributaries in the epiphreatic and phreatic zones. Similar drainage structures have been proven by using tracer tests in the catchment area of Milandre Cave (Perrin et al. 2007) and the Mammoth Cave system (Meiman et al. 2001).

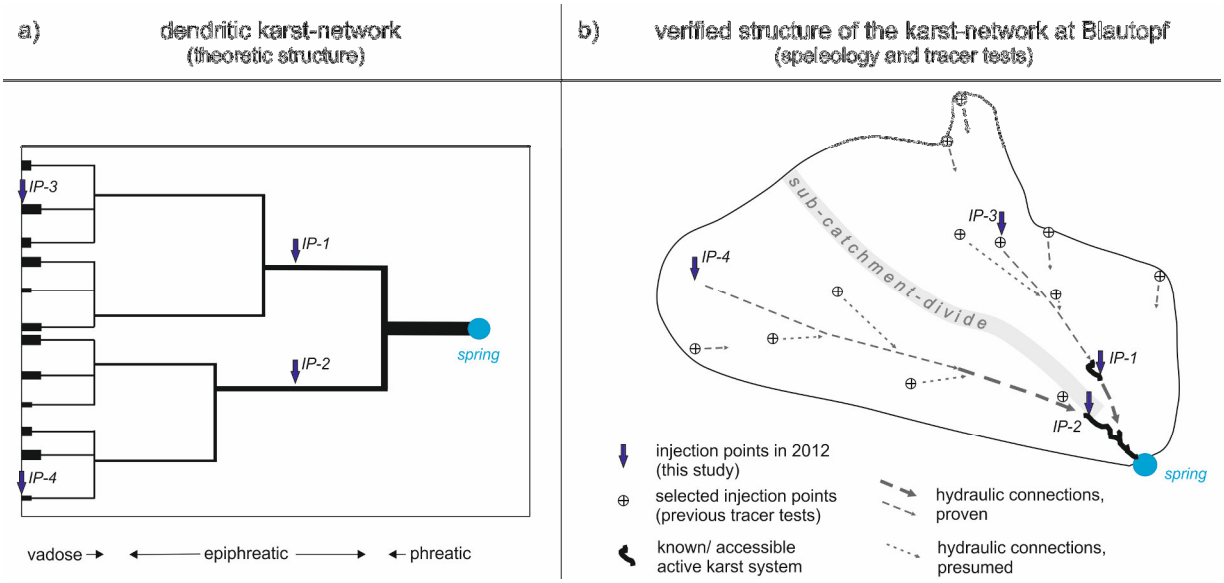

Figure 4.5: (a) Theoretic structure of a hierarchical karst network with a schematic sketch of injection points. (b) Verified structure of the Blautopf spring catchment area that consists of two subcatchments, one draining towards the northern cave and the other towards the southern cave (modified from Lauber et al. 2013). The caves converge about 700 m linear distance upstream of the spring.

4.4.4 Flow velocities and flow parameters in the karst system

Although conventional tracer tests with injections at the surface and monitoring at the spring represent mixed information from the entire flow path, the tracer tests presented in this study made it possible to differentiate flow in vadose, epiphreatic and phreatic cave sections. In the two cave systems, clear relations between flow types, hydraulic gradients and flow velocities

have been found. The highest (mean) flow velocities of 275 m/h were found in the epiphreatic passage between IP-2 and SP-2. Considering a tortuosity of 1.7, maximum mean flow velocities may reach 468 m/h. The hydraulic gradient is highest in this section at about 40‰ (Fig. 4.6). Flow velocities decrease as they approach the main outlet due to the decreasing hydraulic gradient. Above SP-3, flow velocities decrease down to 84 m/h at a gradient of 2‰. The different hydraulic gradients can be attributed to different stages of cave development. The lowest flow velocities of 27 to 47 m/h were found in the phreatic cave passage between SP-3 and the spring, where the conduits are mostly below the level of the spring and thus fully saturated. Approaching the spring, the hydraulically effective cross-sectional area (A) of the phreatic conduit becomes very large, resulting in a decrease of flow velocities (v) according to the condition of flow continuity ($Q=vA$). Additionally, large phreatic conduits produce a high hydraulic conductivity and therefore a very low hydraulic gradient. This leads to impoundment in the phreatic zone and the formation of underground lakes in the upgradient epiphreatic cave passages. As observed at the phreatic cave passage, flow velocities also varied with flow conditions during all four tracer tests. Discharge fluctuated between 0.97 and 1.32 m^3/s, while flow velocities varied between 27 m/h (during lower flow conditions) and 47 m/h (during higher flow conditions).

Spatially, dispersion coefficients vary with flow velocities. The highest value for dispersion, 4920 m^2/h, was calculated for remote parts of the cave system (Fig. 4.6), and can be attributed to the joint effect of rapids and pools in the cave section between IP-2 and SP-2. Similar effects have been observed by Hauns et al. (2001). However, close to the spring, low hydraulic gradients and low flow velocities result in a lower dispersion of about 734 to 1160 m^2/h for in-cave injections (IP-1, IP-2). A decrease in dispersion and flow velocities in proximity to a spring was also observed in a cave system in Slovenia (Gabrovsek et al. 2010).

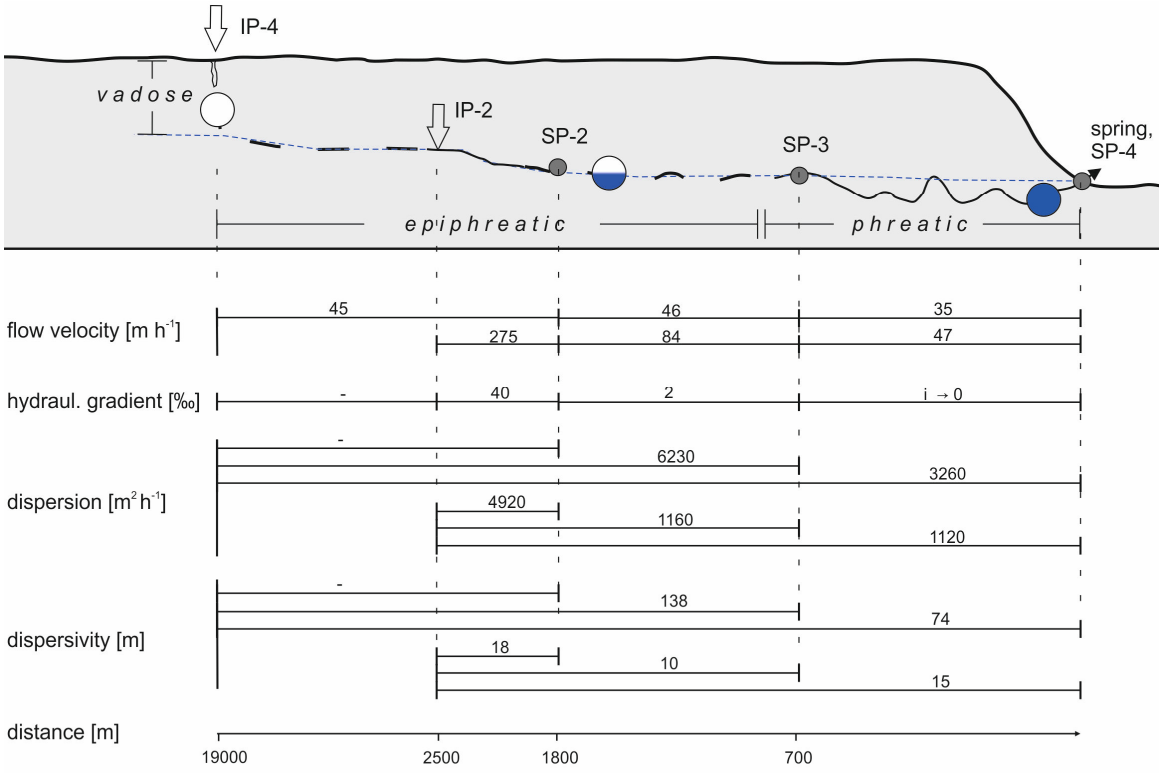

Figure 4.6: Schematic sketch of injection (IP) and sampling points (SP) of the two tracer tests in the southern drainage system (Blue Cave system) and information about vadose, epiphreatic and phreatic cave passages. Below, determined flow and transport parameters are given: flow velocities and hydraulic gradients are calculated for individual cave sections, whereas dispersion and dispersivity values are valid only for sections between IPs and SPs.

The tracer injection at the land surface, at IP-3 (characterized by open shafts), revealed the very low water retention capacity of the vadose zone. Maximum flow velocities of 69 m/h were determined for the vadose and epiphreatic zone between IP-3 and SP-1, whereas only slightly higher flow velocities of 68 to 96 m/h were found for the downgradient cave passage between SP-1 and SP-3 (IP-1, IP-3; Table 4.1, Fig. 4.7). The BTCs of injections IP-1 and IP-3 both exhibit a symmetric peak and a short tailing; that is to say, no essential differences between cave and surface injections have been observed. However, the two injections only deliver information on the active conduit system, where flow velocities are highest. Higher water retention and lower velocities can be expected in the less karstified parts of the vadose zone. Furthermore, the seemingly minor influence of the vadose zone may be attributed to scale effects: observed values of surface injections refer to a large distance and deliver mixed information from the vadose and epiphreatic zones (Fig. 4.7). The thickness of the vadose zone is about 100 m and therefore insignificant in respect to the whole flow path of at least 10 000 m. Results

from IP-3 further exhibit a low dispersion coefficient of 727 m^2/h, which is similar to in-cave values (IP-1, Fig. 4.7). However, geologic profiles show that the karst water lies within the lower karst aquifer and flow paths must cross the marly formation twice in order to drain into the spring (Lauber et al. 2013). Despite this, dispersion does not increase significantly, indicating a high permeability along the flow path.

Concerning the results at IP-4, the generally lower flow velocities can be reduced to low-flow conditions during the tracer test (Fig. 4.6). However, maximum flow velocities are 53 m/h, demonstrating that potential contamination would still reach the spring within a short period of time, even under low discharge from the karst system. In contrast to IP-3, dispersion coefficients from injection IP-4 produce significantly higher values of 3260 to 16 700 m^2/h, likely due to long flow distances and a lower permeability of the vadose zone. These results come from analysis of just the first peak and therefore may have uncertainties.

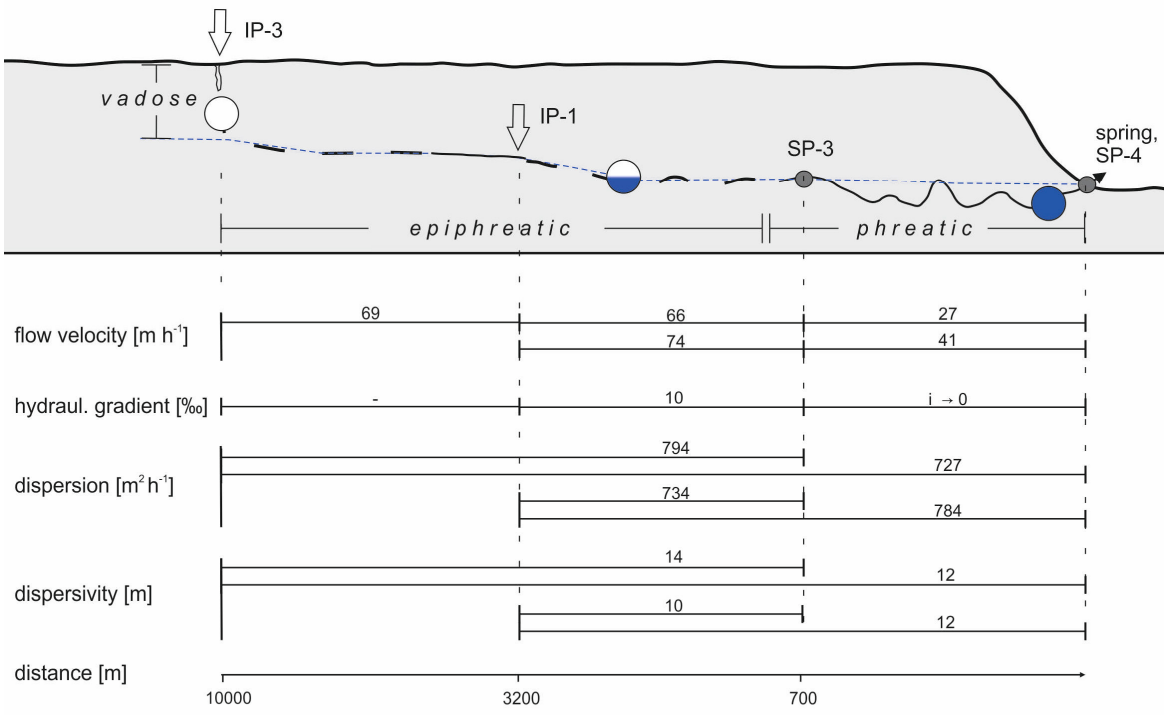

Figure 4.7: Schematic sketch of the two tracer tests in the northern drainage system (Hessenhau Cave), including injection (IP) and sampling points (SP), and information about vadose, epiphreatic and phreatic cave passages. Below, determined flow and transport parameters are given: flow velocities and hydraulic gradients are calculated for individual cave sections, whereas dispersion and dispersivity values are valid only for sections between IPs and SPs.

To eliminate the influence of flow velocity, the dispersivity ($\alpha = D/v$) was calculated for all measuring points. Most values lie within the range of 10 to 18 m (IP-1 to IP-3). There is apparently no significant increase with flow distance within the active cave system. In contrast, the reverse was observed for IP-2: dispersivity decreases with increasing flow distance (Fig. 4.6). This may be due to flow in larger channels with fewer turbulences and heterogeneity. Similar effects have been observed by Gabrovsek et al. (2010) in a cave system in Slovenia. However, Hauns et al. (2001) found a strong correlation between dispersivity and flow distance in a cave system in Switzerland. An increase of dispersivity has also been observed by numerous prior surface tracer tests in the catchment area of Blautopf: Villinger and Ufrecht (1989) found dispersivity values from 12.4 to 38.1 m for distances between 3.7 and 19.0 km, largely in agreement with the values obtained for the two cave streams during the present study.

Results with the 2RNE model of CXTFIT show a high percentage of karst water flowing in the mobile fluid region (89 to 97%). This was calculated for cave and surface injections (IP-1 to IP-3), showing highly karstified and permeable flow paths. The mean value of mass transfer coefficient from in-cave injections is 0.62, demonstrating low mass transfer between the immobile and mobile regions in the epiphreatic and phreatic zones. The higher mean value from surface injections (about 1.2) indicates a higher mass transfer, most likely in the vadose zone.

Large portions of the catchment are dominated by diffuse infiltration. By using water balances, spring hydrograph analyses and natural tracers, previous studies have estimated that the water volume in the fractured rock matrix accounts for 90 to 95% of the total karst water volume, which was estimated at 27 Mm^3. The mean residence time was calculated to be <15 yr (Geyer et al. 2011; Bauer and Selg 2006; Schwarz et al. 2009; Selg and Schwarz 2009). During the tracer tests of this study, water volumes of 0.68 and 1.42 Mm^3 were calculated for the conduits system of each subcatchment area (IP-3 and IP-4, respectively) including the water in the phreatic conduit between the confluence of the subcatchment streams and the spring (Fig. 4.8). The water volume in the phreatic conduit upstream of the spring is about 0.08 Mm^3 and may be taken into consideration only once when calculating the total water in conduits. Thus, the total water volume in conduits is about 2.0 Mm^3 during low-flow conditions (1 m^3/s), and corresponds to a fraction of about 7% of the total karst water of 27 Mm^3. In conclusion, water balances, spring hydrograph analyses and tracer tests deliver comparable estimates for conduit water volumes.

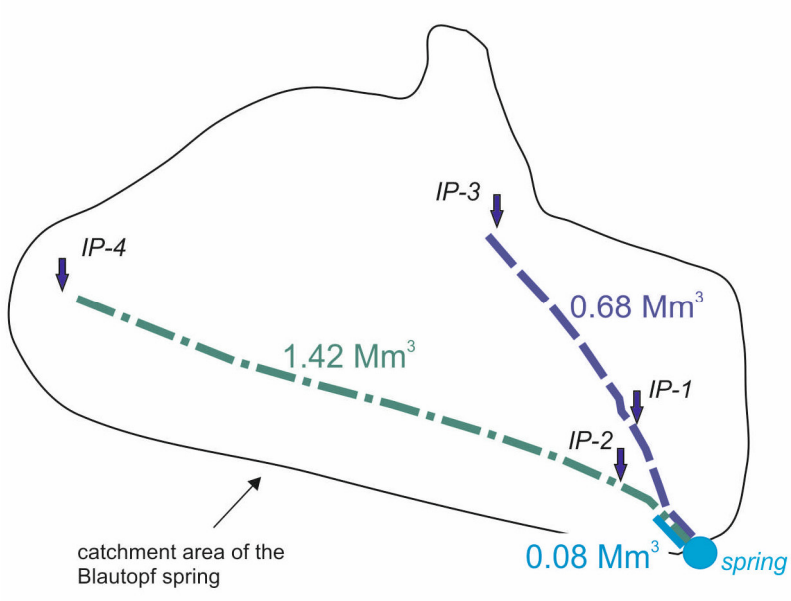

Figure 4.8. Conduit water volumes estimated for each drainage system and the phreatic cave passage on the basis of the tracer test results. The total conduit volume is about 2.0 Mm^3.

4.5 Conclusions

The results of the in-cave dye tracing and monitoring provide detailed knowledge of internal drainage structures and hydraulic properties. It was possible to demonstrate that there is only one hydraulically relevant connection between the two caves, with the confluence located about 700 m (linear distance) upstream of the spring. By combining land surface injections with in-cave monitoring, the dendritic drainage structure of the karst system was able to be characterized for the first time. Within the whole catchment area of the spring, two subcatchment areas were identified, each drained by an active karst conduit contributing about 50% of the discharge from the spring. At a linear distance of approximately 700 m upgradient of the spring, the two conduits converge and form one large phreatic cave passage. In the majority of cases, such unique insights into the drainage structure of karst aquifers are only enabled by in-cave tracer tests. The delineation of subcatchment areas can deliver valuable information regarding prediction of the spread of contaminant plumes in case of accidental release.

For the first time, detailed information on flow velocities and transport parameters were achieved for individual cave passages. Flow velocities vary strongly within the cave systems; highest flow velocities are produced by high hydraulic gradient and are found in epiphreatic

cave passages. Significantly lower flow velocities were determined for the phreatic cave passage with a very low hydraulic gradient and large conduit cross section. This leads to impoundment of water in these parts of the cave system. Due to the heterogeneous distribution of flow velocities, dispersion varies in the cave systems. The highest dispersion was found for epiphreatic conduits with high flow velocity in remote parts of the cave system, whereas low dispersion generally exists in conduits with low flow velocities close to the spring. Dispersivity displays relatively constant values and does not significantly increase with increasing flow path, reflecting strong karstification. In proximity to the spring, large conduits with less turbulence and heterogeneity influence the flow parameters. Although tracer tests in active karst systems are laborious, the benefits are worth the effort since unique information on groundwater flow and flow parameters is obtained.

The volume of the conduit system was estimated and correlated with values from water balances and spring hydrograph analysis. During low-flow conditions, the fraction of conduit water is about 7% of the total karst water. Local rural and agricultural land use affects water quality of the Blautopf. However, tracer tests available to the public have already helped to sharpen awareness of the vulnerability of water resources in the region. The obtained parameters and spatially resolved information allows for a better understanding of the structure of the karst system and may help to protect and preserve karst water resources.

Acknowledgments

We thank all cavers of the caving associations Arge Blautopf and Arge Blaukarst for their excellent cooperation, provision of cave maps and support during the tracer tests, especially Andreas Kücha and Jürgen Bohnert. Financial support was given by the Stuttgarter Hofbräu Environmental Foundation. We acknowledge support by the Deutsche Forschungsgemeinschaft and Open Access Publishing Fund of the Karlsruhe Institute of Technology. We thank Malcolm Field and an anonymous reviewer for valuable review comments and Tim Bechtel for proofreading the manuscript.

Chapter 5

Use of artificial and natural tracers to assess groundwater transit-time distribution and flow systems in a high-alpine karst system (Wetterstein Mountains, Germany)

Reproduced from Lauber, U., Goldscheider, N.: Use of artificial and natural tracers to assess groundwater transit-time distribution and flow systems in a high-alpine karst system (Wetterstein Mountains, Germany). – Hydrogeology Journal, 22, 1807–1824, doi:10.1007/s10040-014-1173-6.

Abstract

Groundwater in mountainous karst regions is vital for regional water budgets and freshwater supply. Owing to increasing water demand and climate change, detailed knowledge of the highly heterogeneous alpine aquifer systems is required. Multi-tracer analyses have been conducted in the steep karstic Wetterstein Mountains, which includes Germany's highest summit, Zugspitze (2,962 m asl). Results of artificial tracer tests demonstrate well-developed flow paths through the unsaturated zone (up to 1,000 m thickness). Flow paths cross topographic divides and contribute to deep drainage systems underneath alpine valleys. Cross-formational flow has been identified. Quantitative analysis of tailing-dominated breakthrough curves and stable isotopes (^{18}O) has enabled determination of the mean transit-time distribution. A fast-flow component with transit times between 3 and 13 days was found in karst conduits and open fissures, dependent on flow conditions. An intermediate-flow component, showing mean transit times of about 2.9 to 4.9 months, was found in well-drained fissures and fractures. A slow-flow component with mean transit times greater than one year is attributable to slow flow and low storage

in the poorly drained fissures and rock matrix. The conceptual model enables a better understanding of drainage, water resources and vulnerability of the high-alpine karst system.

5.1 Introduction

Alpine regions are characterized by high precipitation leading to substantial surface runoff and/or groundwater recharge. Alpine areas form headwaters for regional river systems, such as the Danube and the Rhine, and other large regions benefit from the abundance of water (Viviroli and Weingartner 2004). In the Alps, there are some well-known examples where alpine water resources are used to supply major cities with drinking water, e.g. Vienna and Innsbruck in Austria, and Grenoble in France. However, in most alpine aquifer systems, recharge processes, drainage systems and potentially available water resources are still insufficiently known (Goldscheider 2011). Amongst others, the main challenges are strong heterogeneity and variability: recharge processes highly depend on temporal and spatial distribution of snowmelt and precipitation, drainage follows heterogeneous geologic structures and groundwater volumes are difficult to quantify as groundwater levels and hydraulic rock properties (e.g. porosity, aperture width of fissures, fracture network and karstification) are often not known. In addition, conventional hydrogeological investigation techniques are often difficult to use in alpine regions.

However, climate change and population growth has contributed to an increasing awareness of alpine hydrogeology in the past decade. Future changes in local precipitation, snow cover patterns and glacier storage are likely to affect runoff in alpine headwaters (Bates et al. 2008). Population growth results in increasing demand for drinking water supply, irrigation of agricultural areas and industrial water. As alpine (karst) water resources are likely to become even more important in the future, an increasing number of studies focus on this topic. Interdisciplinary approaches include meteorological research combined with snow and catchment hydrology to characterize the dynamic water resources in mountainous karst regions (Kraller et al. 2012; Marke et al. 2013). Hydrogeological mapping and hydrogeochemical techniques are applied to evaluate the water quality of the available resources (Simsek et al. 2008). Other studies use assessment methods to characterize karst morphology and groundwater vulnerability, considering epikarst, vegetation, infiltration and the karstic network to have a major influence on transit time (Perrin et al. 2004; Plan et al. 2009). Spring hydrograph analysis and hydrochemical methods allow for characterization of infiltration processes of the saturated and unsaturated

zone (Mudarra and Andreo 2011) and enable determination of drainage structures, transit times and recharge processes of alpine karst aquifers (Wetzel 2004; Ozyurt and Bayari 2008; Mudarra et al. 2014). Mean transit times and transit-time distribution have been demonstrated to be an important aspect for understanding dynamic groundwater storage, variable water quality and vulnerability to contamination (Bakalowicz 2005; Worthington 2007; Mueller et al. 2013).

Tracer methods are particularly suitable to assess transit times and flow properties in alpine aquifers, partly because the necessary equipment is manageable. In recent studies, artificial tracer tests were applied in high-alpine karst systems to resolve the influence of heterogeneous geologic structures on karst drainage and recharge processes (Goldscheider 2005; Gremaud et al. 2009; Goldscheider and Neukum 2010; Finger et al. 2012; Kübeck et al. 2013; Mudarra et al. 2014). Tracer tests, conducted under variable flow conditions, have revealed variability of transit times by a factor of 5 or more (Göppert and Goldscheider 2008; Gremaud et al. 2009). As artificial tracers are generally injected into preferential flow paths, flow properties of the conduit system are investigated that result in short transit times and high flow velocities. However, these tracers omit the fissured-porous matrix of the aquifer, which plays an important role with respect to water storage and karst water volumes (Maloszewski et al. 2002; Worthington 2007). To investigate the matrix of karst systems, the use of stable isotopes as natural tracers has been established over the past few decades (Dewalle et al. 1997). Analyses of stable isotopes in spring water allow for estimating transit times of the water, identifying sources and mixing of water, and calculating water volumes in the alpine aquifer (Rodgers et al. 2005; Einsiedl 2005). In contrast to artificial tracer tests, where only preferential flow paths are considered, stable isotope analyses offer the possibility to observe long-term properties of aquifer systems. For these reasons, the combination of artificial and natural tracer tests is particularly favorable to elucidate transit-time distribution in the aquifer.

Facing climate change and increasing water demand, the objective of this study is to develop a conceptual model of a high-alpine karst aquifer in Germany, in the Wetterstein Mountains. The area is part of the headwater of the Loisach River providing runoff for the city of Munich and the surrounding countryside. Special characteristics of this area are steep topographic gradients, a karst aquifer of up to 1,000 m thickness and an unsaturated zone that is almost as thick as the whole aquifer. By combining artificial and natural tracer techniques, this study offers insights into transit-time distribution and flow systems in the karst conduit network and in the fissured-

porous rock matrix of the alpine karst aquifer. The research allows a first assessment of drainage systems and karst water volume, which is needed to manage and to protect the water resources for further generations.

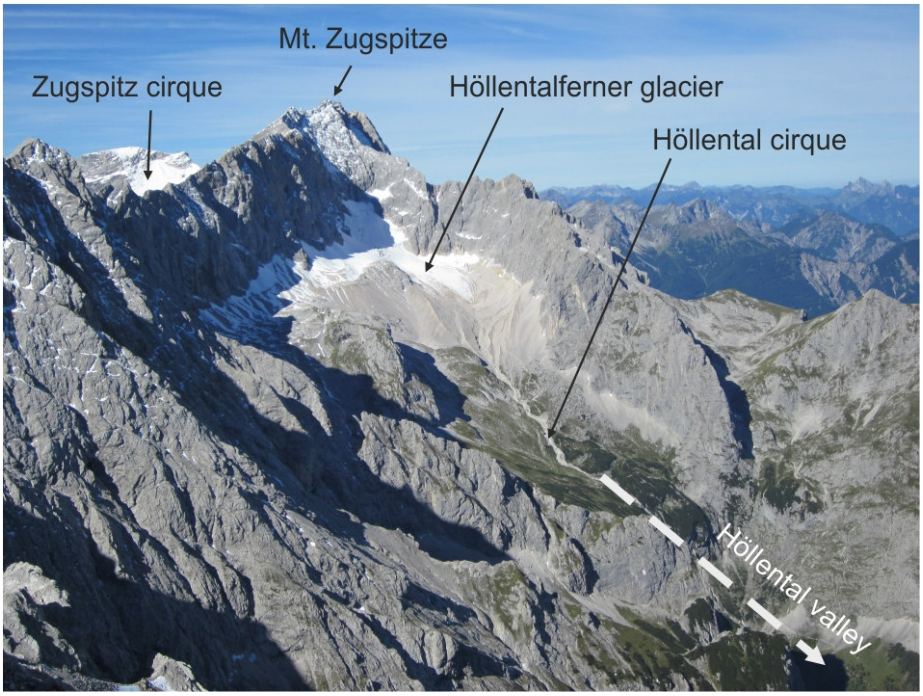

Figure 5.1: Impression of the steep Wetterstein Mountains with the highest summit, Zugspitze (2962 m asl), and the remaining glacier (Höllentalferner). The massive mountain ridges are formed by the up-to-1000-m-thick Wetterstein limestone, the main karst aquifer.

5.2 Field site

5.2.1 Geological setting and karst development

The Wetterstein Mountains are located in the German Alps close to Garmisch-Partenkirchen (700 m above sea level (asl)). They consist of three mountain ridges, including Germany´s highest summit, the Zugspitze (2962 m asl); (Fig. 5.1). The remote, high alpine valleys between the three ridges, Reintal and Höllental are accessible only by foot (Fig. 5.2). The difference in elevation between valley floors and summits is up to 2200 m. Above 2000 m asl, most areas are poorly covered by alpine and nival vegetation (Fig. 5.1) (Küfmann 2003). Two cirques around the highest summit (Höllental and Zugspitz cirques) are still partially covered by vestigial glaciers. With a total extend of about 55 ha and a mean thickness of 12 m and 17 m,

respectively, the two glaciers (Höllentalferner and Nördlicher Schneeferner) are the largest remaining glaciers in Germany (Hagg et al. 2012).

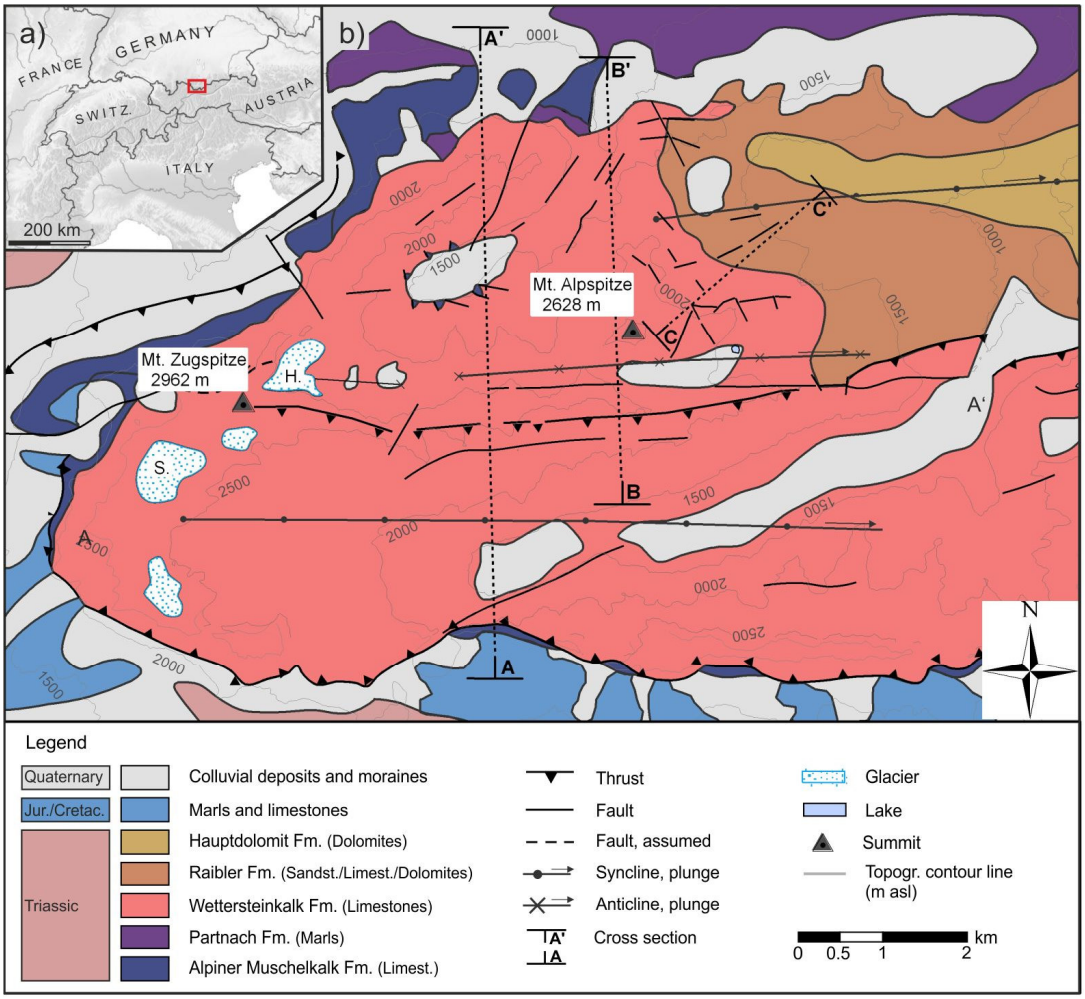

Figure 5.2: (a) Map of the study site (Wetterstein Mountains) in the German Alps and (b) Geologic and tectonic setting of the Wetterstein Mountains. The Wettersteinkalk-Fm. constitutes the main karst aquifer; glaciers: Höllentalferner (H.) and Schneeferner (S.). Geological cross sections are shown in Figs. 5.3, 5.8 and 5.9.

The Wetterstein Mountains formation includes the up-to-1000-m thick Triassic Wetterstein limestone (Fig. 5.2), which can be divided into three groups: a lower, thick and massive reef limestone, a well-bedded limestone, and an upper limestone. There are no distinctive marker horizons within the entire limestone formation, which complicates the determination of stratigraphic positions (Fig. 5.3). Particularly in the northern parts of the area, the marly Partnach Fm. occurs at the base of the karst aquifer, partially substituting the limestone. The underlying strata consist of a sequence of marls and well bedded limestones (Alpiner Muschelkalk Fm.) that act as an aquitard depending on the fraction of marls. The strata are folded and form two

regional synclines and one regional anticline, which appear as valleys and ridges (Fig. 5.3). The fold axes trend W-E and plunge to the east (20-35°). The entire Triassic stratigraphy belongs to the Lechtal nappe of the East Alpine (Austro Alpine) nappe system and has been thrusted over Jurassic and Cretaceous series to the southeast and south (backthrust) (Vidal 1953; Bögel 1960; Miller 1961).

Since the Eocene, the region has generally been steadily uplifting; high mountain chains have dominated the landscape since the early Oligocene (Frisch et al. 2008). Karstification is particularly evident at the cirques, where the slopes are less steep and precipitation and meltwater seep directly into the karst aquifer. At Zugspitz cirque for example, various small to medium sized caves are known; surface karst structures like dolines and karren occur frequently. Strong weathering and karstification together with intensive soil development occurred after the glacial retreat about 11 500 years ago (Grüger and Jerz 2010). However, no larger cave systems are known in this area. In contrast to the cirques, only a few karst features exist in areas where the slopes are steep and vegetation is low. In these areas, physical weathering results in strong jointing so that predominant gravitational erosion aggravates the evolution of prominent karst structures. To date, uplift is highest in this part of the Alps with rates of about 1 mm/a (Frisch et al. 2008).

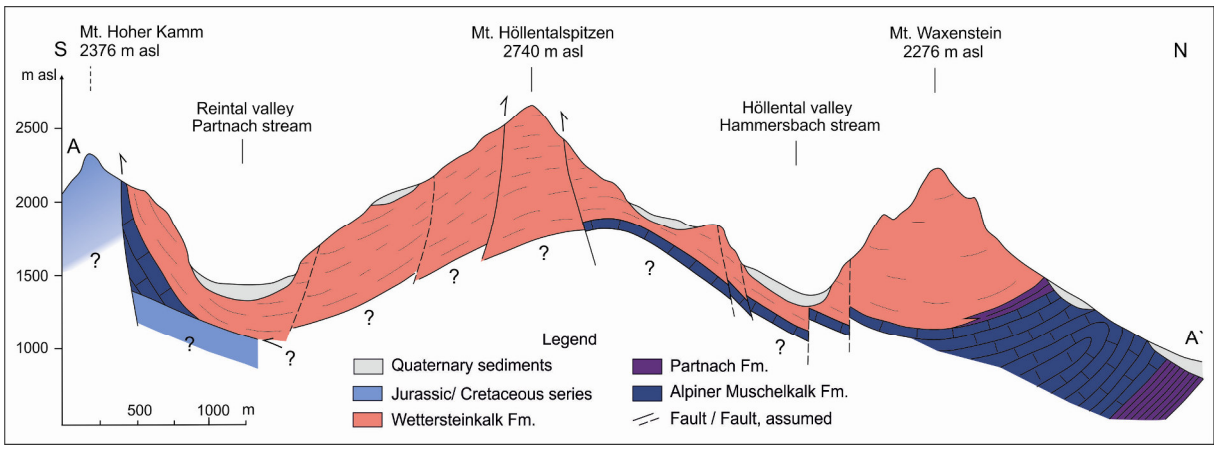

Figure 5.3: Geological cross section A-A` of the Wetterstein Mountains; the three mountain ridges and the two valleys are formed by thick limestone, the main karst aquifer. The cross section is not vertically exaggerated.

5.2.2 Hydrogeology

Several karst springs emanate into alpine streams and rivers flowing east- to northwards into the foreland (Fig. 5.4). The Hammersbach stream has cut deep into the limestone and forms an approximately 100 m deep and narrow gorge in the northern Höllental valley.

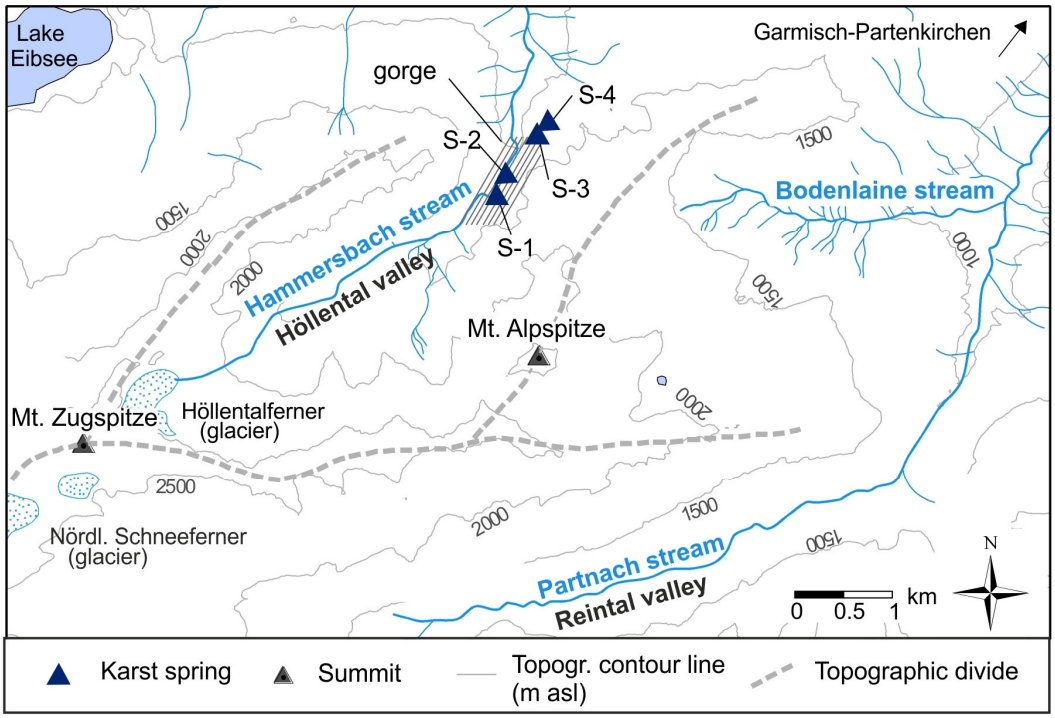

Figure 5.4: Mountain ridges, glaciers, surface waters in the main valleys and selected karst springs in the Wetterstein Mountains; dashed lines indicate topographic water divides.

There are four main karst springs in the northern valley (Fig. 5.4, Table 5.1): Spring S-1, a spectacular karst spring, is situated at a fault zone at the eastern rock face of the gorge. Having a mean runoff of about 260 L/s, water discharges from a karst conduit and falls down into the Hammersbach stream (Fig. 5.5). Thus, only indirect measurements of tracer concentrations are possible by sampling upstream and downstream of the tributary. S-2 is a small spring located at a fault zone on the western side in the gorge at level of the hiking trail. The discharge of the karst conduit is about 7 L/s. The two springs, S-1 and S-2, are perennial. Springs S-3 and S-4 are waterfalls on steep rock faces located at the eastern rock face of the gorge. The exact elevations of the spring orifices are not known. S-3 is an intermittent spring with a mean discharge of about 12 L/s during summer months and without discharge in late autumn. S-4 is also intermittent with a high discharge of up to 200 L/s in wet periods of early summer. The spring

responds rapidly to rain and snowmelt events. In dry periods, the spring runs dry after several days of no rain.

The water temperature of spring S-2 is representative of the mean annual temperature of groundwater in the catchment area. Hydrochemical properties of the three springs S-2 to S-4 are similar. Ca^{2+}, Mg^{2+} and HCO_3^- are the major ions, as is typical for groundwater from limestone. The electrical conductivity of the three karst springs is between 150 and 165 µS/cm reflecting low mineralization. The content of total dissolved solids is between 110 and 170 mg/L.

Table 5.1: Main karst springs in the lower Höllental valley (northern valley of the study area) and their physiochemical characteristics.

Spring no.		S-1	S-2	S-3	S-4
Name		Klamm spring	Tunnel spring	Gorge entrance spring	Rotgraben spring
Description		waterfall at E side of the gorge	spring at W side of the gorge	waterfall at E side of the gorge	waterfall at E side of the gorge
Elevation	[m asl]	~ 1180	~ 1100	~ 1100	~ 1100
Discharge (min/max)	[L/s]	260 (105/490)	7 (4/9)	12 (0/24)	- (0/200)
Type	[-]	perennial	perennial	intermittent	intermittent
Temp.	[°C]	n.a.	4.5	n.a.	n.a.
EC	[µS/cm]	n.a.	148	157	163
pH	[-]	n.a.	8.3	8.3	8.2
Ca^{2+}	[mg/L]	n.a.	22.0	23.5	24.1
Mg^{2+}	[mg/L]	n.a.	4.5	3.8	3.9
Na^+	[mg/L]	n.a.	0.3	0.2	0.1
K^+	[mg/L]	n.a.	0.1	0.1	0.1
Cl^-	[mg/L]	n.a.	0.4	0.3	0.2
NO_3^{2-}	[mg/L]	n.a.	1.2	1.7	1.5
SO_4^{2-}	[mg/L]	n.a.	0.7	0.8	1.1
HCO_3^-	[mg/L]	n.a.	98	104	104

n.a.: not analyzed; no direct measurement at the source is possible

Figure 5.5: View in southern direction from the hiking trail into the gorge to spring S-1; direct sampling at S-1 is not possible.

5.3 Material and methods

5.3.1 Artificial and natural tracer

Two artificial tracer tests have been conducted in the area around Mt. Alpspitze to resolve transit time distributions and drainage structures in the karst conduit system. The fluorescent dye uranine (CAS 518-47-8) was used as the solute tracer.

In 1998, an injection of uranine (2 kg) was performed on 25th of September. The injection point was located in a small cirque at an elevation of 2200 m asl and was selected to define catchment areas and water divides between three alpine valleys, the northern, northeastern and southern valley (Fig. 5.6). The tracer was added to runoff of a small intermittent karst spring, which was seeping into the karst aquifer a few meters below the spring. Discharge was about 0.2 L/s. The injection was conducted after several days without rain. Data have been used to delineate spring catchments but have not been analyzed quantitatively (Goldscheider et al. 1999).

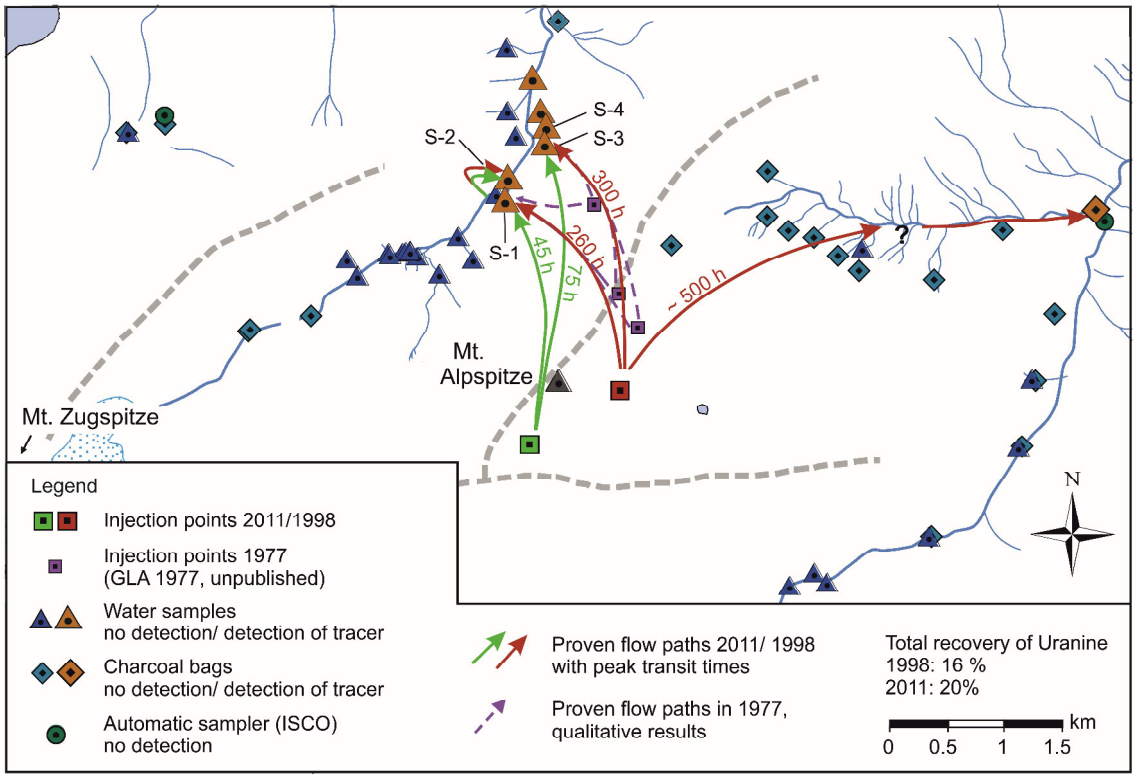

Figure 5.6: Injection points and sampling locations during the two tracer tests, with the location of the four selected karst springs S-1 to S-4. Dashed lines indicate topographic divides. Transit time in hours.

In 2011, 4 kg of uranine were injected on 16th of July at a central cirque in the Wetterstein Mountains at a location, where meltwater of a remaining snowfield was seeping naturally into the aquifer (Figs. 5.6 and 5.7). The injection point was located beyond the apparent topographic catchment area of the northern valley at an elevation of 2350 m asl. High precipitation before and after the injection facilitated drainage through the unsaturated zone. Surrounding valleys were observed by water samples and charcoal bags. At selected sites, automatic samplers (ISCO) were installed.

Two Perkin Elmer spectro-fluorometers (LS 50 B and LS 55) were used to measure uranine in water samples and charcoal bags. The synchronous-scan method was utilized. For calculation of tracer recoveries, discharge measurements were conducted by using the salt-dilution method.

There are data available on previous tracer tests conducted by the Geological Survey in 1977 (Bayerisches Geologisches Landesamt (GLA), unpublished report, 1977) (Fig. 5.6). In that study, the tracers uranine, eosine and sulphorhodamine G were used as tracers and injected in

August 1977 north of Mt. Alpspitze. Qualitative results of the three injections are taken into account in this study in order to resolve drainage structures.

For further characterization of transit-time distribution in fissured-porous rock matrix, isotopic data were collected from the springs. Stable isotopes of oxygen and deuterium were used as natural tracers; samples were collected between May 2011 and October 2012. Sampling intervals were mainly dependent on weather conditions; no sampling was feasible in winter (November to May) due to inaccessibility of the area (deep snow cover and risk of avalanches). During summer, samples were collected once per month in 2011 and every two weeks in 2012.

Figure 5.7: Injection of uranine in July 2011 in the central area of the Wetterstein Mountains at an elevation of about 2,350 m asl.

5.3.2 Climate and isotope data

Climate data were acquired from nearby weather stations, managed by Deutscher Wetterdienst (DWD). One weather station is situated in the community of Garmisch-Partenkirchen, located at 719 m asl. A second weather station is located on the summit of the Zugspitze, 2959 m asl (Fig. 5.2).

The mean monthly air temperature in Garmisch displays a minimum of -2°C in December and January, and a maximum of 17°C in July and August. At the Zugspitze, temperatures are approximately 10°C colder than at Garmisch. The total annual precipitation in 1998 was 1440 mm in Garmisch and 2180 mm at the Zugspitze. In 2011, the total annual precipitation was lower

with 1215 mm in Garmisch and 1,780 mm at the Zugspitze. Precipitation is well distributed over the year (1998 and 2011).

Isotopic data for precipitation at surrounding observation stations were acquired from the Global Network of Isotopes in Precipitation (GNIP) and the Austrian Network for Isotopes in Precipitation (ANIP). Together with isotopic data from Zugspitze, which was provided by the Institute of Groundwater Ecology of the Helmholtz Research Institute in Munich, data were used to estimate the altitude effects in the area. Long-term isotopic data from Garmisch of the years 1978-2009 were used to evaluate seasonal variability of isotopes in precipitation and to estimate mean transit time of water.

5.3.3 Data analysis and modeling

The main direction of flow and hydraulic connections between injection points and springs were determined by positive tracer detection. Basic parameters of the flow system were directly obtained from observed breakthrough curves (BTCs): Maximal flow velocities (v_{max}) were determined with respect to time of first detection (t_0); based on main breakthrough and peak concentration (c_P), dominating transit times (t_{dom}) and velocities (v_{dom}) were derived. To allow comparison, BTCs were normalized by dividing observed concentrations by the injected tracer mass; the resulting unit is m^{-3}.

Using a simple advection-dispersion model (ADM) implemented in the program CXTFIT (Toride et al. 1999), first estimates for mean flow velocities (v) and longitudinal dispersion (D_L) were obtained. Due to the skewness of the BTCs, fitting of the curves lead to coefficients of determination (R^2) of only 0.8. A better fit for the right-skewed BTCs was desired, so, BTCs were modeled with the two-region nonequilibrium (2RNE) model of CXTFIT, which has been successfully applied to characterize transport in karst aquifers (Field and Pinsky 2000; Geyer et al. 2007; Göppert and Goldscheider 2008; Mudarra et al. 2014). By accounting for mobile and immobile fluid phases, the model leads to good fits of the asymmetric BTCs ($R^2 > 0.9$) but less robust values by reason of altogether four fitting parameters. However, the shape of highly irregular BTCs can also result from a combination of two or more peaks provoked by dominating flow components in the turbulent core of karst conduits and laminar flow along margins of the conduit (Massei et al. 2006; Mudarra et al. 2014), variable flow rates or multiple flow paths (Field and Leij 2012). In the present case, the skewness of the BTCs also indicates the presence

of two peaks, whereas the second and lower ones are completely hidden in the long tail. For quantitative evaluation a multi-dispersion model (MDM) has been applied, delineated by (Käss 2004) and implemented in the program TRACI95.

For interpolating seasonal trends of variation and to obtain mean annual values, the isotopic signal in precipitation and spring water were fitted by a seasonal sine wave curves (Dewalle et al. 1997; Rodgers et al. 2005) (Eq. 5.1):

$$\delta^{18}O = y_0 + A[\cos(ct - \theta)] \qquad (5.1)$$

where $\delta^{18}O$ is the modeled isotopic signal, y_0 is the mean annual $\delta^{18}O$, A is the annual amplitude of the signal, c is the radial frequency of annual fluctuations (0.017214 rad/d), t is the time in days after beginning of sampling, and θ is the phase lag or time of the annual peak $\delta^{18}O$ in radians. Amplitudes and uncertainties of the parameters were obtained by fitting the function. Available data for isotopes in precipitation were used in this study. To obtain the input-signal, the weighted monthly mean values from Garmisch (years 1978-2009) were corrected by the mean elevation of the catchment area. This approach does not account for spatial distribution of precipitation within the catchment area and does not include the years 2011 and 2012 (for which data were not available). Therefore, isotopic values were interpreted for 2011 and 2012 by correlating monthly air temperatures and isotopic values for other available years. In snow-dominated alpine catchments, snow accumulation during winter and isotopic contribution of snowmelt in spring and early summer will cause a delay of the input of isotopic depleted winter recharge. Because of the large differences in elevation, temporal and spatial variability of snow accumulation and snowmelt can be expected and evaporation from snow and fractionation processes during snowmelt affect the isotopic compositions of snowmelt input. Because of the high number of unknowns and scarce data in the area, the long-term monthly mean values provide an estimate of the input-signal. Mueller et al. (2013) calculated the effects of different input-signals on transit time estimates in an alpine catchment in the Swiss Alps. According to their findings at transit times of 65 to 105 weeks, there was variation of 10 to 23% between different input-signals.

To estimate mean transit time of the natural tracer, isotopic data were modeled using the lumped-parameter approach implemented in the software FLOWPC (Maloszewski and Zuber 1982). The simple structure of the model requires only a few input parameters and therefore is

suitable to apply in alpine catchment areas, where data are often scarce (Maloszewski et al. 1992, 2002; Mueller et al. 2013). By calculating predefined impulse-response functions (g(τ)) and transit times (τ), the isotopic input signal $\delta^{18}O_{IN}$ is fit to observed values at the spring $\delta^{18}O_{OUT}$ (Eq. 5.2).

$$\delta^{18}O_{out} = \int_0^{\infty} \delta^{18}O_{in}(t-\tau)g(\tau)d\tau \qquad (5.2)$$

The best fit is obtained by trial and error and is quantitatively described by the goodness of the fit, i.e. the root mean square error (RMSE) and the efficiency of the model (EM) (Maloszewski and Zuber 2002). In this study area, the data could be well fitted with the impulse-response function (g(τ)) of an exponential model and a dispersion model. The exponential model, however, was preferred based on the assumption that groundwater flow through the thick unsaturated zone occurs along individual fissures and karst structures in the catchment area. Infiltrating water follows individual flow lines and mixing processes only occur shortly before the outlet. This approach has been applied in alpine catchment areas with thick unsaturated zones (Maloszewski et al. 1992; Mueller et al. 2013). The dispersion model can also account for mixing processes in the unsaturated zone of alpine aquifers (Maloszewski et al. 1992, 2002). The long tailing of the observed BTCs (artificial tracers) indicate that there is at least some water exchange between conduits and fissures. However, the use of the dispersion model requires estimation of two additional parameters, the dimensionless dispersion parameter P_D (=D_L/vx) and the fitting coefficient β, which indicates the proportion of an "old" groundwater component (Maloszewski and Zuber 2002). While these parameters can be estimated (e.g. Maloszewski et al., 2002), the resulting additional uncertainty yields less robust results. The exponential model provides a simpler and less ambiguous approach, and is applied herein. Given the relatively simple structure of the lumped-parameter model and the low number of input data points, results are estimates, but are nonetheless useful.

In addition to the fresh infiltrated water moving through larger fissures, there is generally a slow flow component of the groundwater, which is older than the fresh infiltrated water and contributes to the baseflow of the spring. The isotopic composition at the spring shows a mixture of "old" groundwater and fresh infiltrated water. Using the exponential model, the proportion of the slow flow component was estimated by analyzing the transit-time distribution.

With additional information from discharge measurements, recovery was determined. Conduit volumes (V) were estimated by multiplying the mean discharge (Q_{mean}) and the mean transit time of tracer (t_{mean}) (Field and Nash 1997).

5.4 Results and Discussion

5.4.1 General results of the tracer test in 1998

Uranine was detected at several springs in the northern and in the northeastern valley (Fig. 5.6). Breakthrough curves of S-1, S-2 and S-3 show one clear peak and a long tailing. The first detection of uranine was at S-1 and S-2 193 hours after injection; maximum concentrations of 1.3 µg/L were reached after 260 and 335 hours respectively. At S-3, a maximum of 1.6 µg/L was measured after 260 hours. Peak flow velocities vary between 6 and 9 m/h. Discharge of the springs were largely constant except at S-4, where large variations in spring discharge from 0 to 100 L/s were observed, together with a multi-peaked BTC; the peaks can be related to the discharge, however, with results discussed below.

Recoveries at single springs were quite low and range between 0.3 and 8.1%, with total recovery in the northern valley about 16%. This finding can be related to tracer injection very close to the anticline structure in the central area of the Wetterstein Mountains and is apparently a result of deep infiltration of the tracer and a contribution to regional flow systems (Fig. 5.8).

Results indicate that topographic divides do not correspond with underground catchment areas. Underground flow paths cross the mountain ridge of Mt. Alpspitze and contribute to the drainage of the northern valley (Fig. 5.6). Furthermore, there are obviously flow paths underneath the northern valley itself: uranine was also detected at S-2, at the opposite side of the valley. Between the injection point and S-2 lies the gorge, which cuts deep into the limestone. This is clear evidence for deep flow paths crossing beneath the gorge and demonstrates the presence of deep karst structures (Fig. 5.8). In addition, uranine was also detected in the northeastern valley, where most springs are related to the upper stratigraphic unit, the Raibler Formation (Figs. 5.2 and 5.6). However, tracer was not detected at the individual springs but in the Bodenlaine stream in the valley floor. As uranine must flow from the karst aquifer through the upper strata to emerge to the stream, the positive detection is evidence for cross-formational flow. Drainage follows either direct flow paths or deep flow systems to the valley (Fig. 5.9). In

contrast, results of the tracer test in 1977 (GLA, unpublished report, 1977) showed only drainage to the northern valley; no tracer was detected in the Bodenlaine stream. This demonstrates the strong heterogeneity of the karst drainage, as discussed further below.

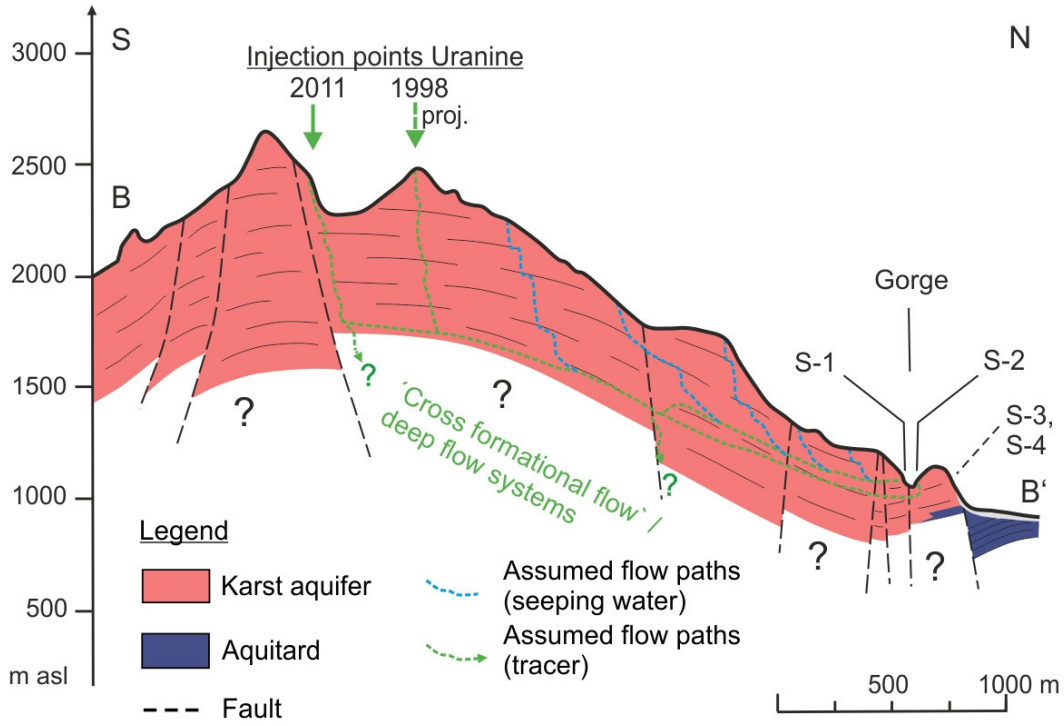

Figure 5.8: Geological cross section B-B` between injection points and springs S-1 to S-4. There is a deep but rapid flow system crossing below the deep gorge. The cross section is not vertically exaggerated.

The results of 1998 were modeled with the MDM; calculated parameters are listed in table 5.1. The multi-peaked BTC of S-4 was not modeled, as the multi-peaks are not a result of several flow paths but are connected to variable runoff at the spring. Therefore, only the first peak was modeled.

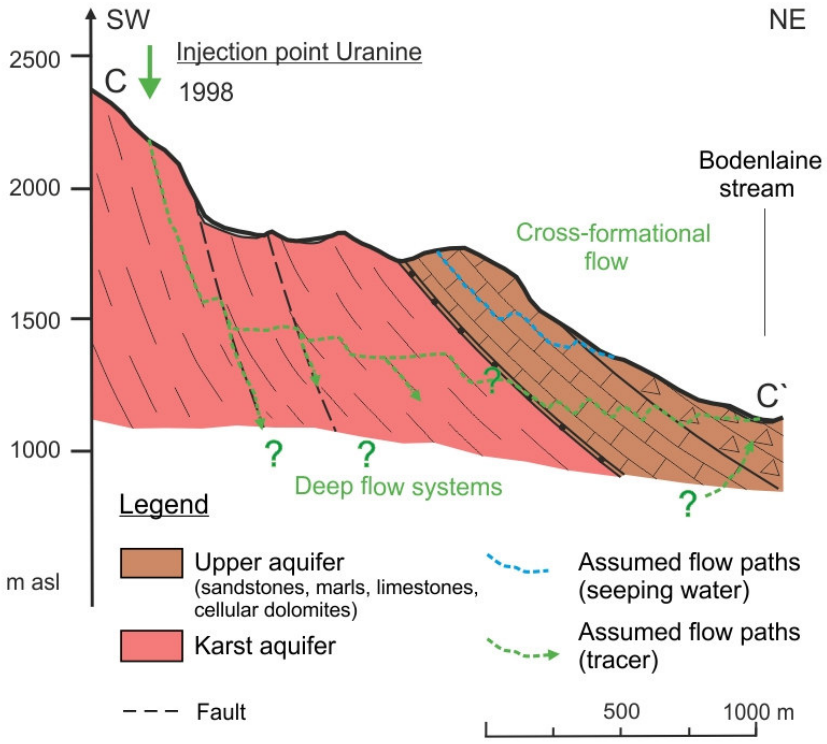

Figure 5.9: Geological cross section C-C` between the 1998 injection point and the valley in the NE. There is cross-formational flow from the karst aquifer through the overlaying formations towards the discharge zone. The cross section is not vertically exaggerated.

5.4.2 General results of the tracer test in 2011

In 2011, underground drainage to the northern valley was observed, although the injection site is located south of the topographic divide. This finding is in accordance with results from 1998. However, no evidence for flow systems to the south or to the valley in the northeast has been found (Fig. 5.6). All breakthrough curves show one single peak and a long tailing. After 44 hours, the tracer reached the springs S-1 and S-3, while at the same time, the maximum of 21 µg/L was reached at S-2, confirming the existence of a deep but rapid flow system crossing below the deep gorge (Fig. 5.8). After 77 hours, maximum concentrations between 5 and 10 µg/L were detected at the other springs. This results in peak flow velocities of 36 to 63 m/h.

Uranine was still detected at S-2, S-3 and S-4 for a sampling campaign in 2012, more than one year later. Concentrations were up to 0.2 µg/L, which is 100 times below maximum concentrations in 2011 but still 100 times above the detection limit (Fig. 5.10). It was not possible to detect low tracer concentrations at S-1, as direct sampling of the spring was not possible. The concentrations at springs S-2 to S-4 fluctuate and give evidence for dilution effects after rain

events (Fig. 5.10). Tracer concentrations declined over the summer down to the detection limit in October 2012, suggesting remobilization of tracer stored in the karst system in 2011. Similar observations were made by Rappl et al. (2010) in the adjacent catchment area of Partnach spring.

Recovery was between 0.8 and 13% at individual karst springs; total recovery of uranine in the northern valley was 20% in 2011. Due to the sampling in 2012, recovery increased at S-2 from 0.8 to 1.3%; at S-3, the increase was from 1.0 to 2.9% and at S-4 it was from 3.7 to 4.0%. Thus, a noteworthy proportion of tracer had been stored in the karst system and released during the following year.

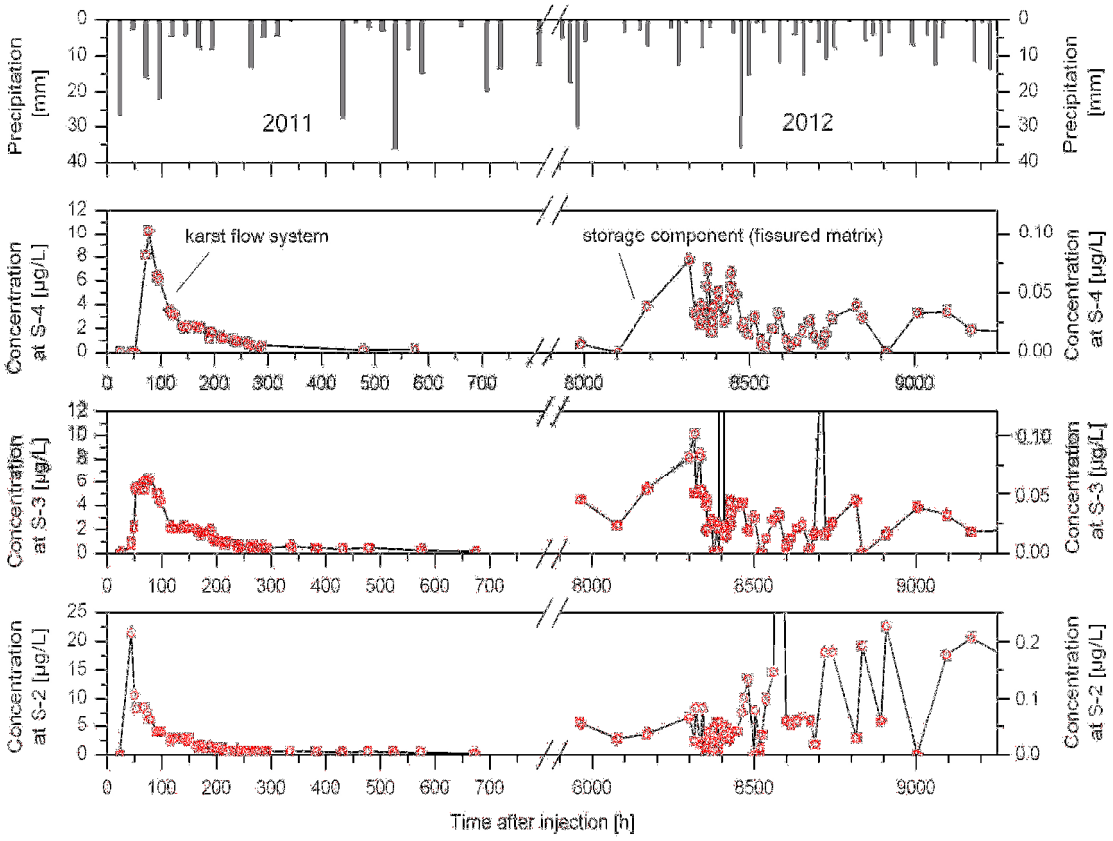

Figure 5.10: Uranine breakthrough curves at three karst springs S-2, S-3 and S-4; the right y-axis scaling is by the factor of 100 lower than the left y-axis scaling. Precipitation data were obtained at the weather station Garmisch (DWD).

The results in 2011 confirm that there are flow paths crossing the topographic divide to S-1 and the deep gorge to S-2 (Fig. 5.8). At S-2, highest concentrations and flow velocities were ob-

served proving well-developed drainage structures and deep karst flow paths are present. However, uranine concentrations at the nearby S-1, located on the SE side of the gorge and thus closer to the injection point, were significantly lower (5 µg/L) than at S-2 (21 µg/L). In contrast to S-2, the water-rich S-1 receives inflow from local water sources causing a higher dilution of the tracer (Fig. 5.8). Differences of flow times and velocities are likely to be a result of hydraulic gradient, as S-2 is located about 80 m lower than S-1.

The results of the analytical modeling (MDM) are listed in table 5.2, discussed below. For comparison with results from 1998, selected BTCs are graphically shown in Fig. 5.11.

5.4.3 Hydrologic variability of the karst drainage network

BTCs show one main peak with a steep rising limb and a long tail, which can be separated into two individual BTCs by analytical modeling with a multi-dispersion model (Fig. 5.11). Thus, the main peak can be related to a BTC representing high mean flow velocities between 35 and 42 m/h in 2011 (Fig. 5.11, Table 5.2). These high flow velocities are attributable to advective and turbulent flow in karst conduits and open fissures. Considering the great thickness of the unsaturated zone, transit times of 50 to 80 h are short. There must be well-developed flow paths within the highly fractured and moderately karstified limestone. The skewness of the BTCs indicates strong tailing effects along the flow path. Analyses with the multi-dispersion model (MDM) for 2011 data revealed that the observed tailing effects are related to a second smaller peak caused by dominating flow velocities between 11 and 18 m/h. These intermediate flow velocities are 2 to 3 times smaller than the observed high flow velocities. Such flow velocities are generally found along rough margins of a main flow channel (Massei et al. 2006), smaller fissures, strata boundaries and stagnant zones. Furthermore, the observed tailing is related to exchange with immobile fluid regions along the flow path, which occur in the thick unsaturated zone and result in persistent tracer concentrations one year after the injection.

Melt water and precipitation before and after the injection of the tracer facilitated flow through the unsaturated zone. The injection points of the two tracer tests were located around Mt. Alpspitze in the central areas of the mountains. Distances to springs were in 2011 only slightly longer than in 1998. In 2011, the mean flow velocities were about 38 m/h on average and thereby 4 to 5 times higher than in 1998 (7.8 m/h) (Fig. 5.11, Table 5.2). Whereas the average of mean transit times was about 286 hours in 1998, mean transit times in 2011 were only 66

hours and thus 4 to 5 times shorter. The observed variability of transit times can be related to weather conditions and seasonal differences between the two tracer tests. In 1998, the tracer test was conducted at the end of September. The month was generally rainy with light snowfall above 2000 m, but there were several days without rain shortly before and after the injection. In 2011, however, the tracer test was conducted in the middle of July in a period with high precipitation. The days before the injection had been rainy; up to 28 mm of rainfall per day was measured during the first week of the tracer test. In addition, there is generally a significant component of snowmelt recharging the karst aquifer during early summer. According to Wetzel (2004) and Rappl et al. (2010), the contribution of snowmelt to the annual runoff is about 30%; the peak is reached in July. As a consequence, the preferential flow paths through the unsaturated zone were fully wetted, and smaller fissures were completely filled with water, especially in July 2011.

The great hydrologic variability of the underground drainage of the karst system is coupled with variable tracer concentrations. In 2011, normalized tracer concentrations were significantly higher than in 1998 (Fig. 5.11, Table 5.2). Values vary by a factor of 2 to 5. Several studies have described the relations between flow conditions and maximum tracer concentrations in karst aquifers (Göppert and Goldscheider 2008; Pronk et al. 2007, 2009). In this case, higher flow velocities result in narrower BTCs and, therefore, higher maximum concentrations.

In 1998, tracer breakthrough at S-4 showed variability of tracer concentrations resulting in a multi-peak BTC (Fig. 5.11). The peaks are directly linked with spring discharge: uranine concentrations increase with increasing discharge, whereas a decrease of concentration was observed with decreasing discharge of the spring (Goldscheider et al. 1999). This suggests that the catchment area enlarges during high-flow conditions as a result of overflow. Tracer from the adjacent injection point can reach the spring and concentrations rise. With the decline of the water level, hydraulic connections are inactive and the catchment area is reduced to a local area. Then, only water from a local origin reaches the spring, resulting in a decrease of uranine concentrations. In contrast, a continuous BTC was observed in 2011, when the spring did not cease flow during the main sampling period. All observed aspects affirm high-flow conditions in 2011: high precipitation and snowmelt led to rapid tracer transport and high spring discharge. Steady high-flow conditions in July 2011 resulted in a continuous BTC; the catchment area of S-4 did not vary during the main breakthrough of the tracer.

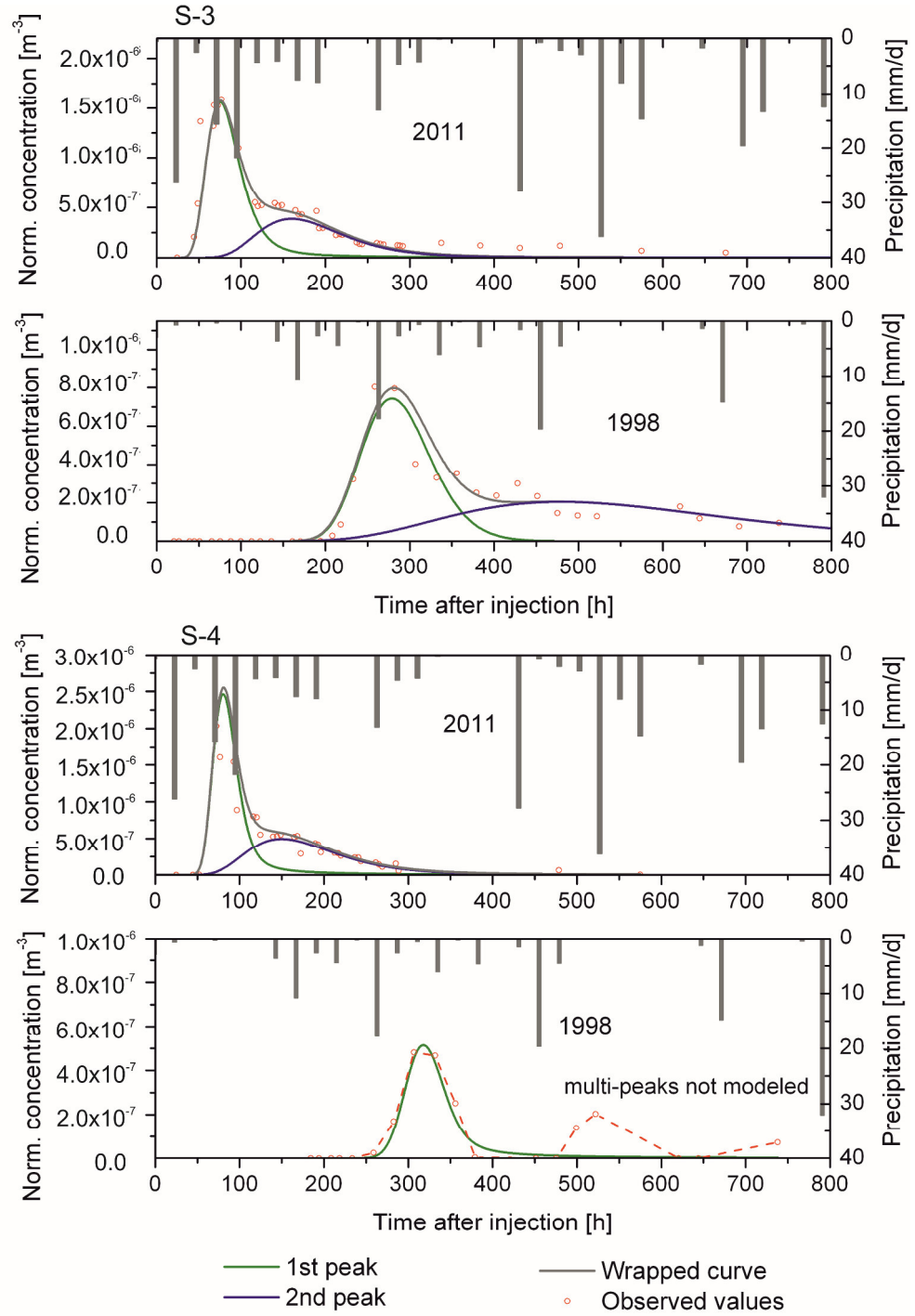

Figure 5.11: Comparison of uranine breakthrough curves at S-3 and S-4, observed and modeled values (multi-dispersion model MDM) from the tracer tests in 1998 and 2011, and precipitation (obtained by DWD, Garmisch).

Table 5.2: Aquifer parameters for karst conduits obtained from artificial tracer tests (uranine).

Spring no.			S-1		S-2		S-3		S-4		Overall comparison		
Test year			1998	2011	1998	2011	1998	2011	1998	2011		1998	2011
General parameters													
Injected tracer mass	M	[kg]	2.0	4.0	2.0	4.0	2.0	4.0	2.0	4.0	av.	2.0	4.0
Distance to spring	x	[m]	1,980	2,200	1,980	2,200	2,350	2,800	2,350	2,800	av.	2,202	2,560
Time of first detection	t_1	[h]	193.4	43.8	193.5	44.0	208.3	44.3	282.8	72.5	av.	219	49.72
Maximal flow velocity	v_{max}	[m/h]	10.2	50.2	10.2	50.0	11.3	63.3	8.3	53.7	av.	10.20	56.16
Peak transit time	t_p	[h]	260.1	43.8	335.0	44.0	258.8	76.8	306.8	77.0	av.	293	63.72
Peak flow velocity	v_p	[m/h]	7.6	50.1	5.9	50.0	9.1	63.3	7.7	36.4	av.	7.6	41.86
Peak concentration	c_p	[µg/L]	1.3	5.1	1.0	21.5	1.6	6.4	1.0	10.3	max	1.6	21.5
Normal peak concentration	c_p/M	[m^{-3}]	6.50E-07	1.28E-06	5.00E-07	5.38E-06	8.00E-07	1.60E-06	5.00E-07	2.58E-06	max.	8.0E-07	5.4E-06
Conduit volume	V	[m^3]	-	73,907	-	1,308	-	4,032	-	19,902	sum	-	99,149
Recovery	R	[%]	8.17	13.01	0.34	0.76	0.80	0.98	0.27	3.65	sum	16.3	20.2
Modeled parameters (MDM)													
1st peak													
Mean flow velocity	v_{mean}	[m/h]	7.7	40.4	-	42.3	8.1	35.2	7.5	34.4	av.	7.8	38.1
Mean transit time (calc.)	t_{mean}	[h]	258	54	-	52	288	80	313	81	av.	286	67
Longitudinal Dispersion	D_L	[m^2/h]	133	5,770	-	5,883	204	3,087	40	1,305	av.	126	4,011
Dispersivity	α	[m]	17	143	-	139	25	88	5	38	av.	16	102
Peclet Number	Pe	[-]	116	17	-	15	94	31	438	73	av.	216	34
2nd peak													
Mean flow velocity	v_{mean}	[m/h]	4.0	12.7	-	15.3	4.1	16.2	-	16.7	av.	4.1	15.2
Mean transit time (calc.)	t_{mean}	[h]	495	172.4	-	143	572	172	-	166.7	av.	534	164
Longitudinal Dispersion	D_L	[m^2/h]	505	4,890	-	3,583	570	2,107	-	2,754	av.	538	3,334
Dispersivity	α	[m]	126	385	-	234	139	130	-	165	av.	133	229
Peclet Number	Pe	[-]	15	8	-	9	16	21	-	17	av.	16	14
Coeff. of determination	R^2	[-]	0.946	0.929	-	0.927	0.951	0.987	0.962	0.991	-	-	-

5.4.4 Results with stable isotopes as natural tracers

The long-term weighted monthly means at Garmisch show a clear seasonal signal of isotopes in precipitation with a minimum of -14.6‰ $\delta^{18}O$ in December and a maximum of -7.0‰ $\delta^{18}O$ in July. The annual mean is -11.2 ± 2.8‰ and the amplitude of the signal is 3.8 ± 0.17‰. In the area, the altitude effect results in a depletion of -0.16‰ per 100 m (Fig. 5.12, Table 5.3), which is in good agreement with values from the Swiss Alps determined by Schürich et al. (2003) and Mueller et al. (2013). The $\delta^{18}O$ values in precipitation were corrected by the mean topographic elevation of the catchment area of 2,000 m, resulting in a shift of the input-signal to annual mean values of -13.2 ± 2.8‰.

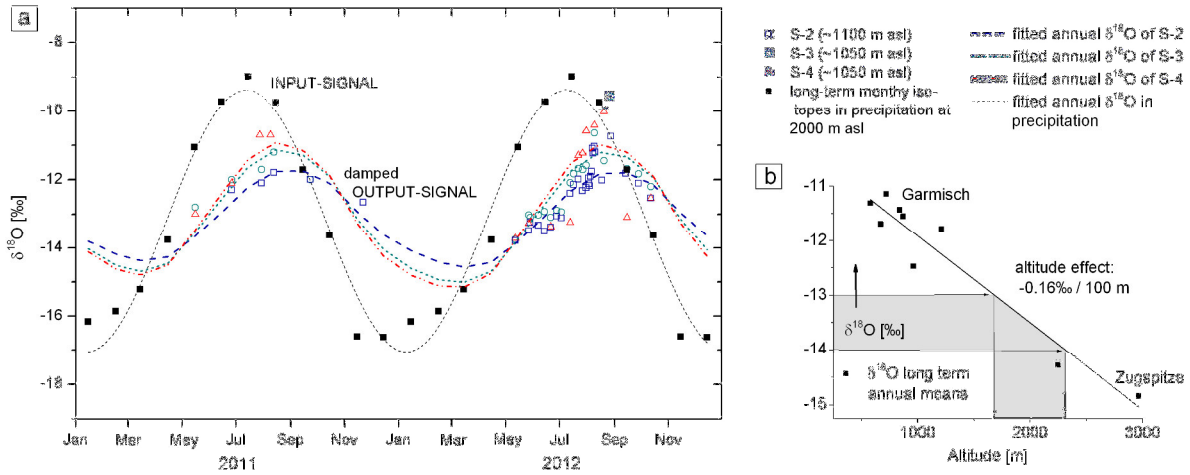

Figure 5.12: (a) Seasonal $\delta^{18}O$ variations in precipitation (weighted monthly mean values at Garmisch, corrected by elevation), and at the springs S-2, S-3 and S-4; monthly values of precipitation are fitted by a sine wave curve (Eq. 5.1) and by the exponential model of FLOWPC. (b) shows the altitude effect in the area.

The seasonal variations are distinct in the isotopic signal at the springs. S-4 had the highest variation during the sampling period, at -13.7‰ $\delta^{18}O$ in May and -10.0‰ $\delta^{18}O$ in August. S-2 and S-3 show slightly lower variation (Fig. 5.12). The observed data were modeled and interpolated using Eq.5.1 only for the summer months, due to inaccessibility of sampling sites in the mountains in winter. The annual means of isotope values at the springs and the uncertainties are between -13.9 ± 0.7‰ and -13.2 ± 0.4‰ $\delta^{18}O$, indicating that the recharge areas are at elevations between 1800 ± 250 and 2300 ± 430 m asl (Fig. 5.12). Considering the uncertainties, including a lack of winter values and the curve fitting, the springs are assumed to have the same catchment area. This is consistent with tracer tests indicating that the catchment area of the three springs is located around Mt. Alpspitze; the mean elevation is 2000 m asl (Fig. 5.6). The

amplitude of the input signal, 3.8 ± 0.17‰, decreases down to values between 1.8 ± 0.25‰ and 2.8 ± 0.81‰ $\delta^{18}O$ at the three springs; there is also a distinct phase lag between input and output signal, varying between 1.1 and 1.8 months (Table 5.3). Considering the statistical monthly variability of 2‰ for isotopes in precipitation and the statistical uncertainties of the amplitude of the springs, which can exceed 0.8‰ because of the lack of winter samples, the amplitudes of the spring data are statistically within the same range. The spring discharge originates from the same groundwater flow component of the aquifer. The fact that the seasonal amplitude of the output signal is still distinctive at all three springs clearly indicates that the mean transit time is less than one year (Trček and Zojer 2009).

To quantify the transit times < 1 year, observed $\delta^{18}O$ values at the springs were fitted with the exponential model. Isotopic input values, interpolated by the monthly mean temperature did not result in a good fit of the model, as the years 2011 and 2012 were about 1°C warmer and the isotopic annual mean of the two years is therefore about 1‰ heavier compared to the annual mean of the springs. Best fitting of the data was obtained by using the long-term weighted annual mean values resulting in mean transit times between 2.9 and 4.9 months (Table 5.3). Although there are uncertainties regarding the input- and the output-signal, the obtained transit times are in good accordance with observed spring characteristics. The mean transit time is highest, at a value of 4.9 months, for S-2, which had a constant discharge over the observation period and to the authors' knowledge does not cease flow. Shorter transit times of approximately 2.9 to 3.3 months were estimated for S-3 and S-4, both of which have a greater variability of discharge and are perennial, with flow ceasing after dry periods in late summer and autumn. Because of the intermittent discharge, fewer water samples were collected from S-4 resulting in the most uncertain results and lowest efficiency of the model (Table 5.3). The proportion of water that is younger than the mean transit time was derived by the distribution of the transit times and is between 53 and 57% for the different springs. This indicates that about 43 to 47% of the discharge is older than the mean transit times and roughly about 22 to 27% is older than twice the mean transit time. In conclusion, there is a proportion of water that is at least older than 6 to 10 months. Considering results of Maloszewski et al. (1983, 1992, 2002), it is likely that the long-term flow component has a mean transit time of several years.

Table 5.3 Mean transit times of natural tracer obtained from stable isotope analysis

Component	Unit	Input-Signal[a]	Spring S-2	Spring S-3	Spring S-4
Observed data					
Number of samples	[-]	24	42	34	28
Mean $\delta^{18}O$[b]	[‰]	-13.2	-13.4	-13.2	-13.9
Std. dev.[b]	[‰]	0.1	0.2	0.4	0.7
Amplitude[b]	[‰]	3.8	1.8	1.9	2.8
Std. dev.[b]	[‰]	0.2	0.3	0.4	0.8
Phase lag[b]	[months]	-	1.8	1.6	1.1
Exponential Model					
Mean transit time (MTT) of tracer	[months]	-	4.9	3.3	2.9
Proportion of water older than 1xMTT	[%]	-	43	46	47
Proportion of water older than 2xMTT	[%]	-	22	25	27
SIGMA[c]	[‰]	-	0.086	0.137	0.247
EM[d]	[-]	-	0.81	0.74	0.32

[a] weighted monthly mean values of Garmisch (1978-2009), corrected by elevation. All precipitation is assumed to infiltrate the aquifer and contribute to spring discharge; snow accumulation and snowmelt contribution is not taken into account

[b] parameters calculated by using Eq. 5.1

[c] goodness of the fit, as described by Maloszewski and Zuber (2002)

[d] efficiency of the model, as described by Maloszewski and Zuber (2002), EM = 1 is ideal fit

5.4.5 Conceptual model of underground drainage and karst aquifer parameters

Most the observed karst springs in the northern valley are situated at fault zones, indicating that karst development and drainage is strongly linked to tectonic weak zones. Thus, drainage structures are highly heterogeneously distributed in the massive limestone.

In the area around Mt. Alpspitze, drainage of the karst aquifer is not controlled by topographic divides. Results of tracer tests with injections in 1977, 1998 and 2011 demonstrate a preferential drainage towards the steep and deep gorge in the north. In this case, drainage structures cross topographic divides, i.e., mountain ridges (Fig. 5.6). Uranine was found in spring S-2, located at the opposite side of the 100 m deep gorge. Velocities of flow to that spring and associated tracer concentrations were the highest of all observed results in 2011. Consequently, there are well-developed and deep drainage structures crossing beneath the narrow gorge with the Hammersbach stream (Fig. 5.8). Additionally, drainage to the gorge occurs transversely to the dip

of the fold axis. In comparison with the other two alpine valleys in the Wetterstein Mountains, the Hammersbach stream has cut the deepest into the karst aquifer. The gorge lies at a relatively low elevation between 1000 and 1100 m asl; as a result of the high hydraulic gradients, drainage is mainly toward this valley.

There is little drainage to the Bodenlaine stream in the NE, as demonstrated by the results of injection in 1998. In this direction, drainage follows the dip of the fold axis. However, the stream is located at an elevation of 1100 to 1300 m asl. As a result, hydraulic gradients are lower in this direction, resulting in minor drainage to the Bodenlaine stream. Additionally, springs are related to the upper stratigraphic unit. Positive detection of dye in the stream provides evidence for cross-formational flow. Flow must occur along strata boundaries, fractures and fault zones in order to cross the stratigraphic units (Fig. 5.9). Linear flow paths are conceivable. According to the local and regional flow pattern in mountainous areas studied by Tóth (1963, 1999), tracer may also enter deep flow paths and follow deep drainage structures to the receiving waters. The presence of further flow paths is also indicated by moderate recoveries of about 20% during each tracer tests. The injected tracer uranine is an ideal tracer with conservative properties. Because tracer tests have demonstrated that karst drainage is related to fractures and fault zones, flow paths may occur along steep tectonic structures contributing to deep drainage and regional flow systems.

Results of the tracer test in 2011 constrain the relative thickness of the unsaturated zone. The tracer was injected close to the anticline structure in a central area of the Mountains. As no tracer was detected in the southern valley, drainage in that direction is unlikely (Fig. 5.6). The saturated zone must be situated at great depth to prevent flow over the anticline structure to the south (Fig. 5.8). The thickness of the unsaturated zone is – in this part of the Mountains – approximately as thick as the karst aquifer. Thus, the anticline acts as a water divide.

The quick breakthrough of the tracer combined with a long tail indicates that there is a large distribution of transit times dominating the drainage in the karst system. The fast-flow component is related to the karst drainage network consisting of conduits and open fissures; corresponding mean transit times are between 2 and 13 days (Fig. 5.13, Table 5.4). Turbulent flow in the core of conduits results in fast transport of water and solutes. The skewness of the BTCs is attributable to lower flow velocities, which occur due to laminar flow at margins of flow

channels, flow through well-drained fractures and fissures, and fluid exchange with immobile fluid regions, e.g. dead-end passages. The fast-flow component is likely to affect spring water quality after precipitation events, as contaminants, e.g. fecal bacteria, are transported to the spring within a short period of time. Thus, storage effects are low.

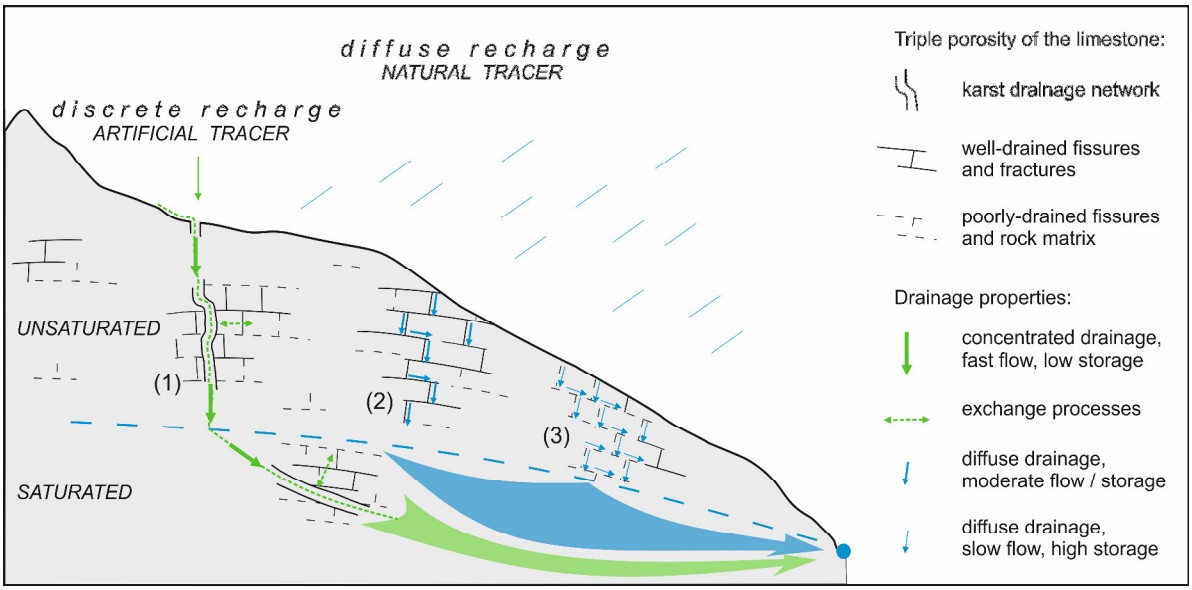

Figure 5.13: Conceptual model of drainage in the investigated alpine karst system, showing triple porosity. Numbers in brackets refer to Table 5.4.

Table 5.4: Summary of the results from artificial and natural tracers characterizing a limestone with triple porosity. Numbers (1), (2) and (3) refer to porosity, as shown in Fig. 5.13.

	(1)	(2)	(3)
Flow path	karst drainage network (conduits and open fractures)	well-drained fissures and fractures	poorly-drained fissures and rock matrix
Recharge	discrete	diffuse	diffuse
Flow velocities	fast flow: 180-1050 m/d	intermediate flow: 15-25 m/d	slow flow: < 1 m/d
Mean transit time of tracer	2-13 days	2.9-4.9 months	few years
Tracer	uranine	stable isotopes (^{18}O)	indirect determined (^{18}O)
Water volume	1 000 / 34 000 m^3 (S-2 / S-4)	90 000 / 500 000 m^3 (S-2 / S-4)	not determined

An intermediate- to slow-flow component has been delineated by tracer concentrations more than one year after the injection in 2011, indicating storage characteristics of the karst system. Percolation through the thick unsaturated zone, which consists of dipping strata, favors flow

along strata boundaries and storage in poorly-drained fissures, voids and joints (Fig. 5.13). In addition, pressure in water filled fissures leads to conduit-matrix exchange. Owing to gradient inversion and matrix diffusion, water can be stored in the fissured rock matrix. With decreasing pressure in the drainage network, water is released out of the karst system slowly and thus contributes to base flow at springs.

An intermediate-flow regime is confirmed by stable isotope results that demonstrate long transit times in the karst system. Although there are uncertainties for the input and output signals, annual oscillation pattern of the isotopic signal at the springs is clearly visible. The signal is considerably dampened and shows a phase shift. The distinct output-signal at the springs indicates a dominant component of flow with a transit time of less than one year. The exponential model enables an estimation of the transit times, indicating that a significant proportion of the spring water has an approximate mean transit time between 2.9 and 4.9 months. Despite the uncertainties, a major flow component with transit times of a few months is in accordance with field observations of spring discharge characteristics. The proportion of the intermediate-flow component of spring discharge is roughly 50%. This indicates that a large amount of new infiltrated water is released out of the karst system after a few months. Intermediate transit times are interpreted as a result of the mainly diffuse infiltration and drainage along numerous well-drained fissures and fractures of the karst system (Fig. 5.13, Table 5.4).

The results of the stable isotope modeling indicate that there is also a slow-flow component of the spring water that is older than the fresh infiltrated water and is probably older than a few years (Table 5.3). The presence of transit times of a few years is, furthermore, very likely (Maloszewski et al. 1983, 1992, 2002) and is in accordance with the conceptual model and triple porosity. The low-flow component with mean transit times in the range of years reflects diffuse infiltration in the poorly-drained fissures and rock matrix of the aquifer. This flow component is particularly important with regard to long-term runoff characteristics of the alpine karst springs and impacts of climate change. High storage capability of the karstic Wetterstein limestone corresponds with observations of Rappl et al. (2010) and Maloszewski et al. (2002).

The average value for dispersion, determined by artificial tracer tests, is 126 m^2/h for the first peak and 539 m^2/h for the second one in 1998 (Table 5.2). In 2011, corresponding values are 4011 m^2/h and 3334 m^2/h respectively. Dispersion is significantly higher in 2011 than in 1998

owing to higher flow velocities and slightly longer flow distances (300 m on average) in 2011. High flow velocities in the main flow channel are associated with large Peclet numbers ($Pe = vx/D_L$) between 17 and 73 (1st peak) and indicate high advective and turbulent flow in the core of the flow path. However, lower Peclet numbers between 8 and 21 arise with lower flow velocities and can be related to well-drained fissures and fractures along the flow path (2nd peak). To clarify dispersive flow, dispersivity ($\alpha = D_L/v$) is taken into account showing the same increase.

For the year 2011, mean transit times of uranine were used to calculation water volumes of the karst drainage network. Karst water volumes of about 100 000 m^3 were determined for the conduit network, whereas individual values range between 1300 m^3 (S-2), 20 000 m^3 (S-4) and 74 000 m^3 (S-1) (Fig. 5.13, Table 5.4). By using mean transit times of the natural tracer, it can be estimated that water volumes of well-drained fissured are significant higher. Values lie between 90 000 m^3 (S-2) and 500 000 m^3 (S-4), excluding estimates for the waterfall and spring S-1, where isotopes could not be measured. These estimated water volumes are applicable for water in conduits and well-drained fissures in the Wetterstein Mountains. Most water is likely to be stored in poorly-drained fissures and rock matrix (Maloszewski et al. 2002; Worthington 2007).

5.5 Conclusions

A combination of artificial and natural tracer investigations was performed in order to resolve drainage structures and transit time distribution of a high-alpine karst system. Underground drainage is not primarily linked with topographic divides: there are well developed drainage structures crossing topographic divides and deep alpine valleys. Observed direction of flow is to the north showing that drainage occurs mainly in the direction of greatest hydraulic gradient to the deep gorge. Therewith, flow is linked to geologic weak zones and occurs transversely to the dip of the main fold axis. Flow is controlled by geologic structures in proximity to the main anticline structure, which acts as a water divide. Cross-formational flow from the main karst aquifer through the overlying formations towards discharge zones has been observed in the northeastern valley and probably occurs along numerous fractures and fault zones.

There is a fast-flow component draining karst conduits and open fissures. Mean transit times vary within several days and highly depend on flow conditions. Flow velocities increase by a factor of 2 to 5 under high flow conditions owing to high precipitation and snowmelt in early summer. Considering the thickness of the unsaturated zone, the fast drainage is evidence for the presence of well-developed karst structures in the Wetterstein limestone. The long tailing of the BTCs is a result of slightly lower flow velocities, dominating on the margins of the karst conduit and well-drained fissures. As expected, calculated water volumes in the karst network are relatively low. An intermediate-flow component has been identified, occurring along well-drained fissures and fractures of the aquifer. Mean transit times of the natural tracer are in the range of a few months. The drainage system benefits from diffuse infiltration. A significant amount of water is stored in these well-drained fissures and contributes a great proportion to the spring discharge. A slow-flow component is attributable to flow and storage in poorly-drained fissures and rock matrix of the karst system. Mean transit times of the natural tracer of a few years are assigned to that flow component. Furthermore, persistent tracer concentrations of artificial tracer prove water storage in poorly-drained fissures. Observed dilution effects after rain events are evidence for conduit-matrix exchange owing to gradient inversion. Poorly-drained fissures and rock matrix are assumed to be the dominant reservoir for water.

The wide range of transit-time distribution demonstrates vulnerability in terms of runoff characteristics and contamination on the one hand and a potential of buffering hydrologic variability on the other hand. Short transit times, between a few days and a few months, reflect low storage capacity, high variability of spring discharge and fast transport of potential pollutants to the spring. Long transit times in the range of years demonstrate high storage capability in poorly-drained fissures and therewith allow attenuation of extreme hydrologic events and retention of contaminants.

Acknowledgements

The authors thank Zhao Chen and several students for their support during the fieldwork and Christine Stumpp from the Helmholtz Zentrum München, Germany, for providing isotopic data from Mt. Zugspitze and helpful comments. We further thank Klaus Fröhlich, MaryLynn Musgrove and an anonymous reviewer for valuable review comments and discussions.

Chapter 6

Hydrogeology of an Alpine rockfall aquifer system and its role in flood attenuation and maintaining baseflow

Based on Lauber, U., Kotyla, P., Morche, D., Goldscheider, N.: Hydrogeology of an alpine rockfall aquifer system and its role in flood attenuation and maintaining baseflow. – Hydrology and Earth System Sciences, 18, 4437–4452, doi:*10.5194/hess-18-4437-2014.*

Abstract

The frequency and intensity of extreme hydrological events in Alpine regions is projected to increase with climate change. The goal of this study is to better understand the functioning of aquifers composed of complex alluvial and rockfall deposits in Alpine valleys and to quantify the role of these natural storage spaces in flood attenuation and baseflow maintenance. Geomorphological and hydrogeological mapping, tracer tests, and continuous flow measurements were conducted in the Reintal (German Alps), where runoff from a karst spring infiltrates a series of postglacial alluvial/rockfall aquifers. During high-flow conditions, groundwater velocities of 30m/h were determined along 500 m; hydrograph analyses revealed short lag times (5 h) between discharge peaks upstream and downstream from the aquifer series; the maximum discharge ratio downstream (22) and the peak recession coefficient (0.196 d^{-1}) are low compared with other Alpine catchments. During low-flow conditions, the underground flow path length increased to 2 km and groundwater velocities decreased to 13m/h. Downstream hydrographs revealed a delayed discharge response after 101 h and peaks damped by a factor of 1.5. These results indicate that alluvial/rockfall aquifers might play an important role in the flow regime and attenuation of floods in Alpine regions.

6.1 Introduction

Snowmelt is a major hydrologic component of flow regimes in Alpine regions; these regimes therefore are particularly sensitive to climate change (Barnett et al. 2005). The temperature in the Alps has increased 2°C since 1901, which is twice the average warming of the Northern Hemisphere (Auer et al. 2007). A shift of snow and precipitation patterns accompanied by higher precipitation in winter and poor snow storage are likely to substantially affect the timing and magnitude of summer discharge. Extreme events, such as floods and droughts, are expected to increase in frequency and intensity/magnitude (Bogataj 2007). Because of the high contribution of Alpine runoff to the total discharge of major streams in Europe, climate change will affect hydrology at lower elevations as well as in Alpine regions.

The assessment of potential effects of climate change on Alpine water resources requires an understanding of recharge and drainage processes. The geological and lithological setting is often complex and has major influence on recharge, storage, and discharge processes (Gremaud et al. 2009; Goldscheider and Neukum 2010). A thorough knowledge of the geologic framework and a conceptual model of the recharge area provide the basis for characterizing Alpine groundwater systems (Plan et al. 2009). To assess underground drainage properties in high-elevated catchments, hydrochemical classification and spring monitoring methods are applied. Such methods allow the characterization of flow components and spring responses to precipitation events so that transit times can be estimated and the presence of preferential flow paths determined (Maloszewski et al. 2002; Wetzel 2004; Mueller et al. 2013). Artificial tracer tests enable the determination of flow velocities, water volumes, and storage capacities within the Alpine aquifer (Goldscheider 2005; Gremaud et al. 2009; Finger et al. 2013). These parameters control the amount of quickflow and baseflow, and thus have a large influence on flood generation and baseflow maintenance.

To investigate discharge properties in Alpine headwaters, spring hydrograph studies have been conducted. It has been demonstrated that soil and vegetation (Badoux et al. 2006), topography (Merz and Blöschl 2009) and subsurface flow components (Zillgens et al. 2007) have major control over discharge response in individual headwater catchments. Discharge properties often used include the discharge response (the ratio between peak discharge and maximum precipi-

tation intensity), the unit conversion factor, and the catchment area (Blume et al. 2007). Furthermore, the discharge ratio, defined here as the ratio between peak discharge and initial discharge, and the time lag between precipitation and the discharge peak at springs and streams are considered (Haga et al. 2005). Stormflow and baseflow recession characteristics can further help to characterize fast and slow discharge components (Millares et al. 2009). The presence of low permeability bedrock, sparse vegetation, and high topographic gradients are likely to cause large amounts of surface runoff, which leads to high peak discharge of Alpine streams and rapid stormflow recession (Wetzel 2003). However, a steady amount of base flow, indicated by low baseflow recession, is particularly important for baseflow maintenance in dry periods and depends greatly on the geologic structure of the aquifer, e.g., the presence of permeable structures, a high effective porosity, or triple porosity such as occur in karst aquifers (Geyer et al. 2008). A detailed understanding of hydrogeological settings and discharge properties is necessary to construct vulnerability maps of Alpine regions, which are particularly affected by floods and droughts. For maintaining and protecting natural retention zones and for developing water management strategies, natural groundwater reservoirs in the Alps need to be understood. Furthermore, the feasibility of engineering works, e.g., dams, river channels, large-scale irrigation schemes, and energy production projects, is determined on the basis of the hydrogeological data. Such knowledge is required for effective flood management and the increase of water storage capacity (Viviroli and Weingartner 2008; Beniston et al. 2011).

Although there is a need to investigate the hydrogeology of Alpine aquifers and their drainage systems, information remains incomplete because of the poor accessibility of Alpine areas and the great effort required to obtain data. Only about 3% of the publications in hydrogeologic journals are related to alpine topics (Goldscheider 2011) and most of those studies focus on fractured and karstic aquifers, e.g., the studies cited above. Few studies deal with the hydrogeology of alpine alluvial/rockfall aquifers, which are frequently found in steep, high alpine valleys (Sinreich et al. 2002; Wassmer et al. 2004; Bichler et al. 2012). Because of the strong interaction between surface flow and subsurface drainage, alluvial/rockfall deposits are likely to influence the discharge pattern of the alpine catchment area. This might be especially important in karst catchments, where concentrated and rapid drainage through karst conduits results in large variability in discharge. To investigate this aspect and to contribute to a better understanding of Alpine aquifers, this study focuses on the hydrogeology of a rockfall aquifer

system in the Reintal (Wetterstein mountains, Germany). Detailed geomorphologic investigations of the sedimentary filling of the Reintal (Hoffmann and Schrott 2003; Schrott et al. 2006; Morche et al. 2007, 2008; Sass et al. 2007) provided the basis for this hydrogeological research, which includes a combination of tracer tests and hydrograph analyses.

The study had five major goals. The initial assessment of the catchment area involves (1) the development of a conceptual model and the identification of discharge components and (2) the characterization of discharge patterns under different flow conditions. A second step involves (3) the determination of drainage parameters of the alluvial/rockfall aquifer and (4) the quantification of discharge characteristics of the system. The final goal of the study was (5) the evaluation of effects on flood buffering and baseflow maintenance of the alluvial/rockfall aquifer system.

6.2 Field site

6.2.1 Geography and Geology

The Wetterstein mountains are located in the Bavarian Alps near the border between Germany and Austria (Fig. 6.1). They consist of three mountain ridges that form some of the highest summits in Germany, including the Zugspitze (2962 m a.s.l.). The deeply incised Reintal has steep mountain slopes and a topographic relief of up to 2000 m between the valley floor and the summits. Above 2000 m a.s.l., vegetation is sparse and bare rocks dominate the landscape. The Zugspitzplatt cirque is still partially covered by vestigial glaciers with a total extent of about 32.6 ha (in 2009).

The geological and lithological setting of the Wetterstein mountains is dominated by Triassic Wetterstein limestone, which is as much as 1000 m thick and forms the main karst aquifer (Fig. 6.2). The underlying strata are comprised of a sequence of marl and well-bedded limestone, the Partnach and Alpine Muschelkalk formations. The folded strata form two large synclines and one anticline, which appear as valleys and ridges. The fold axes trend W–E and plunge to the east (20–35).

Since the Eocene, much of the region has been uplifted almost steadily to a high mountain massif. The exposure of the limestone established the basis for karstification and intense weathering, including gravitational erosion. Karstification is particularly high at the cirques, where topographic gradients are lower and underground drainage dominates. Thus, a well-developed karst conduit system is present at the Zugspitzplatt cirque. In contrast, only small surface karst structures, such as karren, are developed along steep mountain ridges as karren and rillenkarren, are developed along steep mountain ridges as gravitational erosion and frost wedging occur along numerous fissures and fractures.

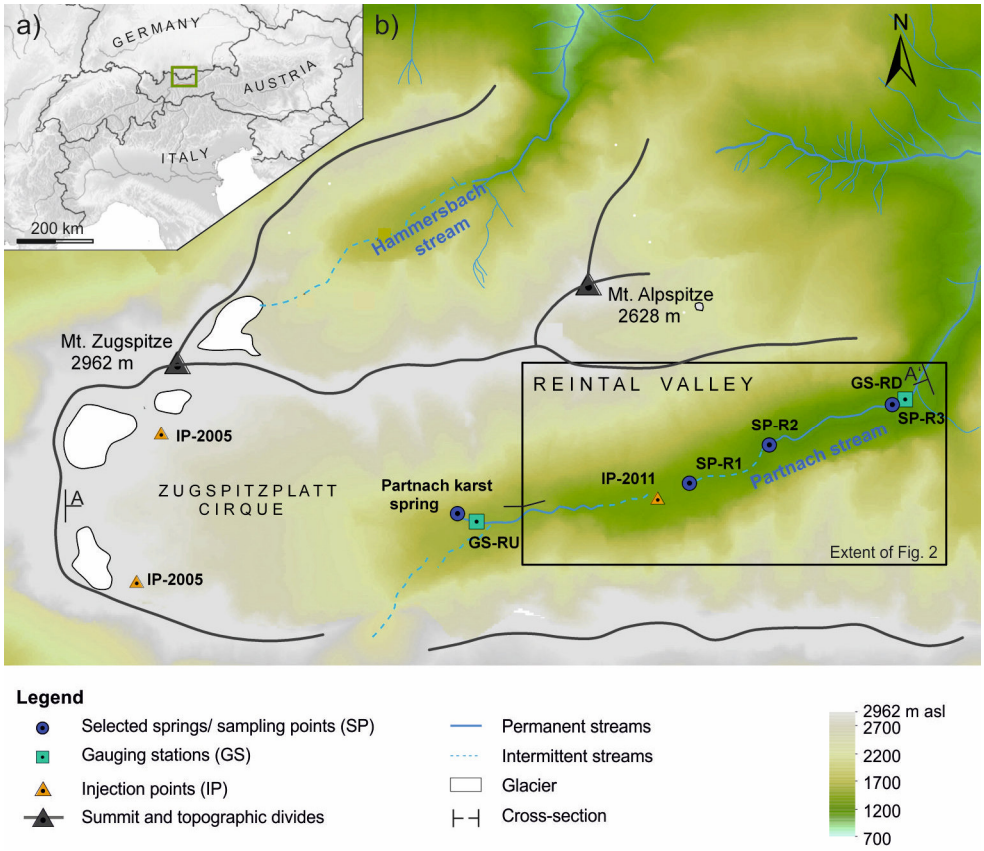

Figure 6.1: (a) Map of the study site (Wetterstein Mountains) in the German Alps; (b) Wetterstein Mountains, including Germany´s highest summit (Mt. Zugspitze), the large Zugspitzplatt cirque, and the high-alpine Reintal valley extending to the east. Tracer injections at the Zugspitz cirque (IP-2005) were conducted by Rappl et al. (2010); IP-2011 is part of this study. GS-RU and GS-RD are gauging stations in the Reintal valley, upstream (RU) and downstream (RD) from the alluvial/rockfall aquifers. The area in the rectangle is shown in detail in Fig. 6.2. A detail of the cross-section A–A' is provided in Fig. 6.4.

During the glaciation in the Quaternary Period, strong glacial erosion caused the present shape of the valleys, including sequences of cirques. After the retreat of glaciers and the melting of

permafrost, several rockslides occurred during the Holocene along the steepened Alpine valley slopes (Haeberli and Beniston 1998). Two major rockslides occurred about 200 and 500 years ago in the Reintal valley (Schmidt and Morche 2006). Mountain lakes formed upstream of the natural rockfall dams, but were gradually filled by sediment. The last remnant of the lower lake disappeared during a high-flow event with associated sedimentation in 2005 (Fig. 6.3). The alluvial plains and rockfall deposits thus have created a series of two alluvial/rockfall aquifers about 2-km long down the valley (Figs. 6.2 and 6.4). The Quaternary sediments are comprised talus sheets and cones, debris cones, rockfall deposits, alluvial fans, avalanche deposits, moraines, and fluvial gravel (Schrott et al. 2006) (Fig. 6.2).

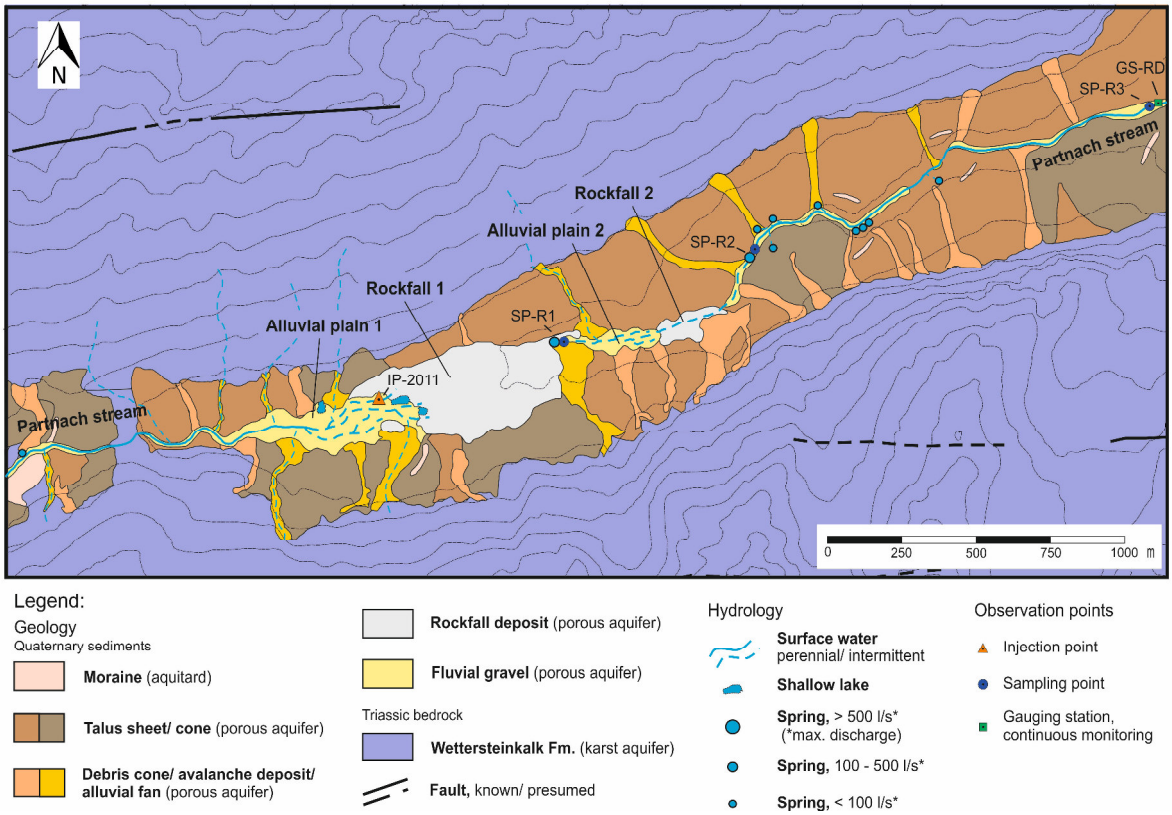

Figure 6.2: Hydrogeologic map of the Reintal valley covered with postglacial sediments, including alluvial plains and rockfall deposits (Schrott et al. 2006). The occurrence and location of surface streams and springs depends on hydrologic conditions. A longitudinal profile is provided in Fig. 6.4.

As a result of gravitational mass movement, the grain-size spectrum of the rockfall deposits, talus sheets, and cones covers a wide range, including large blocks with edge lengths of several meters. The coarse-grained sediments consist mainly of Wetterstein limestone, and the unsorted components form well-drained parts of the alluvial/rockfall aquifer system (Fig. 6.2).

The alluvial plains consist of fluvial gravel, transported by the Alpine stream and surface runoff from steep slopes along the valley. Because of the reduced flow velocity and transport force, the gravel was deposited behind the rockfall dams (Morche and Schmidt 2005). The sediments contain coarse-grained delta sediments and fine limnic sediments developed in proximity to the rockfall deposits. At the surface of the alluvial plain, braided river systems have developed, the location of which shifts following flood events. The unconsolidated alluvial deposits are part of the well-drained alluvial/rockfall aquifer and surface streams infiltrate as a result of the high permeability.

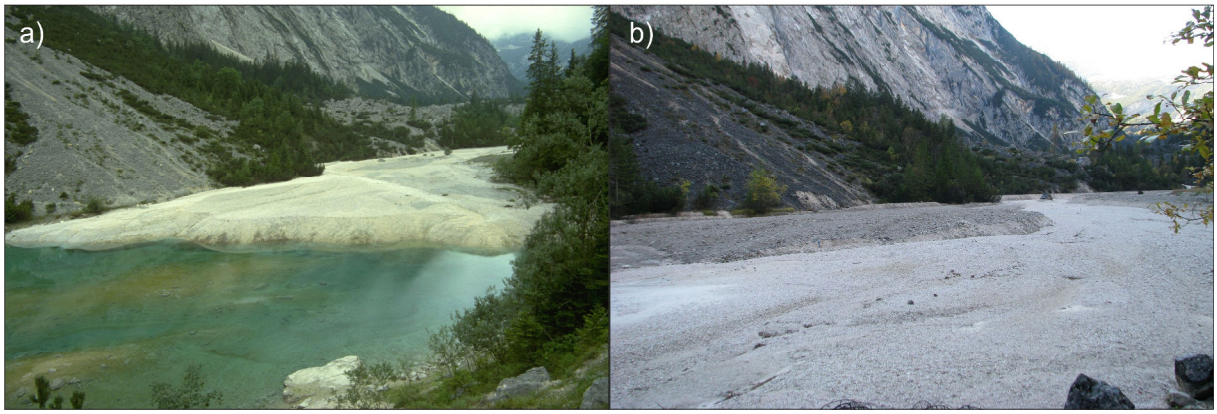

Figure 6.3: View of the second alluvial plain: a) an ephemeral mountain lake created by a natural rockfall dam; b) the same area filled with sediment after a high precipitation event in 2005.

6.2.2 Hydrology and Hydrogeology

The headwater in the Reintal valley, the Partnach stream, forms a tributary of the Loisach river north of the Wetterstein mountains (Fig. 6.1). Discharge is comprised of meltwater from the glaciers, snow, and precipitation. Glacial and snow meltwater contribute about 30% of the annual spring discharge (Wetzel 2004).

In the upper valley, the stream is fed mainly by the Partnach spring (Fig. 6.1). With a mean discharge of 1.2 m^3/s between May and November (2005-2011) and a recorded maximum discharge of 17 m^3/s (2005, Morche et al. 2007), this karst springs is among the largest in the German Alps. The large discharge variability of the karst spring indicates that a well-developed karst conduit system exists in the catchment area. In the lower valley, the hydrology is largely controlled by the Quaternary deposits at the bottom of the valley (Fig. 6.2). As surface water

crosses the alluvial plains, it infiltrates the alluvial sediments and rockfall deposits. Downstream from each alluvial/rockfall deposit is a spring that drains the alluvial/rockfall aquifer system: one spring is intermittent (SP-R1) and one is perennial (SP-R2) (Fig. 6.4). The spring SP-R2 is located in the river bed and its discharge immediately mixes with surface flow if the river is flowing. Several more springs discharge from the river bed downstream from the rockfall deposits. The presence of these springs is attributed to the decrease in the thickness of the Quaternary deposits and the narrowing of the river bed. As a result, stream discharge increases substantially in this part of the valley. The total discharge from the Reintal valley is measured at the downstream end of the valley (gauging station GS-RD, Fig. 6.1). The sampling point SP-R3 is located at the gauging station and comprises groundwater from the alluvial/rockfall deposits and surface runoff. The mean annual discharge associated with the 28 km^2 catchment area during 2005–2011 is about 1.8 m^3/s.

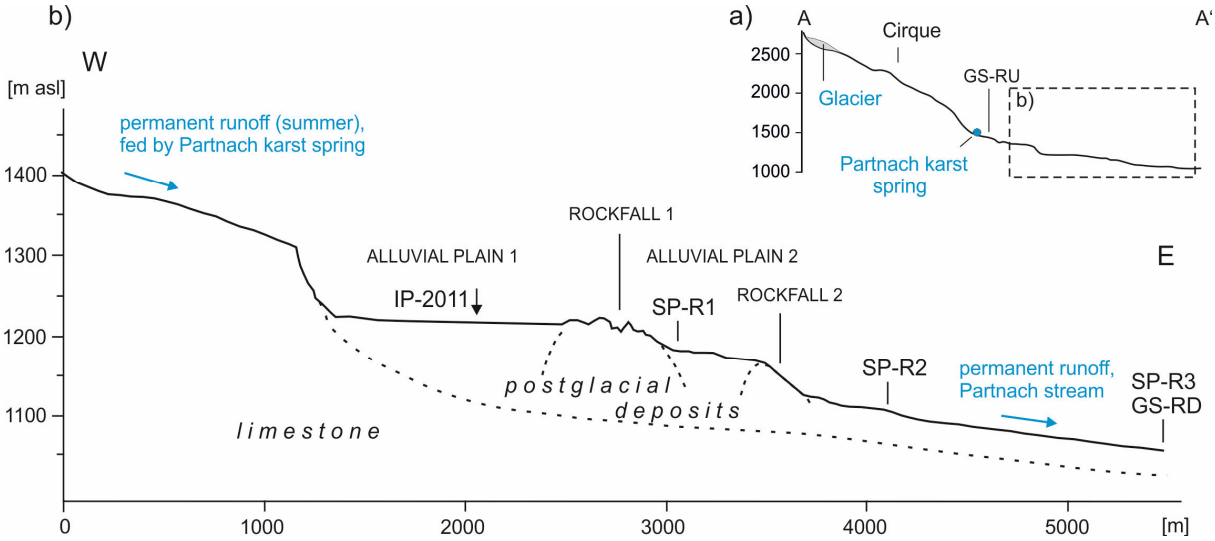

Figure 6.4: (a) Overview over the Reintal valley indicating the major hydrologic inflow from the glacier and the karst spring. (b) Schematic diagram of the alluvial/rockfall aquifer system in the Reintal valley. Although perennial flow exists upstream and downstream, several sinks and springs between the alluvial/rockfall deposits result in intermittent discharge. Cross sections are vertically exaggerated.

6.3 Methods

6.3.1 Artificial tracer tests

To investigate the alluvial/rockfall aquifer system in the valley, a tracer test with 5 kg of the fluorescent dye sodium naphthionate (CAS 130-13-2) was conducted on 19 July 2011. The

injection was performed after several days of rain, which resulted in high discharge at all springs in the valley. Where the stream flows through the upper alluvial plain, it forms a braided river system that completely infiltrates the coarse-grained alluvial/rockfall deposits at several swallow holes (Fig. 6.2). The tracer was injected into one of the numerous swallow holes near the lower end of the alluvial plain, where the infiltration rate into the rockfall deposits was about 6 L/s. The dye was dissolved in a 20 L canister at the injection site and the tracer solution was injected instantaneously. Observation points were located downstream in the valley: at the springs draining the alluvial/rockfall masses (SP-R1 and SP-R2) and further downstream at the outlet of the valley (SP-R3) (Fig. 6.4). Although the samples collected at SP-R1 represent groundwater discharge at the spring, samples at SP-R2 and SP-R3 also contain surface water. Groundwater discharge from spring SP-R2 could only be sampled under low-flow conditions, when the river bed was dry. If the river was flowing, samples from this sampling station were a mixture of spring water and surface runoff. At SP-R3, a mixture of groundwater and surface water was sampled in the stream and enables calculation of tracer recovery from the whole aquifer system. At the spring closest to the injection point (SP-R1), water samples were collected every 30 min during the first 10 h following tracer injection. In the following days, as many as six water samples were collected per day. The final samples were collected three weeks after injection.

Two spectro-fluorimeters (Perkin Elmer, LS 50 B and LS 55) in the hydrogeology laboratory of the Karlsruhe Institute of Technology were used to measure tracer concentration in water samples, using the synchronous-scan-method. Tracer recovery was calculated using data from springs and gauging stations.

6.3.2 Discharge measurements

The two principal gauging stations in the valley are located at the Partnach karst spring upstream from the alluvial/rockfall deposits (site GS-RU) and at the outlet of the alluvial/rockfall aquifer system (site GS-RD) (Fig. 6.1). Water levels were measured every 15 min during observation periods with dataloggers DL 8.4 (EBRU), Orphimedes, and Orpheus K (Ott Hydrometrie) (Schmidt and Morche 2006). Measurements were collected from late spring until late autumn, as snow, ice, and avalanches inhibit measurement in the winter season. Data from 2002–2011 were evaluated, but no measurements were conducted at GS-RU in 2009. Discharge

was measured using a current meter (Ott C2) for a range of flow conditions. At other observation points in the valley, e.g., SP-R1 and SP-R2, discharge was measured manually by the salt-dilution method. Using the dilution technique, sodium chloride was added to the discharge, and the electrical conductivity, i.e., the dilution, was measured downstream, enabling calculation of the discharge (Leibundgut et al. 2009).

6.3.3 Data analysis

All breakthrough curves (BTCs) from the tracer tests were analyzed quantitatively. The time of first detection (t_0), maximum flow velocity (v_{max}), peak transit time (t_{peak}), and peak flow velocity (v_{peak}) were directly determined from the BTCs. Mean flow velocities (v) and dispersion coefficients (D) were quantified using the analytical advection-dispersion model (ADM) implemented in the CXTFIT software (Toride et al. 1999) (Eq. 6.1).

$$\frac{\delta c}{\delta t} = D\frac{\delta^2 c}{\delta c^2} - v\frac{\delta c}{\delta x} \qquad (6.1)$$

The model calculates one-dimensional flow of the tracer indicated by its concentration (c) at a given distance (x) in the direction of flow. The analytical equation is solved by assuming homogeneous flow profiles, a uniform and unidirectional flow field that is constant in time and space, and constant flow parameters (van Genuchten et al. 2012). An inverse modelling tool of the ADM provides best estimates of the two flow parameters (v, D) by fitting a modeled BTC to measured values.

Using additional information from discharge measurements, recovery was calculated according to Käss (2004). Water volume (V) was estimated by multiplying the mean discharge (Q_{mean}) and the mean transit time of the tracer (t_{mean}) (Field and Nash 1997).

In analyzing hydrographs, the best correlation of water level (h) and discharge (Q) is determined by fitting an exponential regression function with the two adjusting variables a and b (Eq. 6.2):

$$Q = a \cdot e^{bh} \qquad (6.2)$$

Coefficients of determination are greater than 0.72 and the standard error is smaller than 0.41 (Table S1 in the Supplement). To compare discharge characteristics from upstream and downstream of the series of alluvial/rockfall aquifers, hydrographs of the years 2006 and 2011 are

presented in this paper as they have the most continuous records. The year 2006 is further characterized by extreme flow conditions. Annual discharge of the catchment is lowest of all observed years and an extreme precipitation event causes extreme high-flow conditions in August. Monthly mean discharge values of 2002 to 2011 are provided in Table S2.

Discharge was analyzed for all precipitation events that caused clear discharge peaks at the gauging stations. Rainfall events that occurred under very unstable discharge conditions, i.e., discharge fluctuations caused by snowmelt or long-lasting rainfall events, could not be analyzed because the occurrence of diffuse discharge peaks made it impossible to select related input and output signals properly. Precipitation data with a sampling interval of 6 h were obtained by Deutscher Wetterdienst (DWD) at the summit of Mt. Zugspitze. As a consequence, the lag time between peak rainfall and peak discharge cannot be quantified at a higher resolution than 6 h. Initial discharge for an event (Q_i) is defined as the discharge rate before the increase began and peak discharge (Q_P) is defined as the discharge maximum. The discharge response ($Q_P/(P_{peak} \cdot f_c \cdot A)$) is calculated by dividing the amount of peak discharge (Q_P, in m^3/s) by the maximum precipitation intensity (P_{peak}, in mm/6h), a unit conversion factor (f_c) that converts discharge units from m^3/s to mm/6h, and the catchment area (A, in km^2) (Blume et al. 2007). The increase of discharge after a precipitation event is described by the discharge ratio Q_P/Q_i. Additionally, the lag time between discharge peaks upstream (site GS-RU) and at the outlet of the catchment (site GS-RD) was determined to assess discharge characteristics of the aquifer system.

Discharge response characteristics were described quantitatively by transfer functions (Asmuth and Knotters 2004). This method can be applied to input signals that are transferred through a system and that result in distinctive output signals dispersed in time. In this case, the transferred signal can be described by an impulse-response function with a lognormal distribution (Eq. 6.3) (Long and Mahler 2013).

$$Q_t = Q_i + \frac{A_{out}}{t\omega\sqrt{2\pi}} e^{-\frac{\left[ln\frac{t}{t_m}\right]^2}{2\omega^2}} \qquad (6.3)$$

where A_{out} is a scaling coefficient that quantifies the area under the curve, and t_m and ω describe mean transit time and its variance. In this study, discharge peak upstream from the alluvial/rockfall aquifer system (GS-RU) was used as the input impulse (t = 0). The output signal downstream from the alluvial/rockfall deposits (GS-RD) occurring at time t after the input impulse was fitted with the function (Q_t, Eq. 6.3). Because additional surface runoff from steep slopes that occurs under mean- to high-flow conditions can interfere with the original input signal, only selected discharge responses under low-flow conditions with one clear input and one clear output signal were analyzed.

To quantify aquifer properties under stormflow and baseflow conditions, recession coefficients (α) were determined from hydrographs upstream (karst drainage) and downstream from the alluvial/rockfall aquifers. The falling limb of the hydrographs represents drainage of groundwater reservoirs that exhibit distinct exponential flow rates for each groundwater reservoir (Bonacci 1993; Bailly-Comte et al. 2010). Recession curve analyses were done using an exponential function (Eq. 6.4):

$$Q_i = Q_0 \cdot e^{-\alpha t} \qquad (6.4)$$

where Q_0 is the initial spring discharge and t is the time step following the decline of spring discharge (Q_t). The recession curve was fitted separately for stormflow and baseflow sections of the hydrograph to obtain the recession coefficient α. Because of the strong linear correlation on a semi-logarithmic plot ($R^2 > 0.9$), the use of Eq. 6.4 was justified (Zillgens et al. 2007).

6.4 Results and Discussion

6.4.1 Conceptual model

The conceptual model of the Alpine valley consists of one karst aquifer and a series of two alluvial/rockfall aquifers. In the upper valley, the karst spring is the principal contributor to stream discharge (Fig. 6.5). All meltwater from glacial ice, snowmelt, and all precipitation in the highly karstified cirque drain through subsurface flow paths to the Partnach karst spring. Tracer tests have shown fast drainage along well-developed karst conduits with linear mean flow velocities of up to 104 m/h (Rappl et al. 2010). The lower valley is comprised of a series of two alluvial/rockfall aquifers (Fig. 6.5), each consisting of an alluvial plain and a rockfall

deposit. The alluvial/rockfall aquifers are linked and characterized by a substantial thickness of postglacial sediments. All discharge from the karst spring infiltrates the first alluvial/rockfall aquifer because of the high permeability of the rockfall deposits (Fig. 6.6). Several sinks and sources, including SP-R1 and SP-R2, exist in the area of the aquifers; the number and location depend on flow conditions and water levels. Total discharge increases towards outlet of the alluvial/rockfall system because of the decreasing thickness of the Quaternary fill and groundwater discharge into the surface stream.

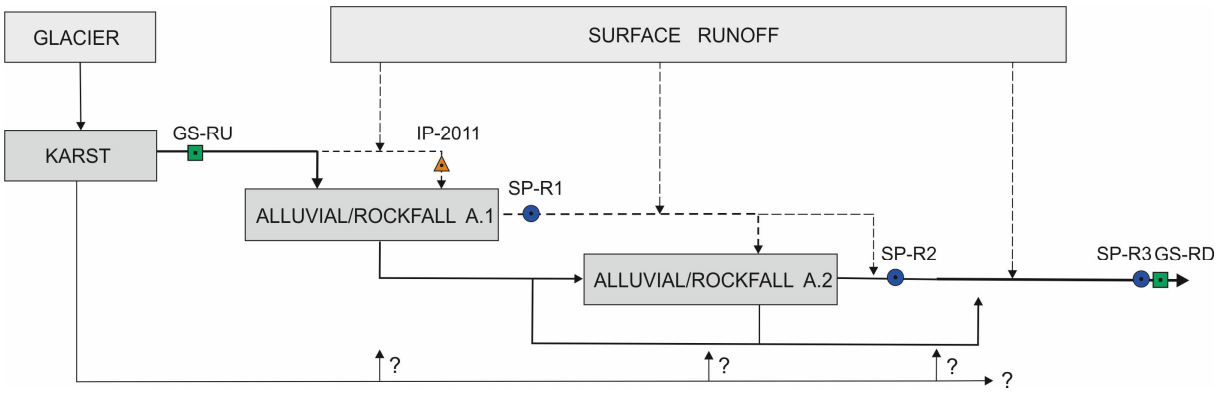

Figure 6.5: Conceptual model of the series of Alpine aquifers in the Reintal valley, which consists of a karst system and two alluvial/rockfall aquifer systems (i.e., alluvial/rockfall A.1 and A.2). Dashed lines indicate ephemeral discharge, solid lines indicate perennial discharge.

Hydraulic connections between the karst system and the alluvial/rockfall aquifer along the valley are of minor hydrologic importance (Fig. 6.6). Infiltration from the alluvial/rockfall aquifer into the karst aquifer can be excluded, as discharge downstream from the alluvial/rockfall deposits (site GS-RD) is larger than at the upstream at site GS-RU. In contrast, Sinreich et al. (2002) demonstrated that the alluvial/rockfall aquifer in the Schwarzwasser valley (Austrian Alps) is drained by the underlying karst aquifer because of a well-developed karst drainage network. In the Reintal valley, a rapid glacial deepening of the valley inhibited the karstification of the limestone below the valley floor.

Here we define low-flow conditions as those under which all discharge from the Partnach karst spring infiltrates the alluvial/rockfall aquifer and follows a 2-km long subsurface flow path until it discharges at SP-R2 at the lower end of the alluvial/rockfall aquifer system (Fig. 6.6). Low-discharge conditions generally occur when baseflow is less than 0.8 m^3/s at site GS-RU and 1.8 m^3/s at site GS-RD. Peak discharge after precipitation events at GS-RU rarely exceeds

2.3 m^3/s. Because the water table is low, there is no flow from spring SP-R1. At low water levels, spring SP-R2 is situated in the river bed as much as 600 m downstream from the alluvial/ rockfall deposits (Morche et al. 2007) (Fig. 6.6). There is no surface runoff from steep slopes of the valley. Low-flow conditions generally occur in late summer, autumn, and winter, when there is little precipitation and no meltwater.

Moderate-flow conditions are characterized mainly as a transition between low- and high-flow and therefore often occur only for a short period of a few hours to a few days. Because the water table is higher than during low-flow conditions, part of the water discharges directly downstream from the first alluvial/rockfall deposits at spring SP-R1 after traveling along a short subsurface flow path of about 500 m (Fig. 6.6). Until 2005, there was a small ephemeral mountain lake on the second alluvial plain, which functioned as a water reservoir and sediment trap (Schmidt and Morche 2006) (Fig. 6.3). Today, discharge from SP-R1 infiltrates into the second alluvial/rockfall aquifer after traveling along a short surface flow path, and drains underground to spring SP-R2 (Fig. 6.6). Because the water level is higher than during low-flow conditions, spring SP-R2 discharges directly downstream from the alluvial/rockfall deposits. During moderate-flow conditions, the steep slopes along the valley contribute a few tens of L/s surface runoff, which is only a small proportion of total stream flow.

High-flow conditions occur after intense or prolonged precipitation events and during peak snow melt in early summer. Because the water table is high, a substantial proportion of the groundwater discharges directly downstream from the first alluvial/rockfall deposits at spring SP-R1, where discharge can exceed 1 m^3/s. While some of the water infiltrates the second alluvial/rockfall aquifer, there is also surface flow over the second alluvial/rockfall deposits (Fig. 6.6). Surface flow and subsurface drainage converge and mix at spring SP-R2. After large precipitation events, fast-flowing streams and torrents from steep slopes along the valley deliver surface runoff. Most high-flow conditions have been observed when peak discharge rates exceed 2.3 ± 0.2 m^3/s at site GS-RD.

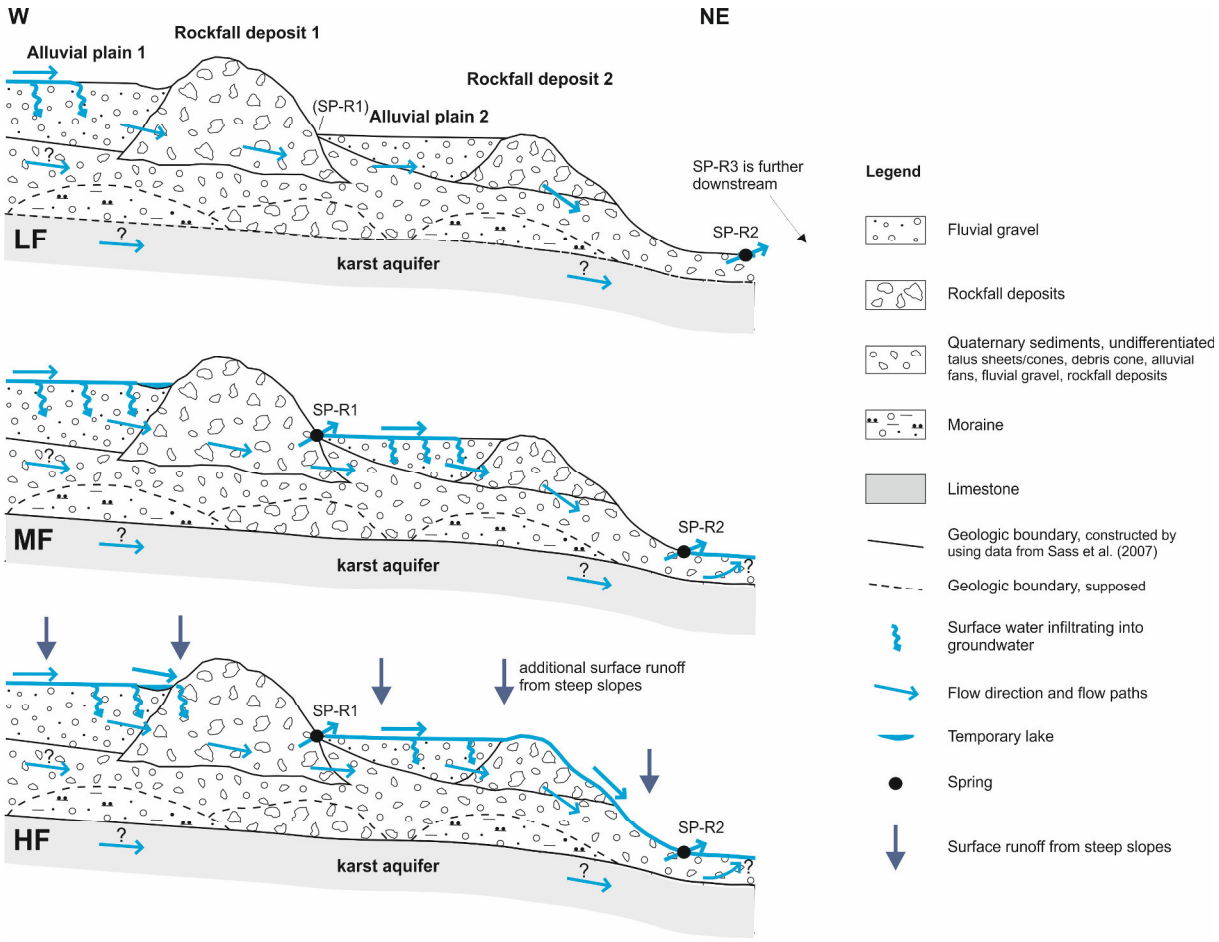

Figure 6.6: Conceptual model of surface and groundwater flow in the series of alluvial/rockfall aquifers of the Reintal valley under low-, moderate-, and high-flow conditions (LF, MF, and HF, respectively. The tracer injection in 2011 was done under high-flow conditions. The length of the section is 1.5 km and is vertically exaggerated.

6.4.2 Drainage properties

The overall results of the tracer test enabled insights into drainage properties of different parts of the alluvial/rockfall system and proportions of flow paths to the total discharge along the valley. The naphthionate was detected at all three sampling points: the two springs SP-R1 and SP-R2 and the outlet of the aquifer system SP-R3 (Fig. 6.4, Table 6.1). High-flow conditions occurred during the first three days after the injection (Fig. 6.6).

The tracer breakthrough curve (BTC) at SP-R1, 500 m downgradient from the injection site, has one clear peak and a short tail (Fig. 6.7a). The tracer was first observed 8 h after the injection, and the tracer peak concentration of 52.1 µg/L was measured 16 h after the injection. The linear peak flow velocity was about 31 m/h. A discharge of 440 L/s was measured during the first 3 days, resulting in a recovery of 30% of the tracer.

At spring SP-R2, the tracer was first detected after 23 h (Fig. 6.7b), and the tracer peak concentration of 21.8 µg/L was measured 28 h after injection. The linear peak flow velocity was 53 m/h. During the first 75 h, the BTC had one sharp peak followed by a decrease of concentration down to 0.6 µg/L. 117 h after injection, the concentration rose slightly to 1.5 µg/L, forming a second, small peak (Fig. 6.7b, Table 6.1). During the first half of the tracer breakthrough (about the first 75 h), flow conditions were high and surface flow occurred downstream from SP-R1 (Fig. 6.6). The main peak of the breakthrough curve at SP-R2 is therefore mostly related to surface flow from SP-R1. However, after 75 h, moderate-flow conditions were reached and all water from SP-R1 infiltrated (Fig. 6.6). We therefore interpret the second increase in tracer concentration as a separate peak related to the peak in subsurface flow. The measured concentration of 1.5 µg/L is 2 to 3 times greater than the values measured before (0.56 µg/L) and after (0.78 µg/L) the peak and thus larger than the measurement error. The natural fluorescent background values of the sample were as low as the values of the samples before and after the second peak so that influence by organic matter content and turbidity can be excluded. Equally, we exclude remobilization of tracer after smaller precipitation events because discharge at the gauging stations decreased gradually. Assuming that the second peak is related to subsurface flow, the linear subsurface flow velocity was 13 m/h and thus substantially less than the linear surface-flow velocity of 53 m/h. During the main part of the tracer breakthrough, mean discharge at this sampling point was about 580 L/s, and tracer recovery was about 21 %.

At site SP-R3, the outlet of the system, the maximum tracer concentrations of 4 µg/L was measured 66 h after injection (Fig. 6.7c). The linear peak flow velocity was 48 m/h. The shape of the tail at SP-R3 indicates the presence of the second peak at this site as well (Fig. 6.7c). Because of high dilution and high dispersion along the surface flow path, the second peak is small but recognizable. The sampling point is about 3.1 km from the injection point. The mean discharge at this site was about 2500 L/s, and tracer recovery was 59%.

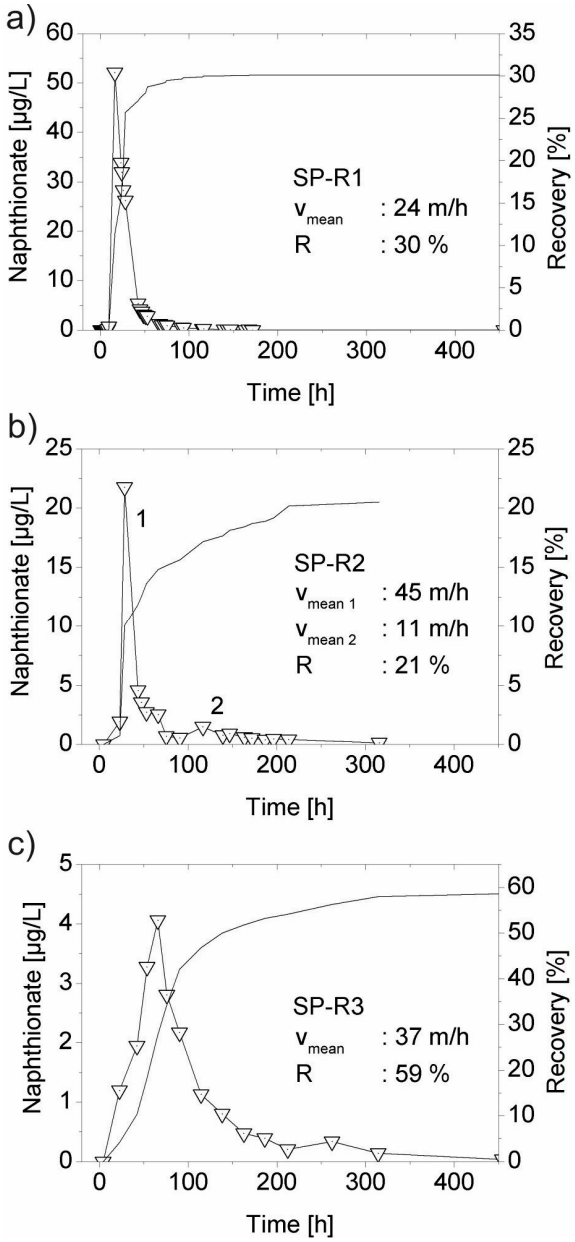

Figure 6.7: Naphthionate breakthrough curves at sampling points SP-R1 (a), SP-R2 (b) and SP-R3 (c) in the Reintal valley. Sampling points were located in the river bed and show dispersion of the tracer downstream the injection point. Total recovery was measured at the outlet of the system at SP-R3.

Hydraulic parameters of the system were determined by ADM modeling of the observed BTCs at the observation points. A dispersion of 630 m^2/h was obtained from data for spring SP-R1 and applies to flow through the high-permeability part of the rockfall aquifer. Results from sites SP-R2 and SP-R3 are influenced by surface flow and are not discussed further. However, high dispersion values for site SP-R3 indicate highly turbulent flow of the stream.

Table 6.1: Results of the 2011 tracer test in the Reintal valley.

		SP-R1	SP-R2	SP-R3
Linear distance	[m]	500	1500	3150
Mean discharge[a]	[L/s]	440	580	2500
First detection	[h]	8.4	23.0	22.5
Max. flow velocity	[m/h]	59.7	65.2	140
Peak transit time (1st peak)	[h]	16.3	28.4	65.8
Peak flow velocity (1st)	[m/h]	30.6	52.8	47.8
Max. concentration (1st)	[µg/L]	52.1	21.8	4.1
Peak transit time (2nd peak)	[h]	-	116.8	262.2
Peak flow velocity (2nd)	[m/h]	-	12.8	12.0
Concentration (2nd)	[µg/L]	-	1.5	0.3
Recovery	[%]	30.0	20.5	58.7
Water volume	[m^3]	25 883	-	-
Mean transit time (1st peak)	[h]	21.3	33.7	85.6
Mean flow velocity (1st)	[m/h]	23.5	44.5	36.8
Dispersion (1st)	[m^2/h]	630	806	15 700
R^2	[-]	0.966	0.945	0.916

[a] mean discharge during main tracer breakthrough

The flow velocities obtained are attributed to different parts within the aquifer system, and tracer recovery demonstrates discharge proportions of flow paths. The flow velocities of 30 m/h along the short flow path from IP-2011 to SP-R1 are very high for a porous aquifer and are attributable to flow through very coarse-grained rockfall deposits with numerous large limestone blocks. Even higher flow velocities of 65 to 81 m/h were measured by a tracer test in an alpine rockfall deposit (Schwarzwasser valley, Austria) and attributed to mechanical and dissolutional enlarged flow paths through large limestone blocks (Sinreich et al. 2002). The tracer recovery of 30% at site SP-R1 indicates that only about 1/3 of spring infiltration discharges directly downgradient from the first alluvial/rockfall deposits. Along the long subsurface flow path to SP-R2, substantially lower flow velocities of 13 m/h occur because flow passes through alluvial gravel. The decreased recovery of 21% at SP-R2 in comparison with recovery at SP-R1 is related to infiltration processes upstream at the alluvial/rockfall aquifer under moderate- to high-flow conditions (Fig. 6.6). The total recovery of the tracer downstream at SP-R3 reaches

59% because stream discharge increases steadily in a downstream direction to the outlet and there are further inflows from the Quaternary sediments into the stream. The tracer test thus demonstrated that there is a large amount of water draining underground.

The total tracer recovery of 59% is well documented with samples collected during the main breakthrough at SP-R3 and continuous discharge measurements at GS-RD. As all of the water from the upper valley drains towards SP-R3, a high recovery was assumed. The unrecovered tracer might attributable to microbial or photo decay, but might also be stored in the alluvial/rockfall aquifers. Storage of groundwater in the alluvial/rockfall system also is indicated by discharge analysis (section 6.4.3). In that case, a difference of about 41% would indicate a relatively large storage capacity of the series of Alpine alluvial/rockfall aquifers.

6.4.3 Discharge characteristics

The hydrographs in the Reintal valley show distinct annual patterns because of the snowmelt-controlled discharge regime. In 2006, discharge begins to increase in mid-April and reaches a characteristic discharge maximum of about 7 m^3/s at the end of June, corresponding to the period of maximum snowmelt (Fig. 6.8). Daily discharge fluctuations of about 100 L/s are attributed to diurnal temperature changes and meltwater production from the glacier and snow fields (Fig. 6.8 and S1 in the Supplement). There are several discharge peaks related to moderate to large precipitation events. Maximum discharge rates of 8 m^3/s at GS-RU and 16 m^3/s at GS-RD were measured after an extreme precipitation event in 2006. With decreasing snowmelt contribution, discharge decreased gradually to 0.5 m^3/s during the second half of 2006 and 2011. As the valley is largely inaccessible during winter months, there has been only one observation (March 2007) that the karst spring is not perennial. The stream at the outlet of the system (site GS-RD) has not been observed to run dry during winter months.

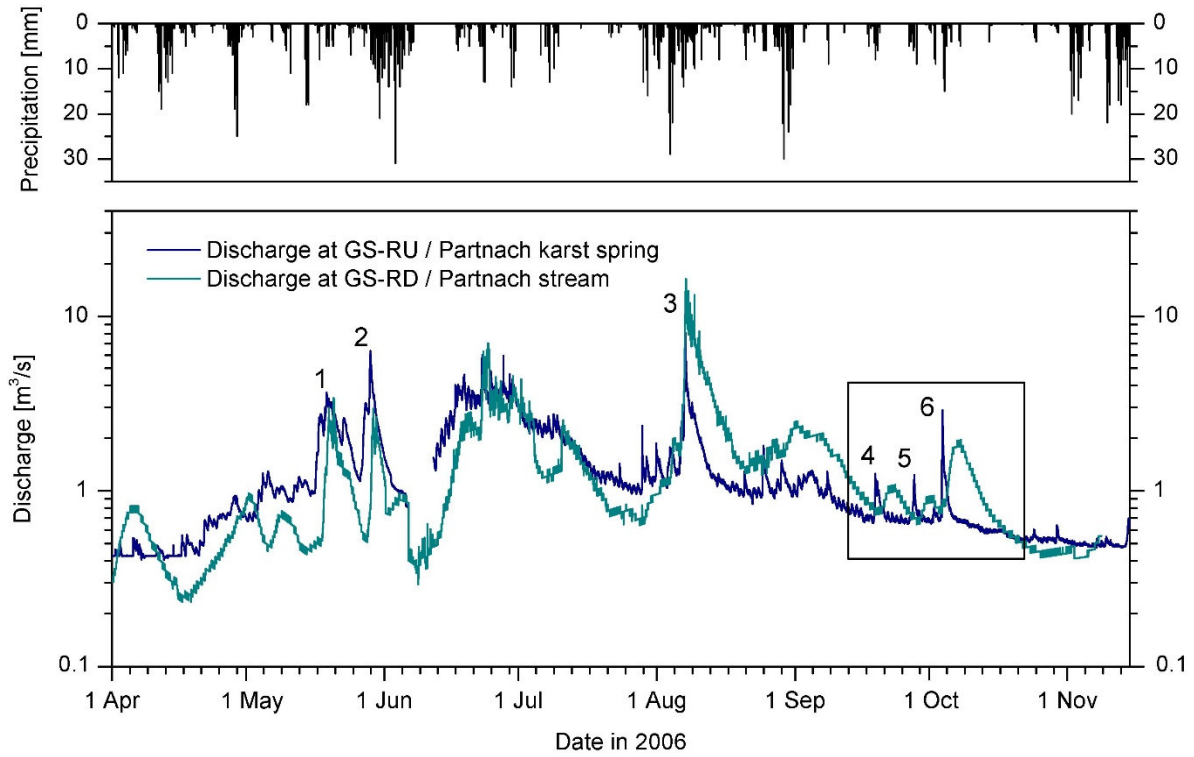

Figure 6.8: Hydrographs at the upstream (Partnach karst spring, site GS-RU) and downstream (Partnach stream, site GS-RD) gauging stations in the Reintal valley in 2006. Precipitation data (6-h time step) was obtained from the weather station at Mt. Zugspitze (DWD).

Hydrologic flow conditions and water levels in the alluvial/rockfall aquifer have a substantial influence on discharge characteristics in the valley. Differences between the hydrographs upstream and downstream from the alluvial/rockfall aquifers depend on surface and subsurface drainage between the two sites. The input signal at the karst spring shows that sharp discharge peaks occur less than 6 h following precipitation events, reflecting concentrated drainage and pressurized flow through a well-developed karst system. In summer (May–August), the sharp input signal at site GS-RU results in rapid and marked discharge responses downstream from the alluvial/rockfall aquifer systems (site GS-RD) (peaks 1–3 and peaks 7–9, Figs. 6.8 and S1). Short lag times of a few hours are associated with precipitation events occurring at high water levels, when subsurface flow paths are short and surface discharge downstream from the upgradient rockfall deposits results in rapid transit of the flood wave (Figs. 6.6 and 6.8). Piston flow effects in the saturated alluvial/rockfall aquifer further accelerate the process. An extremely fast response time of less than 5 h also can be attributed to surface runoff and torrents from steep slopes along the valley (Fig. 6.6).

Recharge events occurring during low-flow conditions result in distinctive wide discharge peaks downstream from the alluvial/rockfall deposits. In spring and autumn, sharp discharge peaks upstream cause delayed flood waves downstream that span several days (peaks 4–6 and 10–11, Fig. 6.8, 6.9 and S1). The mean lag time between maximum discharge at the karst spring (GS-RU) and the outlet of the alluvial/rockfall aquifer (GS-RD) determined by fitting the impulse-response function (Eq. 6.3) is 101 h (Table 6.3). Substantial flood damping is indicated by a decrease in maximum discharge of a factor of 1.5 as the average of three responses (Fig. 6.9). The strong damping effects are attributable to infiltration associated with low water levels, resulting in a long subsurface flow path of up to 2 km and storage within the aquifer (Fig. 6.6). During prolonged periods of low-flow conditions, e.g., during dry periods or in late autumn, flow velocities are expected to decrease as groundwater levels fall and discharge decreases. Lag times determined from the hydrographs can increase to values of as much as 190 h in extreme dry years, e.g., 2003 (Table S3). On the basis of 38 discharge events that occurred during 2002–2011, lag times of about 5, 35, and 101 h between the input at GS-RU and output signal at GS-RD are dominant (Fig. 6.10 and Tables 6.2 and S3). While there is no direct correlation between lag times and individual hydrometeorological parameters (Fig. S2), lag times are related to the hydrologic flow conditions in the alluvial/rockfall aquifer system.

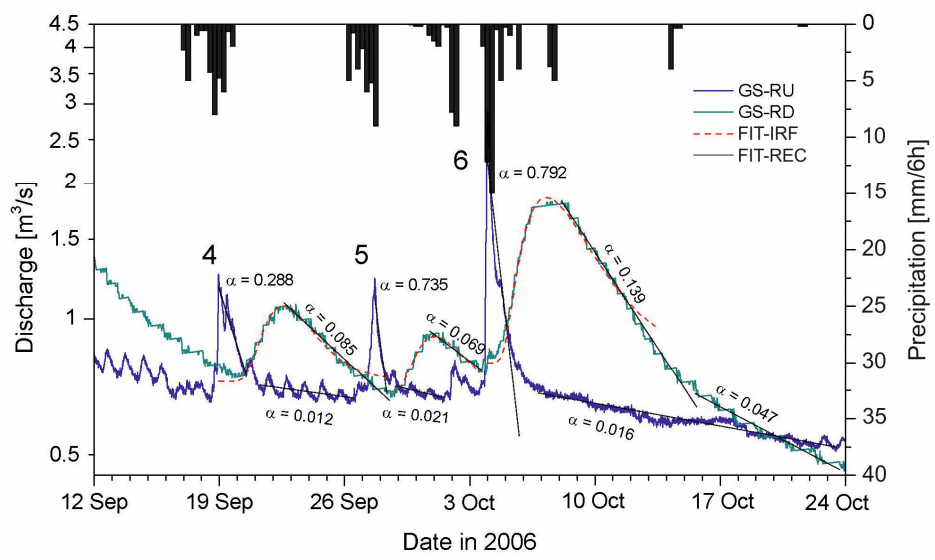

Figure 6.9: Discharge characteristics in late summer and autumn of 2006 in the Reintal valley demonstrating dampening effects of the series of Alpine alluvial/rockfall deposits; GS-RU: discharge from the karst spring upstream the alluvial/rockfall aquifer; GS-RD: discharge downstream at the outlet of the aquifer system; FIT-IRF: fit of impulse-response-function and FIT-REC: fit of recession analysis.

Table 6.2: Discharge characteristics of selected precipitation events in 2006 and 2011. All events with a peak discharge Q_P >2.3 ± 0.2 m^3/s are high-flow events. Q_i: initial discharge; Q_P: peak discharge; discharge response: ratio between direct discharge (Q_P-Q_i) and precipitation, conversion factor and catchment area ($P_{peak} \cdot f_c \cdot A$); discharge ratio: quotient between Q_P and Q_i, lag time: time difference between discharge peak upstream (GS-RU) and downstream (GS-RD) from the rockfall aquifers; flow conditions indicate high-flow (HF) and low- to moderate flow conditions (LF/MF) of the individual events.

Event	Gauging station	P_{SUM} [a]	Peak rainfall in 6h[b]	Q_i	Q_p	Discharge response	Discharge ratio	Lag time	Flow conditions[d]
-	-	mm	mm	$m^3\ s^{-1}$	$m^3\ s^{-1}$	-	-	h	-
20.5.2006	GS-RU	9	5	0.97	3.52	1.338	3.63	38	**HF**
	GS-RD			0.53	3.11	0.481	5.87		
28.5.2006	GS-RU	15	8	1.14	6.03	1.432	5.29	33	**HF**
	GS-RD			0.51	2.63	0.254	5.16		
7.8.2006	GS-RU	49	10	0.96	8.09	1.537	8.43	3.8	**HF**
	GS-RD			0.64	14.40	1.114	22.50		
18.9.2006	GS-RU	17	8	0.65	1.25	0.297	1.92	101[c]	LF
	GS-RD			0.74	1.06	0.103	1.43		
27.9.2006	GS-RU	26	9	0.65	1.22	0.258	1.88	93[c]	LF
	GS-RD			0.67	0.93	0.080	1.39		
4.10.2006	GS-RU	29	15	0.67	2.84	0.360	4.24	106[c]	LF
	GS-RD			0.77	1.80	0.093	2.34		
18.6.2011	GS-RU	39	20	1.65	3.77	0.358	2.28	9.5	**HF**
	GS-RD			2.58	4.96	0.192	1.92		
30.6.2011	GS-RU	30	16	1.34	4.02	0.477	3.00	29	**HF**
	GS-RD			2.04	3.08	0.149	1.51		
7.8.2011	GS-RU	55	31	0.88	2.65	0.162	3.01	36	**HF**
	GS-RD			2.00	3.45	0.086	1.73		
5.9.2011	GS-RU	53	21	0.52	1.96	0.177	3.77	86[c]	LF
	GS-RD			1.04	1.71	0.063	1.64		
18.9.2011	GS-RU	19	15	0.46	1.2	0.152	2.61	105	LF
	GS-RD			1.00	1.6	0.083	1.60		
10.10.2011	GS-RU	30	12	0.45	3.16	0.500	7.02	34	**HF**
	GS-RD			0.9	2.87	0.185	3.19		
mean values (excluding extreme event in 2006)			GS-RU	1.04	2.65	0.389	2.65		
			GS-RD	1.80	3.22	0.188	1.93		

[a] Sum of precipitation until peak discharge at GS-RU

[b] Note that maximum resolution of sum of precipitation is 6 h

[c] Obtained by impulse-response-analysis

[d] predominant flow conditions: high-flow conditions (HF) and low flow conditions (LF); mean-flow conditions (MF) are mainly a transition between LF to HF and therefore are not listed separately

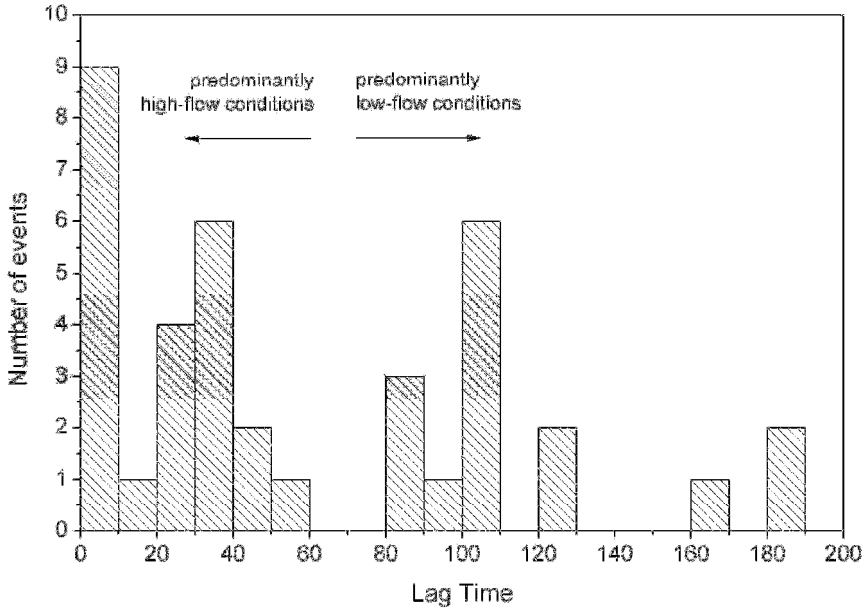

Figure 6.10: Lag times between discharge peaks upstream (GS-RU) and downstream (GS-RD) from the alluvial/rockfall aquifer system, obtained from 38 discharge peaks during 2002–11.

Table 6.3: Results of the impulse-response analysis for three discharge events in 2006. A_{in}: Area under input signal at site GS-RU; A_{out}: area under output signal at site GS-RD; t_m: mean transit time; ω: variance of time; R^2: coefficient of determination from impulse-response function.

Date	A_{in}	A_{out}	t_m	ω	R^2
20.09.2006	10.7	30.5	100.7	0.379	0.915
28.09.2006	5.5	19.4	93.2	0.388	0.897
03.10.2006	24.9	131.1	105.9	0.542	0.972

The discharge ratio downstream from the alluvial/rockfall aquifers is less than that of the Partnach spring, indicating flow damping along the subsurface flow path between the two sites. While the discharge ratio at GS-RU has a mean value of 2.7, the ratio downstream from the aquifer system at site GS-RD has only a mean value of 1.9 (Fig. 6.11a, Table 6.2). The mean values exclude the extreme event in August 2006, which resulted in discharge ratios of 8 at GS-RU and 22 at GS-RD. A substantially higher discharge ratio downstream at GS-RD is the result of a high proportion of surface runoff relative to groundwater discharge. Extreme precipitation intensity followed by a high volume of surface runoff likely causes this discharge response. Nevertheless, the discharge ratio for the Reintal valley is much less than that for other Alpine catchments, e.g., the Lahnenwiesgraben, where a ratio of up to 2500 was reported by Schmidt

and Morche (2006). The Lahnenwiesgraben catchment is largely covered by glacial sediment, and the bedrock is dominated by diverse lithology, including marls and mudstones. Further examples of hydrographs showing annual flood peaks for different catchment areas in Austria are given by Gaál et al. (2012). Analyses indicate that, in addition to the geologic setting, other factors, such as climate and catchment properties, influence discharge characteristics and flood generation processes (Norbiato et al. 2009; Merz and Blöschl 2009; Gaál et al. 2012).

The much larger recession coefficients upstream relative to downstream is evidence of the strong flood-buffering effects of the alluvial/rockfall deposits and demonstrates that they act as a natural retention zone. Analyses of 15 recession events demonstrate that flood recession coefficients at the karst spring (GS-RU) are generally about a factor of 2 to 5 higher than those downstream the alluvial/rockfall deposits (GS-RD) (Figs. 6.10 and 6.11b). One of the highest flood recession coefficient at the karst spring (1.04 d^{-1}) was determined for the extreme precipitation event in August 2006 and is attributed to concentrated recharge and drainage through the karst conduit network. For the same event, the flood recession coefficient downstream at GS-RD was about 0.20 d^{-1}, while the falling limb is gentler and the base of the peak downstream (site GS-RD) generally is broader than at the Partnach spring upstream (site GS-RU). Baseflow recession coefficients at the karst spring and downstream from the alluvial/rockfall aquifer show lowest values of about 0.005 d^{-1} after a long period of 45 days in 2005, at which time the discharge decreased to the lowest values measured (0.56 m^3/s at GS-RU and 0.84 m^3/s at GS-RD). Water storage properties of the alluvial/rockfall aquifer maintain baseflow and perennial discharge at the outlet. An example of an area without drainage through permeable bedrock, such as rockfall deposits, is the Lainbachtal valley in the German Alps. The steep area is dominated by moraine sediments with a low hydraulic permability, resulting in a rapid discharge response and substantially higher flood recession coefficients in the range of 7.2 to 84 d^{-1} (Wetzel 2003). Sinreich et al. (2002) reported recession coefficients in the range of 1.3 to 3.4 d^{-1} for an alpine rockfall deposit in the Schwarzwasser valley in Austria. Surface discharge from a non-karstic catchment area infiltrates the rockfall deposit and the highly fluctuating discharge peaks are damped by the rockfall deposits. In contrast, the moderate flood-recession coefficients in the Reintal valley indicate stronger flood-buffering properties, which could be related to the retention capacity of the alluvial/rockfall aquifer but also to the glacier and the karst aquifer.

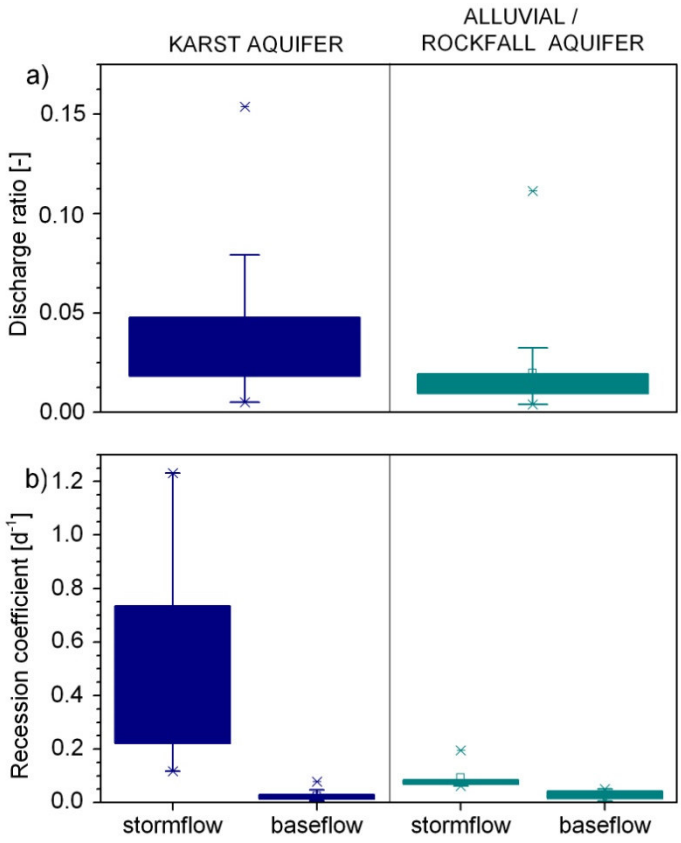

Figure 6.11: Discharge ratios (a) and recession coefficients (b) of the karst aquifer and the alluvial/rockfall aquifer in the Reintal valley.

Infiltration and storage processes are related to water levels in the aquifer system and are highest at low water levels. During low-flow conditions, flood-buffering of recharge events plays an important role because of the high infiltration of water into the series of alluvial/rockfall deposits and because of long subsurface flow paths (Fig. 6.6). This is shown by the long lag times and the damped discharge ratio at GS-RD. Substantial infiltration was also observed during early summer in 2006, when discharge downstream from the alluvial/rockfall aquifers (site GS-RD) was about 0.4 m^3/s lower than that upstream at the karst spring (site GS-RU) (Fig. 6.8). The observations in 2006 indicate replenishment of the aquifer after low-flow conditions during the winter. At high water levels, when infiltration and subsurface flow paths are shortest, flood-buffering effects are at a minimum because of the high proportion of overland flow. This is indicated by rapid transit of the flood wave but, nevertheless, moderate flood recession (Fig.6.9). Even under high-flow conditions, flood recession is less than 0.2 d^{-1} and thus much smaller than for the karst system.

In conclusion, the alluvial/rockfall deposits have a large influence on the overall discharge of the high-alpine karstic catchment area. Discharge ratios and their distribution of values are much smaller for the alluvial/rockfall aquifer than for the karst aquifer, except for the extreme event in 2005 (Figs. 6.6 and 6.11a). Similarly, flood recession coefficients are much smaller for the alluvial/rockfall aquifer (Figs. 6.6 and 6.11b). While the discharge response in the karst aquifer occurs very rapidly – within 6 h of the precipitation event – the peak discharge downstream from the alluvial/rockfall aquifer occurs after a great range of lag times, between 5, 35, and 101 h (Figs. 6.6 and 6.10). The observed flood-buffering potential in the Reintal valley therefore is related to the underground drainage properties and the water storage capacity of the permeable alluvial/rockfall deposits, which are natural retention zones.

High magnitude rockfall deposits (bergsturz, rockslide) have a persistent and large impact on sediment transfer and ecosystems in high mountain basins. The interaction between surface and subsurface flow inhibits large sediment output in the catchment; sediment deposition occurs in the alluvial plains (Schmidt and Morche 2006; Morche et al. 2007). Braided-river systems on the alluvial plains and infiltration and storage in the alluvial/rockfall aquifer system enable the development of unique Alpine ecosystems in the Reintal valley. Because the flood-buffering properties of the aquifer system prevent abrasive fluvial erosion, vegetation can grow close to the stream bed.

6.5 Conclusions and outlook

The alluvial/rockfall aquifer system of the Reintal valley has a substantial influence on the discharge and water storage in the high-alpine valley. The valley is characterized by a series of karst and alluvial/rockfall aquifers that affect discharge from the Alpine catchment. Depending on the hydrologic flow conditions, the surface and underground flow patterns change substantially in the valley. Under high-flow conditions, discharge peaks at the outlet of the valley occurred about 5 h after discharge peaks in the upper part of the valley. Because of high water levels, subsurface flow paths along the valley are short, and subsurface flow velocities of 30 m/h dominated in the coarse-grained rockfall deposits. Flood recession curves were substantially wider downstream than upstream, indicating that the strong interaction of surface and subsurface flow along the alluvial/rockfall aquifer system buffers flood flow. The greatest flood-damping effects were observed in response to recharge events that occurred under low-flow

conditions during the autumn. Because of low water levels, subsurface flow path lengths increased and water discharged only downstream from the alluvial/rockfall deposits. Flow velocities decreased to 13 m/h along the long subsurface flow path. After recharge events, dominant lag times of 101 h occurred together with a decrease in peak discharge by a factor of 1.5. The storage properties of the aquifer enable replenishment and a slow release of water and thus provide baseflow during periods of low flow.

Flood-buffering and storage effects in the Reintal valley are a result of the presence of three natural retention zones: the glacier, the karst aquifer, and the alluvial/rockfall aquifer. In comparison with catchment areas underlain by impermeable bedrock, concentrated drainage and short transit times through well-developed karst structures result in a moderate discharge ratio, moderate flood recession and short discharge response after precipitation events. Because of underground drainage and lower flow velocities through alluvial/rockfall deposits, discharge ratios and flood recession coefficients decreased substantially and the discharge response occurred with a time lag of several hours downstream in the valley. Thus, the alluvial/rockfall aquifer is of great hydrogeologic importance for the discharge characteristics of the high-alpine valley.

The presence of such natural retention zones might be important with regard to climate change, i.e., floods and droughts. Other high Alpine valleys might also have hydrogeologic settings conducive to flood damping and baseflow maintenance. Better understanding of the hydrogeology of Alpine headwaters could be a useful tool for improved water management and the development of risk maps.

Acknowledgements

We acknowledge support by Deutsche Forschungsgemeinschaft and Open Access Publishing Fund of Karlsruhe Institute of Technology. The work of David Morche was funded by DFG (grant numbers SCHM 472/12-1-3, SCHM 472/15-1 and MO 2068/3-1). We thank Barbara Mahler for valuable comments and proof-reading the manuscript, and Andy Long, Michael Sinreich and two anonymous reviewers for helpful suggestions which improved the manuscript.

Supplementary material

Table S1: Statistics of the two gauging stations GS-RU and GS-RD, n = number of measurements, R^2 = coefficient of determination, SE = standard error.

Gauging station	Observation period	n	R^2	SE
GS-RU	2002-2008	38	0.89	0.39
GS-RU	2010-2011	14	0.72	0.41
GS-RD	2002-2005	58	0.91	0.39
GS-RD	2005-2006	6	0.97	0.40
GS-RD	2007-2011	81	0.90	0.37

Table S2: Monthly mean discharge downstream from the alluvial/rockfall aquifer at GS-RD. The year 2006 is characterized by very low discharge in comparison with the other years.

	2002	2003	2004	2005	2006	2007	2008	2010	2011
	28.4.-24.10.	18.7.-11.12.	2.6.-9.11.	11.3.-18.11.	15.3.-18.11.	10.2.-6.12.	18.4.-20.11.	2.3.-24.11.	15.3.-14.10.
February	-	-	-	-	-	0.24	-	-	-
March	-	-	-	0.8	-	0.31	-	0.41	0.46
April	-	-	-	1.18	0.48	0.70	0.92	0.62	0.84
May	2.66	-	-	2.35	0.95	2.86	2.13	1.85	1.75
June	3.74	-	3.55	3.54	1.75	3.83	4.33	3.52	2.60
July	3.28	-	3.99	3.63	1.32	2.64	2.54	2.92	2.22
August	3.46	-	2.81	2.68	2.75	1.63	2.92	2.35	1.87
September	2.25	1.4	2.06	1.50	1.28	-	1.77	1.74	1.33
October	1.88	1.46	1.82	1.35	0.81	-	1.07	0.93	1.40
November	-	0.84	-	0.91	-	0.40	0.73	0.94	-

Table S3: Discharge characteristics of selected precipitation events in 2002–2011. Hydrographs from 2006 and 2011 are presented in Figs. 6.8 and 6.9. All events with a peak discharge Q_P >2.3 ± 0.2 m³/s are high-flow events. Q_i: initial discharge; Q_P: peak discharge; discharge response: ratio between direct discharge (Q_P-Q_i) and precipitation, conversion factor and catchment area ($P_{peak} \cdot f_c \cdot A$); discharge ratio: quotient between Q_P and Q_i, lag time: time difference between discharge peak upstream (GS-RU) and downstream (GS-RD) from the rockfall aquifers; Flow conditions indicate high-flow (HF) and low- to moderate flow conditions (LF/MF) of the individual events.

Event	Gauging station	P_{SUM} [a]	Peak rainfall in 6h[b]	Q_i	Q_p	Discharge response	Discharge ratio	Lag time	Flow conditions[d]
-	-	mm	mm	$m^3 s^{-1}$	$m^3 s^{-1}$	-	-	h	-
1.8.2002	GS-RU	18	9	2.01	5.28	1.115	2.63	4.5	**HF**
	GS-RD			2.82	5.92	0.509	2.10		
4.8.2002	GS-RU	18	18	1.97	3.39	0.358	1.72	5.4	**HF**
	GS-RD			3.40	3.90	0.168	1.15		
6.8.2002	GS-RU	21	13	1.98	4.12	0.602	2.08	5.0	**HF**
	GS-RD			3.54	5.43	0.323	1.53		
11.8.2002	GS-RU	66	22	1.78	7.76	0.670	4.36	4.5	**HF**
	GS-RD			3.10	12.17	0.428	3.93		
20.8.2002	GS-RU	29	16	1.46	2.34	0.278	1.60	14	**HF**
	GS-RD			2.55	3.04	0.147	1.19		
1.9.2002	GS-RU	26	16	0.94	2.20	0.261	2.34	85[c]	LF
	GS-RD			1.90	2.24	0.108	1.18		
29.8.2003	GS-RU	12	12	0.81	2.10	0.333	2.59	105[c]	LF
	GS-RD			1.08	1.58	0.102	1.46		
10.9.2003	GS-RU	35	19	0.65	1.83	0.183	2.82	187[c]	LF
	GS-RD			1.08	1.86	0.076	1.72		
4.10.2003	GS-RU	35	21	0.66	1.21	0.109	1.83	186	LF
	GS-RD			1.08	2.57	0.095	2.38		
20.8.2004	GS-RU	89	70	1.69	2.92	0.079	1.73	40	**HF**
	GS-RD			2.47	3.07	0.034	1.24		
26.8.2004	GS-RU	69	27	1.52	2.89	0.203	1.90	29	**HF**
	GS-RD			2.57	3.46	0.099	1.35		
22.9.2004	GS-RU	68	25	0.71	2.88	0.219	4.06	125[c]	LF
	GS-RD			1.59	2.47	0.076	1.55		
30.9.2004	GS-RU	12	7	1.47	1.82	0.494	1.24	103[c]	LF
	GS-RD			2.21	2.61	0.288	1.18		
16.8.2005	GS-RU	41	28	1.30	2.99	0.203	2.30	43	**HF**
	GS-RD			1.98	3.45	0.095	1.74		
2.10.2005	GS-RU	14	14	0.98	2.48	0.337	2.53	102[c]	LF
	GS-RD			1.55	1.99	0.110	1.28		

Event	Gauging station	P_{SUM} [a]	Peak rainfall in 6h[b]	Q_i	Q_p	Dis-charge response	Dis-charge ratio	Lag time	Flow condi-tions[d]
-	-	mm	mm	$m^3 s^{-1}$	$m^3 s^{-1}$	-	-	h	-
20.5.2006	GS-RU	9	5	0.97	3.52	1.338	3.63	38	**HF**
	GS-RD			0.53	3.11	0.481	5.87		
28.5.2006	GS-RU	15	8	1.14	6.03	1.432	5.29	33	**HF**
	GS-RD			0.51	2.63	0.254	5.16		
7.8.2006	GS-RU	49	10	0.96	8.09	1.537	8.43	3.8	**HF**
	GS-RD			0.64	14.40	1.114	22.50		
18.9.2006	GS-RU	17	8	0.65	1.25	0.297	1.92	101[c]	LF
	GS-RD			0.74	1.06	0.103	1.43		
27.9.2006	GS-RU	26	9	0.65	1.22	0.258	1.88	93[c]	LF
	GS-RD			0.67	0.93	0.080	1.39		
4.10.2006	GS-RU	29	15	0.67	2.84	0.360	4.24	106[c]	LF
	GS-RD			0.77	1.80	0.093	2.34		
26.6.2007	GS-RU	32	18	1.05	2.1	0.222	2.00	22	**HF**
	GS-RD			2.77	2.85	0.122	1.03		
2.7.2007	GS-RU	69	21	0.79	1.97	0.178	2.49	35	**HF**
	GS-RD			2.32	4.67	0.172	2.01		
9.7.2007	GS-RU	36	28	0.85	2.99	0.203	3.52	23	**HF**
	GS-RD			2.94	5.24	0.145	1.78		
24.7.2007	GS-RU	9	7	0.78	1.47	0.399	1.88	56	**HF**
	GS-RD			1.69	2.47	0.273	1.46		
9.8.2007	GS-RU	29	10	0.67	1.15	0.219	1.72	34	**HF**
	GS-RD			1.1	2.20	0.170	2.00		
16.8.2008	GS-RU	118	38	0.84	2.93	0.147	3.49	3.5	**HF**
	GS-RD			2.01	7.73	0.157	3.85		
11.9.2008	GS-RU	10	10	0.61	0.92	0.175	1.51	161[c]	LF
	GS-RD			1.54	2.02	0.156	1.31		
17.7.2010	GS-RU	45	18	1.41	3.06	0.323	2.17	3.2	**HF**
	GS-RD			2.35	3.9	0.168	1.66		
23.7.2010	GS-RU	37	25	1.14	2.45	0.186	2.15	4.3	**HF**
	GS-RD			2.03	2.83	0.088	1.39		
25.9.2010	GS-RU	45	24	0.56	0.64	0.051	1.14	83[c]	LF
	GS-RD			1.16	1.27	0.041	1.09		
13.11.2010	GS-RU	12	6	0.31	0.55	0.174	1.77	122[c]	LF
	GS-RD			0.89	1.01	0.130	1.13		
18.6.2011	GS-RU	39	20	1.65	3.77	0.358	2.28	9.5	**HF**
	GS-RD			2.58	4.96	0.192	1.92		
30.6.2011	GS-RU	30	16	1.34	4.02	0.477	3.00	29	**HF**
	GS-RD			2.04	3.08	0.149	1.51		

Event	Gauging station	P_{SUM} [a]	Peak rainfall in 6h[b]	Q_i	Q_p	Discharge response	Discharge ratio	Lag time	Flow conditions[d]
-	-	mm	mm	$m^3 s^{-1}$	$m^3 s^{-1}$	-	-	h	-
7.8.2011	GS-RU	55	31	0.88	2.65	0.162	3.01	36	**HF**
	GS-RD			2.00	3.45	0.086	1.73		
5.9.2011	GS-RU	53	21	0.52	1.96	0.177	3.77	86[c]	LF
	GS-RD			1.04	1.71	0.063	1.64		
18.9.2011	GS-RU	19	15	0.46	1.2	0.152	2.61	105	LF
	GS-RD			1.00	1.6	0.083	1.60		
10.10.2011	GS-RU	31	12	0.45	3.16	0.500	7.02	34	**HF**
	GS-RD			0.9	2.87	0.185	3.19		
mean values (excluding extreme event in 2006)			GS-RU	1.04	2.65	0.389	2.65		
			GS-RD	1.80	3.22	0.188	1.93		

[a] Sum of precipitation until peak discharge at GS-RU

[b] Note that maximum resolution of sum of precipitation is 6 h

[c] Obtained by impulse-response-analysis

[d] predominant flow conditions: high-flow conditions (HF) and low flow conditions (LF); mean-flow conditions (MF) are mainly a transition between LF to HF and therefore are not listed separately

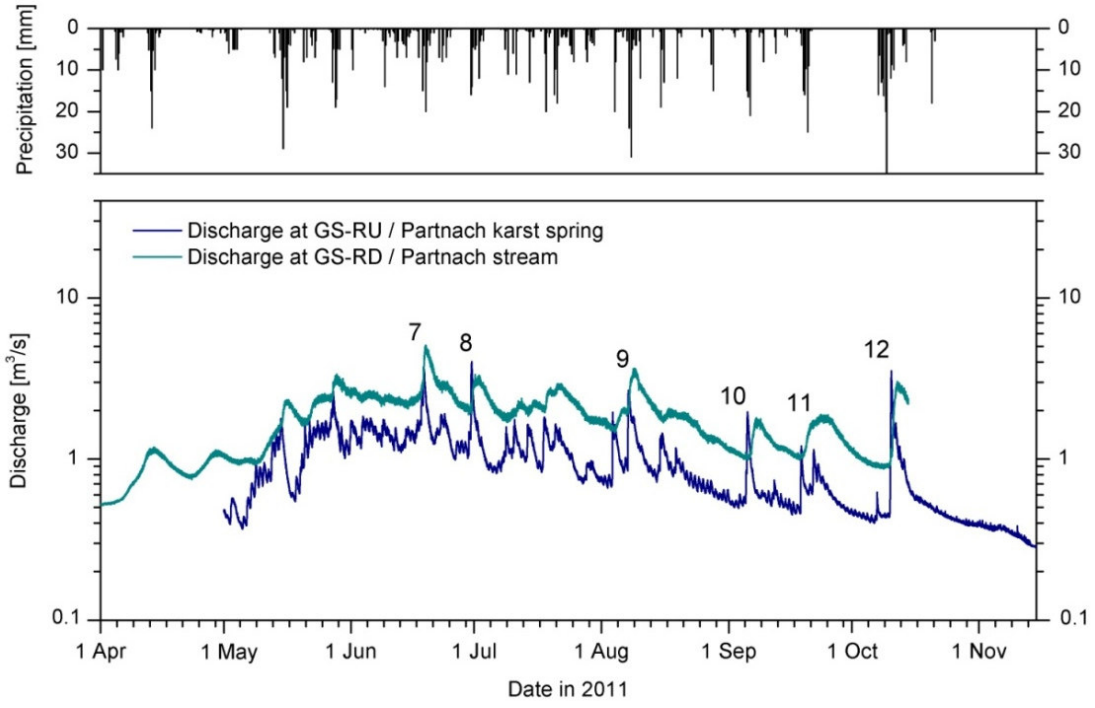

Figure S1: Hydrographs at the upstream (Partnach karst spring, site GS-RU) and downstream (Partnach stream, site GS-RD) gauging stations in the Reintal valley in 2011. Precipitation data (6-h time step) was obtained from the weather station at Mt. Zugspitze (DWD).

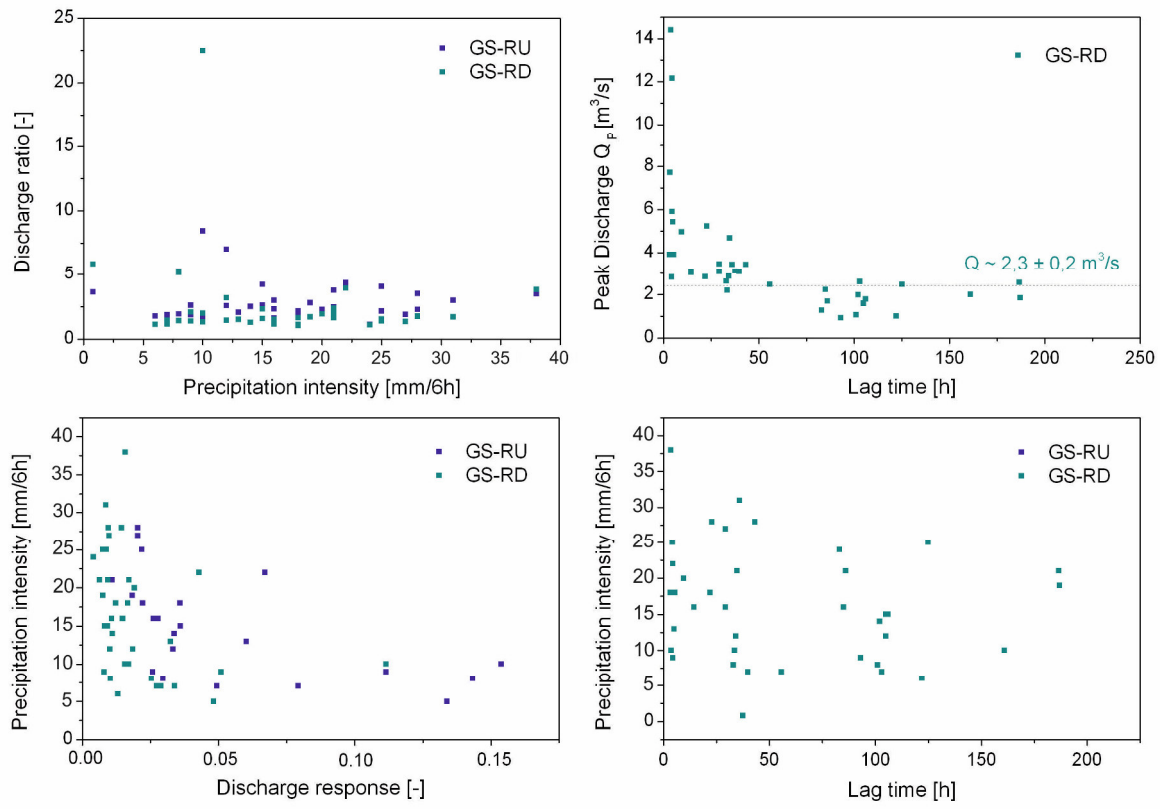

Figure S2: a) Precipitation intensity vs. discharge ratio, b) lag time vs. peak discharge, c) discharge response vs. precipitation intensity, and d) lag time vs. precipitation intensity at the gauging stations upstream (GS-RU) and downstream (GS-RD) from the alluvial/rockfall aquifer.

Chapter 7

Summary

This thesis is composed of four studies that address the identification of underground drainage structures and the quantification of transit-time distributions and other flow parameters in three different types of karst aquifer systems. In this chapter, results of the studies are summarized and new findings are presented for the three different systems: the conduit-dominated system, the fissured karst system, and the system comprised of a karst and porous-media aquifer. Additionally, new findings of the applied methods are addressed.

7.1 Drainage structures

Underground drainage in karst aquifer systems is highly dependent on the presence and structure of flow paths. In this thesis, preliminary information about the presence of preferential flow paths and their structure was obtained by evaluating the hydrogeologic setting, considering geomorphologic evolution and karst development, and using data from speleological research in the catchment areas. There are large differences between the individual karst systems with respect to their underground drainage patterns and properties. Karst systems characterized by a well-developed conduit and cave system can be classified as conduit-dominated karst systems, while karstified systems with a less developed conduit system can be described as fissured karst systems.

In the catchment area of the Blautopf, it is known from geologic and tectonic investigations that caves are developed along tectonic weak zones (Ufrecht 2009). In the Wetterstein Mountains, results of the tracer tests indicate that underground drainage is also predominantly linked to fractures and tectonic weak zones. Because of the inclination and orientation of the fault structures, underground flow paths can cross mountain ridges and occur underneath deep valleys. In the thick limestone with an up-to-1000-m thick unsaturated zone, drainage follows the hydraulic gradient to the deepest outlet of the system, independent of the dip of the fold axis. Young infiltrated water follows cross-formational flow paths and can contribute to deep flow systems.

The stratigraphic flow control in the Wetterstein Mountains is low because of the high degree of fault tectonics. Cross-formational flow has also been identified in the conduit-dominated catchment area of the Blautopf, where the tracer tests indicate that there are well-developed flow paths through the marly formation, which was previously considered impervious. Considering new geologic findings, the cross-formational flow is attributed to fractures and solutionally enlarged fissures related to the presence of sponge-reefs in the relatively thin marly formation. Cross-formational flow occurs because the apparent karst water table is low and lies in the lower karst aquifer. In these two karst systems – the conduit-dominated Blautopf catchment and the fissured Wetterstein Mountains system – underground drainage is linked to tectonic structures.

The structure of karst drainage is highly dependent on the degree of karstification. In the conduit-dominated karst system, the Blautopf catchment, karst development has proceeded to such an extent that a wide and large system of caves is present, forming a distinctive drainage network. By conducting the first tracer tests inside the active cave systems in the catchment area, the dendritic structure of karst drainage was characterized. Two main branches of drainage, the two active caves, have developed in the catchment area and merge to one main conduit about 700 m upstream from the main spring, the Blautopf. Such hierarchical drainage structures are known from numerical modeling of highly karstified systems, but have rarely been demonstrated in the field because of the lack of accessible active caves. Detailed knowledge about drainage structures is important with respect to the spread of potential contamination within the aquifer. Results demonstrate that potential contamination in one sub-catchment, e.g., poor water quality downstream of a wastewater treatment plant, will not affect water quality in the second sub-catchment. In contrast to the conduit-dominated catchment area of the Blautopf, a steady uplift of the alpine karst area of the Wetterstein Mountains and the dominance of strong mechanical and gravitational erosion has resulted in a fissured karst system. Karst development is at an early to intermediate stage, where several small-scale karst conduits coexist in the system and drainage occurs to a number of springs. The tracer tests show a wide spreading of the injected tracer and a positive detection at several springs. Thus, potential contaminants entering the system may be widely distributed in the groundwater.

The karst systems are characterized by concentrated flow through solutionally-enlarged conduits and diffuse flow through the fissured rock matrix. In the catchment area of the Blautopf,

focus was on the hydraulic characterization of the well-developed flow paths. The tracer tests demonstrated low storage and retention properties of well-developed conduit system in the unsaturated and saturated zone. Besides this, the presence of diffuse flow structures had already been illustrated by other authors (Armbuster and Selg 2006; Selg and Schwarz 2009; Geyer et al. 2011). In the fissured karst system of the Wetterstein Mountains, three dominant drainage structures were identified. Results with artificial and natural tracers indicate that there is 1) the karst drainage network characterized by concentrated recharge and fast drainage, 2) a network of well-drained fissures characterized by diffuse recharge, moderate flow and moderate storage, and 3) a coexisting network of poorly-drained, smaller fissures that is characterized by diffuse recharge, slow flow and high storage properties. Based on tracer test results (i.e. the long tailing of the breakthrough curves) there is strong interaction between the conduits and the fissured network. This interaction results in groundwater storage and natural attenuation of potential contaminants entering the karst system.

7.2 Transit-time distributions and hydraulic parameters

The quantification of transit times and hydraulic parameters is crucial for the assessment and management of karst water resources. However, the large temporal and spatial variability of flow and transport parameters within karst systems and the dynamics of karst aquifers are still major challenges in karst hydrogeology. New findings resulting from this thesis contribute to a better understanding of transit-time distributions and related flow structures.

In the conduit-dominated catchment of the Blautopf, the main objective was to spatially and temporally resolve hydraulic parameters of the conduit system. Because tracer tests were conducted inside the cave system, this work is one of few studies to determine real flow parameters directly in epiphreatic and phreatic cave passages. Results of tracer injections and measured tracer breakthrough curves at several observation points in the cave indicate that flow velocities were highly variable within individual cave passages. Linear flow velocities of up to 275 m/h were found in the epiphreatic passage, where hydraulic gradients were highest. In contrast, flow velocities in the phreatic passage were one order of magnitude lower than in the epiphreatic section. The decrease of flow velocities is attributable to the high hydraulic conductivity of the large conduit and, accordingly, extremely low hydraulic gradients. In addition to flow velocities, other hydraulic parameters, such as dispersion, were highly variable along the underground

flow path. Resulting transit times in the conduit system are short, between a few hours to a few days, indicating rapid transport of potential contaminants from the surface to the spring. The duality of karst drainage is particularly evident in this karst area considering that the mean transit time is in the range of 15 years (Geyer et al. 2011). Because of diffuse recharge and slow drainage in the fissured rock matrix, a high storage volume in the fissured matrix of the Blautopf karst system provides steady baseflow of at least 250 L/s.

To determine hydraulic parameters of underground drainage in the fissured karst system, a combination of artificial and natural tracer methods was used. Results of tracer tests with uranine and evaluation of stable isotopes indicate that three flow compartments contribute to spring discharge in the fissured karst system. There is a large range of transit times in the karst conduits of the system (varying between 2 and 13 days) which is dictated by flow conditions. Under high-flow conditions, e.g., after precipitation events or during snow-melt, transit times are a factor of 5 shorter than under low-flow conditions, which dominate during periods with less precipitation and no meltwater contribution, e.g., in the second half of the year. A long tailing of all breakthrough curves is indicative of interaction and hydraulic exchange with the fissured rock matrix originating from high water pressure in the phreatic karst conduits. Substantially longer transit times of about a few months were indicated by the evaluation of natural tracers. The intermediate transit times are attributed to intermediate percolation through the well-drained fissured rock matrix. These results are consistent with observations of spring discharge that indicate that several karst springs run dry in the late summer and autumn of each year. Results from artificial and natural tracers indicate that there are also transit times of a few years that are attributed to the poorly-drained fissures and rock matrix. The detection of uranine more than a year after the injection provides important insight into properties of the fissured rock matrix, such as storage of groundwater, retardation, and dilution of potential contaminants. Additionally, the alpine water resource is likely vulnerable to climatic changes. The results of this research are an important contribution to the assessment and evaluation of alpine water resources.

For a better understanding of the dynamics of a karst system, tracer tests in the conduit-dominated and fissured karst systems were conducted under different flow conditions. Results of these tracer tests show that during high-flow conditions, transit times are 3 to 5 times shorter than under low-flow conditions. This effect was observed in both the conduit-dominated and

the fissured karst systems. Two different effects in the different karst systems were documented based on the maximum tracer concentration and the dilution of tracer. In the strongly karstified catchment area of the Blautopf, the highest tracer concentrations were measured under low-flow conditions. Low water volumes result in a low dilution of tracer, because epiphreatic to phreatic drainage passages play an important role in the conduit-dominated karst system. In contrast, the highest tracer concentrations were found under high-flow conditions in the high-alpine fissured karst system in the Wetterstein Mountains. This effect is attributed to high flow velocities that cause fast drainage to the spring and a sharp BTC with high maximum concentrations. Because of drainage through a thick unsaturated zone, dilution of the tracer is minimal in the fissured karst system.

Most studies in karst hydrogeology focus on the underground drainage of the karst aquifer itself because the high heterogeneity is challenging to characterize. This thesis is one of the first to investigate discharge characteristics of a system consisting of a karst and a porous-media (alluvial/rockfall) aquifer, with special focus on the behavior of natural retention zones. By analyzing hydrographs of the karst and the porous-media system it was possible to constrain flood-buffering effects of the alluvial/rockfall aquifer that influence discharge of the whole catchment. The discharge variability at the outlet of the valley is damped. Depending on flow conditions and water levels in the system, underground drainage through the alluvial/rockfall aquifer results in a delayed discharge peak after recharge events of more than 101 hours. Recession curve analyses at the karst spring and at the outlet indicate that flood recession coefficients are lower than in other alpine catchment areas, i.e., areas that are dominated by impermeable rocks. Because of groundwater storage in the fissured karst system and in the porous-media aquifer, baseflow recession coefficients are low. However, the karst spring is intermittent and occasionally runs dry during winter months, although there is permanent discharge from the valley because of the storage characteristics of the porous-media system. In conclusion, the alluvial/rockfall aquifer has a major influence on discharge of the karstic catchment area, provides strong flood-buffering effects, and enables groundwater storage and a slow release of groundwater during periods with low-flow.

7.3 Evaluation of the applied methods

To obtain hydrogeologic knowledge and quantitative data about hydraulic parameters in the different catchment areas, a combination of different approaches has been applied. The selection of different investigating methods is highly dependent on the specific research focus, as particular techniques assess only specific drainage structures, e.g. conduits or fissured networks. In this thesis, artificial tracer tests, analyses of stable isotopes, and evaluations of hydrographs facilitated quantitative characterization of underground drainage properties.

Tracer tests with artificial tracers are a powerful tool in karst hydrogeology to assess conduit drainage. In conjunction with knowledge of the hydrogeologic setting and karst development, carefully designed tracer tests can provide valuable information for the delineation of catchment areas and the development of conceptual models. In this thesis, tracer tests allowed for the determination of transit times and flow velocities in the fast draining karst conduit system, which is crucial for groundwater management of the aquifer and the estimation of potential flow paths of contaminants. The method was especially suitable in areas that are difficult to access, i.e., alpine areas and caves, because the necessary equipment was manageable. Tracer tests were also conducted under different flow conditions, which enabled assessment of the dynamics of the drainage system for variable transit times and different effects of dilution in the individual karst systems. Additionally, it was possible to use a tracing technique that has rarely been applied in karst hydrogeology – tracer tests were conducted inside a cave system to obtain detailed insights into the structure of karst drainage and related flow parameters. Tracer injection and observation in accessible passages of the conduit system allowed for the resolution of flow parameters for epiphreatic and phreatic cave passages. In combination with injection on the land surface in remote parts of the catchment area, it was possible to determine the hierarchical structure of karst drainage. It can be concluded that such unique insights into the drainage structure of karst aquifers were only possible from in-cave tracer tests. Although such tracer tests are laborious, the benefits are worth the effort since unique information about groundwater flow and flow parameters can be obtained.

The combined use of artificial and natural tracer methods was applied in this thesis to assess underground drainage properties in a fissured karst system. Fissured karst systems are characterized by the absence of an accessible conduit and cave system that prohibits in-cave tracer

tests to resolve the internal drainage structure. While the artificial tracing method provides information about fast drainage structure, i.e., the conduit system, natural tracers generally deliver information about diffuse and slow flow paths. Even if data for isotopes in precipitation or at the springs are scarce, a simplified evaluation of stable isotopes is still possible using a lumped-parameter model. Such evaluation is especially important in areas that are difficult to access and where data collection is difficult, e.g., in alpine areas. Long-term data from nearby precipitation stations and monthly water samples from springs provided sufficient input data. Data modeling with the program FLOWPC provided an evaluation of intermediate to slow transit times through the aquifer. The combination of artificial and natural tracers was suitable to develop a detailed conceptual model of the fissured karst system and to assess the fast and the slow drainage system. The approach resulted in 1) detection of three flow compartments comprising a fast-, an intermediate- and a slow-flow component, 2) determination of the distribution of transit times in these three flow compartments, and 3) estimates of the contribution of the flow components to spring discharge. The results illustrate the triple porosity of the karst system and allow for estimation of available karst water resources.

To investigate a complex aquifer system comprising a karst and a porous-media aquifer, a combination of tracer tests and discharge analysis was conducted. Based on a conceptual model of the alluvial/rockfall system describing the hydrogeology and the surface water-groundwater interaction, the tracer test was used to determine subsurface transit times and flow velocities in the alluvial/rockfall system. Available long-term discharge data for two different sites in the valley allowed for the detailed evaluation of discharge characteristics. Results indicate that the following parameters were particularly suitable to describe the system: the discharge ratio, the recession coefficients, and the lag times of discharge peaks. In this study, the lag times between discharge peaks upstream and downstream in the valley was found to be a crucial parameter to describe the system. Sharp discharge peaks of the hydrographs were evaluated manually, while an impulse-response function was applied to evaluate the lag times of wide discharge peaks. Long-term records were especially useful, as extreme events could be considered. However, the temporal resolution of precipitation data with a time step of 6 h was too low to evaluate discharge responses of the system. In conclusion, the applied approach was very useful to quantify flood-buffering and dampening effects of the porous-media aquifer in the karstic catchment area.

Chapter 8

Synthesis

8.1 Conclusions

Karst aquifer systems are characterized by highly heterogeneous drainage that makes it difficult to assess the groundwater resource. Sustainable management of karst water resources requires a detailed understanding of these complex aquifer systems. The identification of hydraulically important drainage structures and the quantification of related transit-times are crucial parameters that provide reliable predictions about availability, storage capability and vulnerability of the water resource. Basic information about the geological and hydrological setting and a review of available data are necessary to develop an initial conceptual model of the system. Depending on the hydrogeological setting and the main research question, suitable methods of study need to be selected and adjusted if necessary. Especially in karst hydrogeology, special methods are required to investigate these heterogeneous aquifers. In this thesis, a combination of artificial tracer tests, natural tracer analyses, and discharge analyses was applied to assess drainage structures and related transit-time distributions of three different karst aquifer systems: a conduit-dominated aquifer, a fissured karst system, and a karstic catchment area influenced by a hydraulic linkage between a karst and porous-media drainage system. The results are an important contribution to the general understanding of karst hydrogeology and the scope of application of the different methods used.

With respect to the research questions of this thesis (section 1.2), results indicate that:

- In the conduit-dominated and in the fissured karst system, flow paths are linked to geologic weak zones. Groundwater flow occurs transversely to the dip of the fold axis draining to the deepest outlet of the system. Cross-formational flow was observed in both karst systems. The well-developed drainage network has a hierarchical structure.

- The conduit-dominated karst system is characterized by short transit times of a few days from the land surface to the discharging spring, which is highly dependent on flow conditions. The highest flow velocities were associated with epiphreatic cave passages, while flow velocities in the phreatic cave passage were an order of magnitude lower. Low retention properties result in high vulnerability with respect to water quality.

- In the fissured karst system, a range of transit times occurred. Short transit times of a few days were associated with well-developed karst conduits, which were highly dependent on flow conditions. Intermediate transit times of a few months occurred in the well-drained fissured network, and long transit times > 1 year were estimated for the poorly drained fissured network. Because of the high proportion of short and intermediate transit times, the karst water resources are highly vulnerable with respect to water quality and quantity.

- In the fissured karst system drainage through a thick unsaturated zone results in strong interaction between karst conduits and the fissured system. Storage is attributable to conduit-matrix exchange as a result of gradient inversion. In the conduit-dominated system, diverse effects of the unsaturated zone occur depending on the degree of karstification.

- Alluvial/rockfall aquifers can play an important role as natural retention zones in karstic catchment areas. Because of strong interaction between surface flow and underground drainage, alluvial/rockfall aquifers can dampen and delay flood waves after high precipitation events.

Additionally, based on the different methods and approaches used, results indicate that:

- In-cave dye tracing and monitoring can provide detailed knowledge of internal drainage structures and demonstrates the dendritic structure of karst conduits. Detailed information on flow velocities and transport parameters can be achieved for individual cave passages.

- The combined use of artificial and natural tracers was crucial to assess dominant flow compartments in heterogeneous karst drainage systems. In combination with discharge

characteristics of springs these methods provided specific information about karst water resources and vulnerability.

- The development of a hydrogeologic model, supported by a combination of tracer tests and discharge analysis, provided unique insights into the role of a porous-media aquifer in a karstic catchment. Parameters such as flow velocities, discharge ratios, lag times, i.e., the use of an impulse-response function, and recession coefficients were particularly useful to describe the hydrogeologic system and develop the conceptual model.

- The methods and approach employed are suitable in areas that are difficult to access.

8.2 Perspectives and outlook

Karst groundwater systems are dynamic and respond rapidly to hydrologic conditions and climate changes. Understanding the controls on groundwater composition, transit times and vulnerability of groundwater with respect to contamination is critical for managing and protecting groundwater resources in the future (Hartmann et al. 2014). Hydraulic parameters of underground drainage are critical for an accurate description of aquifer permeability (White 2003; Mohrlok 2014; Geyer and Goldscheider 2014). Numerical models are fundamental tools for the development of groundwater management strategies. Parameterization is a well-recognized challenge for numerical models in karst systems (Geyer et al. 2013). Detailed information about conduit geometry and aquifer structure, together with spatially distributed flow parameters, is necessary input for distributed parameter models (Doummar et al. 2012). Simulations of karst systems with numerical modeling approaches are rare, partly because of sparse information about flow parameters in real karst systems (Jeannin 2001; Worthington 2009; Morales et al. 2010). In this thesis, detailed knowledge about the conduit system in the catchment area of the Blautopf was determined and spatially resolved information about transport parameters was obtained by tracer tests; these results provide a unique opportunity for future numerical modeling. An especially challenging aspect of numerical modeling is the simulation of saturated and unsaturated flow in karstified systems (Kordilla et al. 2012). In the cave system of the Blautopf catchment, epiphreatic and phreatic sections of the cave are accessible and hydraulic parameters were obtained for each zone. In combination with available long-term discharge data from the Blautopf, the results of this thesis provide a foundation for distributed parameter models and

enable the solution of aquifer dynamics with respect to climate change and subsurface transport of contaminants.

Quantification of the contribution of different flow compartments to spring discharge is critical to evaluate the vulnerability of the karst system with respect to water quantity and quality. Based on artificial and natural tracer analyses in the alpine catchment area of the Wetterstein Mountains, it was possible to distinguish three flow compartments characterized by a large distribution of transit times. The contribution of these flow compartments was roughly estimated by spring discharge characteristics. Methods such as the evaluation of environmental tracers are required to quantify the contribution of groundwater with different transit times (Maloszewski et al. 2002; Einsiedl et al. 2009; Geyer et al. 2011). For further characterization of the thick unsaturated zone, with special focus on transit times and storage processes, hydrochemical methods can be applied (Mudarra and Andreo 2011; Mudarra et al. 2014). The combined use of these tracers and correction of the results can eliminate non-unique results and estimate the groundwater age (Johnston et al. 1998, Geyer 2008).

Alpine water resources and discharge from alpine headwaters are vital for large regions of Europe. However, alpine aquifer systems are especially vulnerable because of the snow dominated flow regime and a strong warming of the alpine climate within the past 100 years. Climate studies predict an increase in the frequency, intensity and magnitude of extreme events, such as floods and droughts (Bogataj 2007). With this in mind, underground drainage properties are key factors for the estimation of groundwater storage and discharge processes within alpine catchments. Knowledge of drainage structures and related transit-times enables estimation of alpine water resources and their vulnerability with respect to changing climate conditions. Furthermore, the presence of natural retention zones, such as alpine rockfall aquifers, can have a major effect on discharge characteristics of alpine karstic catchment areas. Results of this thesis indicate that other alpine valleys might also have hydrogeologic settings conducive to flood dampening and baseflow maintenance. A better understanding of the hydrogeology of alpine headwaters could be crucial for improved water management in the Alps and the development of risk maps.

Acknowledgements

This work was made possible with the help and support of many people. Therefore, I would like to thank…

… my supervisor Prof. Dr. Nico Goldscheider for giving me the opportunity to do a PhD at the Institute. You supported me with regard to my work and also with respect to all the problems I encountered during my thesis. Thanks for the personal and constructive cooperation.

… Prof. Dr. Tim Bechtel for the great field trip and his friendly willingness to be co-referee.

… Zhao Chen for the great time in the office, for his support in the field, discussions and helpful suggestions.

… all students, Patrick Kotyla, Christina Bethke, Marc Ohmer, Lisa Blechschmitt, Charlotte Bethge, Philipp Holz, Matthias Ertelt, as well as Andreas Hartmann and Veronica Ivan for their commitment, reliable sampling and great time together in the field.

… Wolfgang Ufrecht and all cavers of the caving group ARGE Blautopf and ARGE Blaukarst, especially Andreas Kücha and Jürgen Bohnert, for the great collaboration in the field and the great experience on the cave trip into the Blauhöhlensystem.

… the Geo Workshop, especially Mr. Grunvinck and Hagen Steger, for technical support regarding installations in the field.

… the hydrogeology and the engineering working group and the laboratory team at our Institute for the enjoyable collaboration.

… the tenant farmers, family Auer, of the mountain hut (Höllentalangerhütte) for their hospitality and support during the field work and the free use of the material cableway for transportation of samples and field equipment.

… Andreas Wolf and (Höhlenforscher München) for providing data about caves and for helping with installations in the Wetterstein Mountains.

… David Morche from the University in Halle for the good collaboration and for providing discharge data from the Reintal valley.

…. Barbara Mahler who supported me before and during my stay at the U.S. Geological Survey in Austin, Texas in the United States.

… all the people who spend their free time to review the manuscripts of my thesis and my articles: Barbara Mahler, MaryLynn Musgrove, Andreas Hartmann, Manuela Hübsch.

Finally, I especially want to thank my husband Steffen who supported and encouraged me throughout the time – during field work and during the week by phone. I´m also very grateful to my parents, Doris und Jürgen Bellmann, who made all efforts to support me.

Declaration of authorship

Study 1


FACHBEITRAG

Neue Erkenntnisse zur Struktur der Karstentwässerung im aktiven Höhlensystem des Blautopfs

Ute Lauber · Wolfgang Ufrecht · Nico Goldscheider

Citation: Lauber, U., Ufrecht, W., Goldscheider, N. (2013): Neue Erkenntnisse zur Struktur der Karstentwässerung im aktiven Höhlensystem des Blautopfs. – Grundwasser, 18: 247-257, doi: 10.1007/s00767-013-0239-z.

Declaration of authorship: Ute Lauber (UL) planned the tracer test in consultation with Wolfgang Ufrecht (WU), Nico Goldscheider (NG). The installations, injections and sampling were conducted by UL with the support by the cavers (ARGE Blautopf and ARGE Blaukarst), WU, NG, and students from the institute (KIT). The analyses in the laboratory were done under supervision and responsibility of UL. UL evaluated and interpreted the results of the tracer tests in consultation with WU and NG and wrote the manuscript. The final manuscript was reviewed by all authors.

Study 2


Hydrology and Earth System Sciences

Spatially resolved information on karst conduit flow from in-cave dye tracing

U. Lauber[1], W. Ufrecht[2], and N. Goldscheider[1]

Published by Copernicus Publications on behalf of the European Geosciences Union.

Citation: Lauber, U., Goldscheider, N., Ufrecht, W. (2014): Spatially resolved information on karst conduit flow from in-cave dye-tracing. – Hydrol. Earth Syst. Sci., 18, 435–445, doi: 10.5194/hess-18-435-2014.

Declaration of authorship: Ute Lauber (UL) planned the tracer test in consultation with Wolfgang Ufrecht (WU), Nico Goldscheider (NG). The installations, injections and sampling were conducted by UL with the support by the cavers (ARGE Blautopf and ARGE Blaukarst), WU, NG, and students from the institute (KIT). The analyses in the laboratory were done under supervision and responsibility of UL. UL evaluated and interpreted the results of the tracer tests in consultation with NG and wrote the manuscript. The final manuscript was reviewed by NG.

Study 3

Hydrogeology Journal
DOI 10.1007/s10040-014-1173-6

Use of artificial and natural tracers to assess groundwater transit-time distribution and flow systems in a high-alpine karst system (Wetterstein Mountains, Germany)

Ute Lauber · Nico Goldscheider

Abstract Groundwater in mountainous karst regions is vital for regional water budgets and freshwater supply. Owing to increasing water demand and climate change, detailed knowledge of the highly heterogeneous alpine aquifer systems is required. Multi-tracer analyses have been conducted in the steep karstic Wetterstein Mountains, which includes Germany's highest summit, Zugspitze (2,962 m asl). Results of artificial tracer tests demonstrate well-developed flow paths through the unsaturated zone (up to 1,000 m thickness). Flow paths cross topographic divides and contribute to deep drainage systems underneath alpine valleys. Cross-formational flow has been identified. Quantitative analysis of tailing-dominated breakthrough curves and stable isotopes (^{18}O) has enabled determination of the mean transit-time distribution. A rapid-flow component with transit times between 3 and 13 days was found in karst conduits and open fissures, dependent on flow conditions. An intermediate-flow component, showing mean travel times of about 2.9–4.9 months, was found in well-drained fissures and fractures. A slow-flow component with mean travel times greater than 1 year is attributable to slow flow and fine storage in the poorly drained fissure and rock matrix. The conceptual model enables a better understanding of drainage, water resources and vulnerability of the high-alpine karst system.

Keywords Karst · Alpine hydrogeology · Tracer tests · Stable isotopes · Germany

Received: 28 November 2013 / Accepted: 31 July 2014

© Springer-Verlag Berlin Heidelberg

U. Lauber (✉) · N. Goldscheider (✉)
Institute for Applied Geosciences, Division of Hydrogeology, Karlsruhe Institute of Technology (KIT), Kaiserstr. 12, 76131, Karlsruhe, Germany
e-mail: ute.lauber@kit.edu
Tel.: 0721-608 45061
e-mail: goldscheider@kit.edu

Published online: 23 August 2014

Introduction

Alpine regions are characterized by high precipitation leading to substantial surface runoff and/or groundwater recharge. Alpine areas form headwaters for regional river systems such as the Danube and the Rhine, and other large regions benefit from the abundance of water (Viviroli and Weingartner 2004). In the Alps, there are some well-known examples where alpine water resources are used to supply major cities with drinking water, e.g. Vienna and Innsbruck in Austria, and Grenoble in France; however, in most alpine aquifer systems, recharge processes, drainage systems and potentially available water resources are still insufficiently known (Goldscheider 2011). Amongst others, the main challenges are strong heterogeneity and variability: recharge processes highly depend on temporal and spatial distribution of snowmelt and precipitation, drainage follows heterogeneous geologic structures and groundwater volumes are difficult to quantify as groundwater levels and hydraulic rock properties (e.g. porosity, aperture width of fissures, fracture network and karstification) are often not known. In addition, conventional hydrogeological investigation techniques are often difficult to use in alpine regions.

Nevertheless, climate change and population growth has contributed to an increasing awareness of alpine hydrogeology in the past decade. Future changes in local precipitation, snow cover patterns and glacier storage are likely to affect runoff in alpine headwaters (Jasper et al. 2004). Population growth results in increasing demand for drinking-water supply, irrigation of agricultural areas and industrial water. As alpine (karst) water resources are likely to become even more important in the future, an increasing number of studies focus on this topic. Interdisciplinary approaches include environmental research combined with snow and catchment hydrology to characterize the dynamic water resources in mountainous karst regions (Kraller et al. 2012; Marke et al. 2013). Hydrogeological mapping and hydrogeochemical techniques are applied to evaluate the water quality of the available resources (Simsek et al. 2008). Other studies use assessment methods to characterize karst morphology and groundwater vulnerability, considering epikarst, vegetation, infiltration and the karstic network to have a major influence on transit time (Perrin et al. 2003; Plan et al. 2009). Spring hydrograph analysis and hydrochemical methods allow for characterization of infiltration processes of the saturated and

Citation: Lauber, U., Goldscheider, N.: Use of artificial and natural tracers to assess groundwater transit-time distribution and flow systems in a high-alpine karst system (Wetterstein Mountains, Germany). – Hydrogeol. J., 22, 1807–1824, doi:10.1007/s10040-014-1173-6.

Declaration of authorship: Ute Lauber (UL) planned the tracer test with artificial tracers in consultation with Nico Goldscheider (NG). The tracer tests were conducted with support of NG, Zhao Chen and several students from the institute (KIT). The development of the concept and sampling of stable isotopes were done by UL, analysis were conducted in the laboratory of the Institute of Mineralogy and Geochemistry by Gesine Preuss. UL evaluated the results and wrote the manuscript. The final manuscript was reviewed by NG.

Study 4

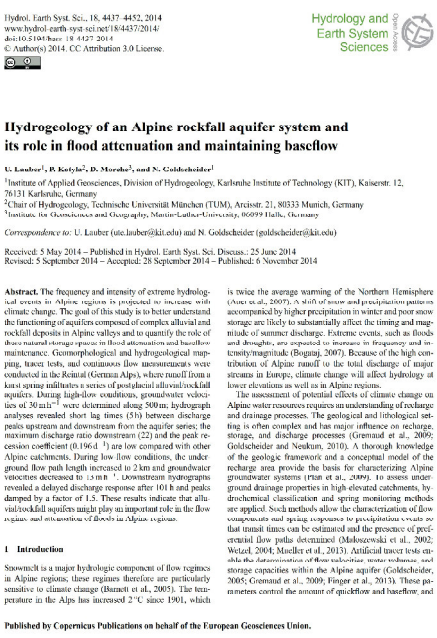

Hydrol. Earth Syst. Sci., 18, 4437–4452, 2014
www.hydrol-earth-syst-sci.net/18/4437/2014/
doi:10.5194/hess-18-4437-2014
© Author(s) 2014. CC Attribution 3.0 License.

Hydrology and Earth System Sciences

Hydrogeology of an Alpine rockfall aquifer system and its role in flood attenuation and maintaining baseflow

U. Lauber[1], P. Kotyla[2], D. Morche[3], and N. Goldscheider[1]

[1]Institute of Applied Geosciences, Division of Hydrogeology, Karlsruhe Institute of Technology (KIT), Kaiserstr. 12, 76131 Karlsruhe, Germany
[2]Chair of Hydrogeology, Technische Universität München (TUM), Arcisstr. 21, 80333 Munich, Germany
[3]Institute for Geosciences and Geography, Martin-Luther-University, 06099 Halle, Germany

Correspondence to: U. Lauber (ute.lauber@kit.edu) and N. Goldscheider (goldscheider@kit.edu)

Received: 5 May 2014 – Published in Hydrol. Earth Syst. Sci. Discuss.: 25 June 2014
Revised: 5 September 2014 – Accepted: 28 September 2014 – Published: 6 November 2014

Abstract. The frequency and intensity of extreme hydrological events in Alpine regions is projected to increase with climate change. The goal of this study is to better understand the functioning of aquifers composed of complex alluvial and rockfall deposits in Alpine valleys and to quantify the role of these natural storage spaces in flood attenuation and baseflow maintenance. Geomorphological and hydrogeological mapping, tracer tests, and continuous flow measurements were conducted in the Reintal (German Alps), where runoff from a karst spring infiltrates a series of postglacial alluvial/rockfall aquifers. During high-flow conditions, groundwater velocities of 30 m h^{-1} were determined along 500 m; hydrograph analyses revealed short lag times (5 h) between discharge peaks upstream and downstream from the aquifer series; the maximum discharge ratio downstream (22) and the peak recession coefficient (0.196 d^{-1}) are low compared with other Alpine catchments. During low-flow conditions, the underground flow path length increased to 2 km and groundwater velocities decreased to 1.5 m h^{-1}. Downstream hydrographs revealed a delayed discharge response after 101 h and peaks damped by a factor of 1.5. These results indicate that alluvial/rockfall aquifers might play an important role in the flow regime and attenuation of floods in Alpine regions.

1 Introduction

Snowmelt is a major hydrologic component of flow regimes in Alpine regions; these regimes therefore are particularly sensitive to climate change (Barnett et al., 2005). The temperature in the Alps has increased 2 °C since 1901, which is twice the average warming of the Northern Hemisphere (Auer et al., 2007). A shift of snow and precipitation patterns accompanied by higher precipitation in winter and poor snow storage are likely to substantially affect the timing and magnitude of summer discharge. Extreme events, such as floods and droughts, are expected to increase in frequency, intensity/magnitude (Bogunj, 2007). Because of the high contribution of Alpine runoff to the total discharge of major streams in Europe, climate change will affect hydrology at lower elevations as well as in Alpine regions.

The assessment of potential effects of climate change on Alpine water resources requires an understanding of recharge and drainage processes. The geological and lithological setting is often complex and has major influence on recharge, storage, and discharge processes (Gremaud et al., 2009; Goldscheider and Neukum, 2010). A thorough knowledge of the geologic framework and a conceptual model of the recharge area provide the basis for characterizing Alpine groundwater systems (Plan et al., 2009). To assess underground drainage properties in high-elevated catchments, hydrochemical classification and spring monitoring methods are applied. Such methods allow the characterization of flow components and spring responses to precipitation events so that transit times can be estimated and the presence of preferential flow paths determined (Maloszewski et al., 2002; Wetzel, 2004; Mueller et al., 2013). Artificial tracer tests enable the determination of flow velocities, water volumes, and storage capacities within the Alpine aquifer (Goldscheider, 2005; Gremaud et al., 2009; Finger et al., 2013). These parameters control the amount of quickflow and baseflow, and

Published by Copernicus Publications on behalf of the European Geosciences Union.

Citation: Lauber, U., Kotyla, P., Morche, D., Goldscheider, N. (2014): Hydrogeology of an alpine rockfall aquifer system and its role in flood attenuation and maintaining baseflow. – Hydrol. Earth Syst. Sci., 18, 4437–4452, doi:10.5194/hess-18-4437-2014.

Declaration of authorship: Ute Lauber (UL) planned the tracer tests in consultation with Nico Goldscheider (NG). Patrick Kotyla (PK) was involved in the sampling and conducted discharge measurements. Analysis and evaluation of the results were conducted by PK in consultation with UL. David Morche (DM) provided the discharge data. UL created a concept for analyzing the hydrographs, conducted the evaluation, interpreted the overall results and wrote the manuscript. The final manuscript was reviewed by all authors and Barbara Mahler.

References

Arbeitsgemeinschaft Blautopf (2011): Faszination Blautopf – Vorstoß in unbekannte Höhlenwelten. – 160 p., Ostfildern (Thorbecke).

Armbuster, V., Selg, M. (2006): Der Abfluss des Blautopfs im Spiegel der Grundwasserneubildung (Oberjura-Karst, Süddeutschland). – Tübinger Geowiss. Arbeiten, C 98, 1–16.

Asmuth, J.R., von Knotters, M. (2004): Characterising groundwater dynamics based on a system identification approach. – J. Hydrol., 296(1-4), 118–134, doi: 10.1016/j.jhydrol.2004.03.015.

Auer, I., Böhm, R., Jurkovic, A., Lipa, W., Orlik, A., Potzmann, R., Schöner, W., Ungersböck, M., Matulla, C., Briffa, K., Jones, P., Efthymiadis, D., Brunetti, M., Nanni, T., Maugeri, M., Mercalli, L., Mestre, O., Moisselin, J.-M., Begert, M., Müller-Westermeier, G., Kveton, V., Bochnicek, O., Stastny, P., Lapin, M., Szalai, S., Szentimrey, T., Cegnar, T., Dolinar, M., Gajic-Capka, M., Zaninovic, K., Majstorovic, Z., Nieplova, E. (2007): HISTALP—historical instrumental climatological surface time series of the Greater Alpine Region. – Int. J. Climatol., 27(1), 17–46, doi:10.1002/joc.1377.

Badoux, A., Witzig, J., Germann, P.F., Kienholz, H., Lüscher, P., Weingartner, R., and Hegg, C. (2006): Investigations on the runoff generation at the profile and plot scales, Swiss Emmental. – Hydrol. Process., 20, 377–394, doi:10.1002/hyp.6056.

Bailly-Comte, V., Martin, J.B., Jourde, H., Screaton, E.J., Pistre, S., Langston, A. (2010): Water exchange and pressure transfer between conduits and matrix and their influence on hydrodynamics of two karst aquifers with sinking streams. – J. Hydrol., 386(1-4), 55–66, doi:10.1016/j.jhydrol.2010.03.005.

Bakalowicz, M. (2005): Karst groundwater: a challenge for new resources. – Hydrogeol. J., 13(1), 148–160.

Barnett, T.P., Adam, J.C., Lettenmaier, D.P. (2005): Potential impacts of a warming climate on water availability in snow-dominated regions. – Nature, 438 (7066), 303–309, doi:10.1038/nature04141.

Bartenbach, M., Möbius, R., Aigner, T. (2009): Neue Daten zur Geologie (Schichtenfolge, Fazies) des Oberjuras im Einzugsgebiet des Blautopfs. – Laichinger Höhlenfreund, 44, 73–88.

Bartenbach, M., Ufrecht, W. (2009): Stratigraphie und Fazies des Oberjuras im Umfeld der Blaubeurer Talschlinge – Ergebnisse einer Bohrung und Untertagekartierung im Blauhöhlensystem. – Laichinger Höhlenfreund, 44, 89–106.

Bates, B.C., Kundzewicz, Z., Wu, S., Palutikof, J. (2008): Climate change and water. – IPCC Technical paper VI. IPCC Secretariat, 210 p., Geneva.

Bauer, M., Selg, M. (2006): Altersstruktur und mittlere Verweilzeit im Grundwasser des Blautopfs und anderer Quellen und Brunnen im Oberjura-Karst Süddeutschlands. – Tübinger Geowiss. Arbeiten, C 98, 17–44.

Beniston, M., Stoffel, M., Hill, M. (2011): Impacts of climatic change on water and natural hazards in the Alps: Can current water governance cope with future challenges? Examples from the European "ACQWA" project. – Environ. Sci. Policy, 14(7), 734–743, doi:10.1016/j.envsci.2010.12.009.

Bichler, B., Reischer, M., Höfer-Öllinger, G., Zagler, G., Whlidal, S., and Spötl, C. (2012): Hydrogeology of the Untersberg and the adjacent Salzburg basin (Interactions of karst and porous aquifers). – Pangeo Austria 2012, Abstractband Geo Wissenschaft plus Praxis, p.27, Salzburg.

Blume, T., Zehe, E., Bronstert, A. (2007): Rainfall runoff response, event-based runoff coefficients and hydrograph separation. – Hydrol. Sci. J., 52(5), 843–862, doi:10.1623/hysj.52.5.843.

Bogataj, L.K. (2007): How will the Alps Respond to Climate Change? Scenarios for the Future of Alpine Water. – In: The Water Balance of the Alps, 88 p., Innsbruck (Innsbruck university press).

Bögel, H. (1960): Der geologische Bau des Wettersteingebirges und seiner Umgebung. – Jb. D. Ö. A. V. München, 80, 20–27.

Bohnert, J. (2009): Zum Stand der speläologischen Erforschung von Hessenhauhöhle (7524/117) und Seligengrundhöhle (7524/119) durch die Arbeitsgemeinschaft Blaukarst. – Laichinger Höhlenfreund, 44, 37–44.

Bonacci, O. (1993): Karst springs hydrographs as indicators of karst aquifers. – Hydrol. Sci. J., 38(1), 51–62, doi:10.1080/02626669309492639.

Clark, I.D., Fritz, P. (1997): Environmental isotopes in hydrogeology. – 328 p., Boca Raton (Lewis).

COST 65 (1995): Hydrogeological aspects of groundwater protection in karstic areas, Final report (COST action 65). – European Comission, Directorat-General XII Science, Research and Development, Report EUR 16547 EN, 446 p., Brüssel, Luxemburg.

Dewalle, D., Edwards, P.J., Swistock, B.R., Aravena, R., Drimmie, R.J. (1997): Seasonal isotope hydrology of three Appalachian forest catchments. – Hydrol. Process., 15, 1895–1906, doi:10.1002/(SICI)1099-1085(199712)11:15<1895::AID-HYP538>3.3.CO;2-R.

Doummar, J., Sauter, M., Geyer, T. (2012): Simulation of flow processes in a large scale karst system with an integrated catchment model (Mike She) – Identification of relevant parameters influencing spring discharge. – J. Hydrol., 426-427, 112–123, doi:10.1016/j.jhydrol.2012.01.021, 2012.

Dreybrodt, W., Romanov, D., Kaufmann, G. (2010): Evolution of caves in porous limestone by mixing corrosion: A model approach. – Geol. Cro., 63(2), doi:10.4154/gc.2010.09.

Einsiedl, F. (2005): Flow system dynamics and water storage of a fissured-porous karst aquifer characterized by artificial and environmental tracers. – J. Hydrol., 312, 312–321, doi:10.1016/j.jhydrol.2005.03.031.

Einsield, F., Maloszewski, P., Stichler, W. (2009): Multiple isotope approach to the determination of the natural attenuation potential of a high-alpine karst system. – J. Hydrol., 365, 113-121, doi: 10.1016/j.jhydrol.2008.11.042.

Field, M.S., Nash, S.G. (1997): Risk assessment methodology for karst aquifers: 1. Estimating karst conduit-flow parameters. – Environ. Monit. Assess., 47, 1–21, doi: 10.1023/A:1005753919403.

Field, M.S., Pinsky, P.F. (2000): A two-region nonequilibrium model for solute transport in solution conduits in karstic aquifers. – J. Contam. Hydrol., 44, 329–351, doi:10.1016/S0169-7722(00)00099-1.

Field M.S., Leij F.J. (2012): Solute transport in solution conduits exhibiting multi-peaked breakthrough curves. – J. Hydrol., 440, 26–35, doi:10.1016/j.jhydrol.2012.03.018.

Finger, D., Heinrich, G., Gobiet, A., Bauder, A. (2012): Projections of future water resources and their uncertainty in a glacierized catchment in the Swiss Alps and the subsequent effects on hydropower production during the 21st century. – Water Resour. Res., 48, W02521, doi:10.1029/2011WR010733.

Finger, D., Hugentobler, A., Huss, M., Voinesco, A., Wernli, H., Fischer, D., Weber, E., Jeannin, P.-Y., Kauzlaric, M., Wirz, A., Vennemann, T., Hüsler, F., Schädler, B., Weingartner, R. (2013): Identification of glacial meltwater runoff in a karstic environment and its implication for present and future water availability. – Hydrol. Earth Syst. Sci., 17(8), 3261–3277, doi:10.5194/hess-17-3261-2013.

Ford, D., Williams, P.W. (2007): Karst hydrogeology and geomorphology. – 562 p., Chichester, England (John Wiley & Sons).

Frisch, W., Kuhlemann, J., Dunkl, I. (2008): Die geomorphologische Entwicklung der Ostalpen. – Mitt. Österreich. Geogr. Ges., 150, 123–162.

Gaál, L., Szolgay, J., Kohnová, S., Parajka, J., Merz, R., Viglione, A., and Blöschl, G. (2012): Flood timescales: Understanding the interplay of climate and catchment processes through comparative hydrology. – Water Resour. Res., 48, W04511, doi:10.1029/2011WR011509.

Gabrovsek, F., Romanov, D., Dreybrodt, W. (2004): Early karstification in a dual-fracture aquifer: the role of exchange flow between prominent fractures and a dense net of fissures. – J. Hydrol., 299(1–2), 45–66, doi:10.1016/j.jhydrol.2004.02.005.

Gabrovsek, F., Kogovsek, J., Kovacic, G., Petric, M., Ravbar, N., Turk, J. (2010): Recent results of tracer tests in the catchment of the Unica River (SW Slovenia). – Acta Carsologica, 39, 27–37.

Geyer, T., Birk, S., Licha, T., Liedl, R., Sauter, M. (2007): Multitracer Test Approach to Characterize Reactive Transport in Karst Aquifers. – Ground Water, 45, 36–45, doi:10.1111/j.1745-6584.2006.00261.x.

Geyer, T. (2008): Process-based characterisation of flow and transport in karst aquifers at catchment scale. – PhD Thesis Georg-August-Univ., 103 p., Göttingen.

Geyer. T., Birk, S., Liedl, R., Sauter, M. (2008): Quantification of temporal distribution of recharge in karst systems from spring hydrographs. – J. Hydrol., 348(3-4), 452–463, doi:10.1016/j.jhydrol.2007.10.015.

Geyer, T., Selg, M., Gudera, T., Sauter, M. (2011): Langzeitabflussverhalten der Gallusquelle und des Blautopfs – relative Bedeutung der Matrix und des Großkluftsystems. – Laichinger Höhlenfreund, 46, 63–74.

Geyer, T., Birk, S., Reimann, T., Dorfliger, N., Sauter, M., (2013): Differentiated characterization of karst aquifers: some contributions. – Carbonates and Evaporites, 28, 41-46, doi: 10.1007/s13146-013-0150-9.

Geyer, T., Goldscheider, N. (2014): Herausforderungen bei der Charakterisierung von Karstgrundwasserleitern. – Grundwasser, 19 (1), p. 3, doi:10.1007/s00767-013-0251-3.

GLA Bayerisches Geologisches Landesamt (1977): Bericht des Bayerischen Geologischen Landesamtes über den Markierungsversuch im Osterfelder-Gebiet bei Garmisch-Partenkirchen im August/ September 1977. – Unpublished report, file number 318-IV/2a-1931, Munich.

Goldscheider, N., Brosemer, M., Umlauf, N., Hötzl, H. (1999): Karstentwässerung im Gebiet der Alpspitze (Wettersteingebirge, Bayerische Kalkhochalpen). – Laichinger Höhlenfreund, 34(2), 47–68.

Goldscheider, N. (2005): Fold structure and underground drainage pattern in the alpine karst system Hochifen-Gottesacker. – Eclogae Geol. Helv., 98(1), 1–17, doi: 10.1007/s00015-005-1143-z.

Goldscheider, N., Drew, D. (2007): Methods in Karst Hydrogeology. – 264 p., London (Taylor & Francis).

Goldscheider, N., Meiman, J., Pronk, M., Smart, C. (2008): Tracer tests in karst hydrogeology and speleology. – Int. J. Speleol., 37(1), 27–40, doi:10.5038/1827-806X.37.1.3.

Goldscheider, N., Neukum, C. (2010): Fold and fault control on the drainage pattern of a double-karst-aquifer system, Winterstaude, Austrian Alps. – Acta Carsologica, 39(2), 173–186.

Goldscheider, N. (2011): Alpine Hydrogeologie. – Grundwasser, 16, p.1, doi:10.1007/s00767-010-0157-2.

Göppert, N., Goldscheider, N. (2008): Solute and Colloid Transport in Karst Conduits under Low- and High-Flow Conditions. – Ground Water, 46(1), 61–68, doi:10.1111/j.1745-6584.2007.00373.x.

Gremaud, V., Goldscheider, N., Savoy, L., Favre, G., Masson, H. (2009): Geological structure, recharge processes and underground drainage of a glacierised karst aquifer system, Tsanfleuron-Sanetsch, Swiss Alps. – Hydrogeol. J., 17(8), 1833–1848, doi:10.1007/s10040-009-0485-4.

Grüger, E., Jerz, H. (2010): Untersuchung einer Doline auf dem Zugspitzplatt. Ein palynologischer Beitrag zur holozänen Gletschergeschichte im Wettersteingebirge. – Quaternary Sci. J., 59, 66–75.

Haeberli, W., Beniston, M. (1998): Climate change and its impacts on glaciers and permafrost in the Alps. – Ambio, 27(4), 258–265.

Haga, H., Matsumoto, Y., Matsutani, J., Fujita, M., Nishida, K., Sakamoto, Y. (2005): Flow paths, rainfall properties, and antecedent soil moisture controlling lags to peak discharge in a granitic unchanneled catchment. – Water Resour. Res., 41, W12410, doi:10.1029/2005WR004236.

Hagg, W., Mayer, C., Mayr, E., Heilig, A. (2012): Climate and glacier fluctuations in the Bavarian Alps in the past 120 years. – Erdkunde, 66(2), 121–142.

Hartmann, A., Goldscheider, N., Wagener, T., Lange, J., Weiler, M. (2014): Karst water resources in a changing world: Review of hydrological modeling approaches. – Rev. Geophys., doi:10.1002/2013RG000443.

Hauns, M., Jeannin, P.-Y., Atteia, O. (2001): Dispersion, retardation and scale effect in tracer breakthrough curves in karst conduits. – J. Hydrol., 241(3-4), 177–193, doi:10.1016/S0022-1694(00)00366-8.

Hoffmann, T., Schrott, L. (2003): Determining sediment thickness of talus slopes and valley fill deposits using seismic refraction – a comparison of 2D interpretation tools. – Z. Geomorph. N.F. Suppl.-Bd., 127, 71–87.

Jeannin, P.-Y. (2001): Modeling flow in phreatic and epiphreatic karst conduits in the Holloch cave (Muotatal, Switzerland). – Water Resour. Res., 37 (2), 191–200, doi: 10.1029/2000WR900257.

Johnston, C.T., Cook, P.G., Frape, S.K., Plummer, L.N., Busenberg, E., Blackport, R.J. (1998): Ground water age and nitrate distribution within a glacial aquifer beneath a thick unsaturated zone. – Ground Water, 36(1), 171–180, doi:10.1111/j.1745-6584.1998.tb01078.x.

Käss, W. (2004): Geohydrologische Markierungstechnik. – 557 p., Stuttgart (Borntraeger).

Kiraly, L. (2003): Karstification and Groundwater Flow. – Speleogenesis and Evolution of Karst Aquifers, 1 (3), 1–26.

Kordilla, J., Sauter, M., Reimann, T., Geyer, T. (2012): Simulation of saturated and unsaturated flow in karst systems at catchment scale using a double continuum approach. – Hydrol. Earth Syst. Sci., 16 (10), 3909–3923, doi: 10.5194/hess-16-3909-2012.

Kovács, A., Perrochet, P. (2008): A quantitative approach to spring hydrograph decomposition. – J. Hydrol., 352 (1-2), 16–29, doi:10.1016/j.jhydrol.2007.12.009.

Kraller, G., Warscher, M., Kunstmann, H., Vogl, S., Marke, T., Strasser, U. (2012): Water balance estimation in high Alpine terrain by combining distributed modeling and a neural network approach (Berchtesgaden Alps, Germany). – Hydrol. Earth Syst. Sci., 16: 1969–1990, doi:10.5194/hess-16-1969-2012.

Kübeck, C., Maloszewski, P.J., Benischke, R. (2013): Determination of the conduit structure in a karst aquifer based on tracer data-Lurbach system, Austria. – Hydrol. Process, 27(2), 225–235, doi:10.1002/hyp.9221.

Kücha, A., Jantschke, H. (2009): Zum Stand der speläologischen Erforschung der Blautopfhöhle im Blauhöhlensystem (7524/30). – Laichinger Höhlenfreund, 44, 9–22.

Küfmann, C. (2003): Soil types and eolian dust in high-mountainous karst of the Northern Calcareous Alps (Zugspitzplatt, Wetterstein Mountains, Germany). – Catena, 53(3), 211–227, doi:10.1016/S0341-8162(03)00075-4.

Lauber, U., Ufrecht, W., Goldscheider, N. (2013): Neue Erkenntnisse zur Struktur der Karstentwässerung im aktiven Höhlensystem des Blautopfs. – Grundwasser, 18, 247–257, doi:10.1007/s00767-013-0239-z.

Leibundgut, Ch., Maloszewski, P., and Külls, Ch. (2009): Tracers in Hydrology. – 415 p., West Sussex (Wiley-Blackwell).

Long, A.J., Mahler, B.J. (2013): Prediction, time variance, and classification of hydraulic response to recharge in two karst aquifers. – Hydrol. Earth Syst. Sci., 17(1), 281–294, doi:10.5194/hess-17-281-2013.

Mahler, B.J., Personne, J.C., Lods, G.F., Drogue, C. (2000): Transport of free and particulate-associated bacteria in karst. – J. Hydrol., 238(3-4), 179–193, doi:10.1016/S0022-1694(00)00324-3.

Maloszewski, P., Zuber, A. (1982): Determining the turnover time of groundwater systems with the aid of environmental tracers: 1. models and their applicability. – J. Hydrol., 57(3-4), 207-231, doi:10.1016/0022-1694(82)90147-0.

Maloszewski, P., Rauert, W., Stichler, W., Herrmann, A. (1983): Application of flow models in an alpine catchment area using tritium and deuterium data. – J. Hydrol., 66, 310–330, doi:10.1016/0022-1694(83)90193-2.

Maloszewski, P., Rauert, W., Trimborn, P., Herrmann, A., Rau, R. (1992): Isotope hydrological study of mean transit times in an alpine basin (Wimbachtal, Germany). – J. Hydrol., 140, 343–360, doi:10.1016/0022-1694(92)90247-S.

Maloszewski, P., Stichler, W., Zuber, A., Rank, D. (2002): Identifying the flow systems in a karstic-fissured-porous aquifer, the Schneealpe, Austria, by modelling of environmental 18O and 3H isotopes. – J. Hydrol., 256(1-2), 48–59, doi:10.1016/S0022-1694(01)00526-1.

Maloszewski, P., Zuber, A. (2002): Manual on lumped-parameter models used for the interpretation of environmental tracer data in groundwaters. – In: Use of Isotopes for Analyses of Flow and Transport Dynamics in Groundwater Systems, 1–50, Vienna.

Marke, T., Strasser, U., Kraller, G., Warscher, M., Kunstmann, H., Franz, H., Vogel, M. (2013): The Berchtesgaden National Park (Bavaria, Germany): a platform for interdisciplinary catchment research. – Environ. Earth Sci., 69(2), 679–694, doi:10.1007/s12665-013-2317-z.

Massei, N., Lacroix, M., Wang, H.Q., Mahler, B.J., Dupont, J.P. (2002): Transport of suspended solids from a karstic to an alluvial aquifer: the role of the karst/alluvium interface. – J.Hydrol., 260(1-4), 88-101, doi: 10.1016/S0022-1694(01)00608-4.

Massei, N., Wang, H.Q., Field, M.S., Dupont, J.P., Bakalowicz, M., Rodet, J. (2006): Interpreting tracer breakthrough tailing in a conduit-dominated karstic aquifer. – Hydrogeol. J., 14, 849–858, doi:10.1007/s10040-005-0010-3.

Mayer, J. (1681): Vorstellung Deß jüngst-erschienenen Cometen/… Deme beyegefügt Eine wahrhaffte Erzehlung und Beschreibung/deß im Decembri obigen Jahrs entstandenen weit-beschreyten Erdbruchs bey Blaubeyren. – 56 p., Ulm (Kühnen).

Meiman, J., Groves, C., Herstein, S. (2001): In-cave dye tracing and drainage basin divides in the Mammoth Cave karst aquifer, Kentucky. – US Geological Survey Water Resources Investigations Report, 01–4011, 179–185, Virginia (USA).

Merz, R., Blöschl, G. (2009): A regional analysis of event runoff coefficients with respect to climate and catchment characteristics in Austria. – Water Resour. Res., 45, W01405, doi:10.1029/2008WR007163.

Millares, A., Polo, M.J., Losada, M.A. (2009): The hydrological response of baseflow in fractured mountain areas. – Hydrol. Earth Syst. Sci., 13(7), 1261–1271.

Miller, H. (1961): Der Bau des westlichen Wettersteingebirges. – Dt. geol. Ges. Hannover (113): 409–426.

Mohrlok, U. (2014): Numerische Modellierung der Grundwasserströmung im Einzugsgebiet der Gallusquelle unter Festlegung eines Drainagesystems. – Grundwasser, 19, 73–85, doi: 10.1007/s00767-013-0249-x.

Mook, W.G. (2006): Introduction to isotope hydrology. Stable and radioactive isotopes of hydrogen, oxygen and carbon. – 256 p., London (Taylor & Francis).

Morales, T., Valderrama, I., Uriarte, J., Antigüedad, I., Olazar, M. (2007): Predicting travel times and transport characterization in karst conduits by analyzing tracer-breakthrough curves. – J. Hydrol., 334, 183–198, doi:10.1016/j.jhydrol.2006.10.006.

Morales, T., Uriarte, J.A., Olazar, M., Antigüedad, I., Angulo, B. (2010): Solute transport modelling in karst conduits with slow zones during different hydrologic conditions. – J. Hydrol., 390 (3-4), 182–189, doi:10.1016/j.jhydrol.2010.06.041.

Morche, D., Schmidt, K.-H. (2005): Particle size and particle shape analyses of unconsolidated material from sediment sources and sinks in a small Alpine catchment (Reintal, Bavarian Alps, Germany). – Z. Geomorphol. N.F., Suppl.-Bd., 138, 67–80.

Morche, D., Schmidt, K.H., Heckmann, T., Haas, F. (2007): Hydrology and geomorphic effects of a high-magnitude flood in an alpine river. – Geogr. Ann. A, 89(1), 5–19.

Morche, D., Witzsche, M., Schmidt, K.H. (2008): Hydrogeomorphological characteristics and fluvial sediment transport of a high mountain river (Reintal Valley, Bavarian Alps, Germany). – Z. Geomorphol., 52, 51–77, doi:10.1127/0372-8854/2008/0052S1-0051.

Mudarra, M., Andreo, B. (2011): Relative importance of the saturated and the unsaturated zones in the hydrogeological functioning of karst aquifers: The case of Alta Cadena (Southern Spain). – J. Hydrol., 397(3-4), 263–280, doi:10.1016/j.jhydrol.2010.12.005.

Mudarra, M., Andreo, B., Marín, A. I., Vadillo, I., Barberá, J. A. (2014): Combined use of natural and artificial tracers to determine the hydrogeological functioning of a karst aquifer: the Villanueva del Rosario system (Andalusia, southern Spain). – Hydrogeol. J., doi:10.1007/s10040-014-1117-1.

Müller, M.H., Weingartner, R., Alewell, C. (2013): Importance of vegetation, topography and flow paths for water transit times of base flow in alpine headwater catchments. – Hydrol. Earth Syst. Sci., 17(4), 1661–1679, doi:10.5194/hess-17-1661-2013.

Norbiato, D., Borga, M., Merz, R., Bloschl, G., Carton, A. (2009): Controls on event runoff coefficients in the eastern Italian Alps. – J. Hydrol., 375(3-4), 312–325, doi:10.1016/j.jhydrol.2009.06.044.

Ozyurt, N.N., Bayari, C.S. (2008): Temporal variation of chemical and isotopic signals in major discharges of an alpine karst aquifer in Turkey: implications with respect to response of karst aquifers to recharge. – Hydrogeol. J., 16(2), 297–309, doi:10.1007/s10040-007-0217-6.

Palmer, A.N. (1991): Origin and morphology of limestone caves. – Geol. Soc. Am. Bull., 103(1), 1–21, doi:10.1130/0016-7606(1991)103<0001:OAMOLC>2.3.CO;2.

Perrin, J., Pochon, A., Jeannin, P.-Y., Zwahlen, F. (2003): Vulnerability assessment in karstic areas: validation by field experiments. – Environ. Geol., 46, 237–245, doi:10.1007/s00254-004-0986-3.

Perrin, J., Jeannin, P.-Y, Cornaton, F. (2007): The role of tributary mixing in chemical variations at a karst spring, Milandre, Switzerland. – J. Hydrol., 322(1-2), 158–173, doi:10.1016/j.jhydrol.2006.06.027.

Perrin, J., Luetscher, M. (2008): Inference of the structure of karst conduits using quantitative tracer tests and geological information: example of the Swiss Jura. – Hydrogeol. J., 16, 951–967, doi:10.1007/s10040-008-0281-6.

Pilli, A., Sapigni, M., Zuppi, G.M. (2012): Karstic and alluvial aquifers: a conceptual model for the plain - Prealps system (northeastern Italy). – J. Hydrol., 464, 94–106, doi: 10.1016/j.jhydrol.2012.06.049.

Plan, L., Decker, K., Faber, R., Wagreich, M., Grasemann, B. (2009): Karst morphology and groundwater vulnerability of high alpine karst plateaus. – Environ. Geol., 58(2), 285–297, doi:10.1007/s00254-008-1605-5.

Pronk, M., Goldscheider, N., Zopfi, J. (2006): Dynamics and interaction of organic carbon, turbidity and bacteria in a karst aquifer system. – Hydrogeol. J., 14(4), 473–484, doi: 10.1007/s10040-005-0454-5.

Pronk, M., Goldscheider, N., Zopfi, J. (2007): Particle-Size Distribution As Indicator for Fecal Bacteria Contamination of Drinking Water from Karst Springs. – Environ. Sci. Technol., 41 (27), 8400–8405, doi:10.1021/es071976f.

Pronk, M., Goldscheider, N., Zopfi, J., Zwahlen, F. (2009): Percolation and Particle Transport in the Unsaturated Zone of a Karst Aquifer. – Ground Water, 47(3), 361–369, doi:10.1111/j.1745-6584.2008.00509.x.

Rappl, A., Wetzel, K.-F., Büttner, G., Scholz, M. (2010): Dye tracer investigations at the Partnach Spring (German Alps). – Hydrogeol. Wasserbewirts., 54(4), 220–230.

Ravbar, N., Engelhardt, I., Goldscheider, N. (2011): Anomalous behaviour of specific electrical conductivity at a karst spring induced by variable catchment boundaries: the case of the Podstenjšek spring, Slovenia. – Hydrol. Process., 13, 2130–2140, doi: 10.1002/hyp.7966.

Regierungspräsidium Tübingen (2009): Hydrogeologische Erkundung Baden-Württemberg, Mittlere Alb. – Vol. 3: Hydrogeologischer Bau, Grundwasserhaushalt, 23 p., Tübingen.

Reimann, T., Geyer, T., Shoemaker, W.B., Liedl, R., Sauter, M. (2011): Effects of dynamically variable saturation and matrix-conduit coupling of flow in karst aquifers. – Water Resour. Res., 47, W11503, doi:10.1029/2011WR010446.

Rodgers, P., Soulsby, C., Waldron, S. (2005): Stable isotope tracers as diagnostic tools in upscaling flow path understanding and residence time estimates in a mountainous mesoscale catchment. – Hydrol. Process., 19(11), 2291–2307, doi:10.1002/hyp.5677.

Sass, O., Krautblatter, M., Morche, D. (2007): Rapid lake infill following major rockfall (bergsturz) events revealed by ground-penetrating radar (GPR) measurements, Reintal, German Alps. – Holocene, 17(7), 965–976, doi:10.1177/0959683607082412.

Schmidt, K.H., Morche, D. (2006): Sediment output and effective discharge in two small high mountain catchments in the Bavarian Alps, Germany. – Geomorphol., 80(1-2), 131–145, doi:10.1016/j.geomorph.2005.09.013.

Schrott, L., Götz, J., Geilhausen, M., Morche, D. (2006): Spatial and temporal variability of sediment transfer and storage in an Alpine basin (Bavarian Alps, Germany). – Geogr. Helvetica, 61(3), 191–200.

Schürch, M., Kozel, R., Schotterer, U., Tripet, J.-P. (2003): Observations of isotopes in the water cycle – the Swiss National Network (NISOT). – Environ. Geol., 45, 1–11, doi:10.1007/s00254-003-0843-9.

Schwarz, K., Barth, J.A.C., Postigo-Rebollo, C., Grathwohl, P. (2009): Mixing and transport of water in a karst catchment: a case study from precipitation via seepage to spring. – Hydrol. Earth Syst. Sci., 13, 285–292, doi:10.5194/hess-13-285-2009.

Selg, M., Schopper, M., Straub, R. (2006): Kurzzeitdynamik und Direktabfluss des Blautopfs (Oberjura-Karst, Süddeutschland). – Tübinger Geowiss. Arbeiten, C 98, 45–72.

Selg, M., Schwarz, K. (2009): Am Puls der schönen Lau – zur Hydrogeologie des Blautopf-Einzugsgebietes. – Laichinger Höhlenfreund, 44, 45–72.

Simsek, C., Elci, A., Gunduz, O., Erdogan, B. (2008): Hydrogeological and hydrogeochemical characterization of a karstic mountain region. – Environ. Geol., 54(2), 291–308, doi:10.1007/s00254-007-0817-4.

Sinreich, S., Goldscheider, N., and Hötzl, H. (2002): Hydrogeologie einer alpinen Bergsturzmasse (Schwarzwassertal, Vorarlberg). – Beiträge zur Hydrogeologie, 53, 5–20.

Smart, P.L., Hobbs, S.L. (1986): Characterisation of carbonate aquifers: A conceptual base. – In: Graves, B.J., Lehr, J.H., Butcher, K., Crawford, N.C. (eds.), Proceedings of the Environmental Problems in Karst Terranes and their Solutions Conference, 28-30. Oct. 1986, 1–14, Bowling Green.

Smart, C.C. (1988): Artificial tracer techniques for the determination of the structure of conduit aquifers. – Ground Water, 26, 445–453, doi:10.1111/j.1745-6584.1988.tb00411.x.

Toride, N., Leij, F.J., van Genuchten, M.T. (1999): The CXTFIT code for estimating transport parameters from laboratory or field tracer experiments. – Research Report No. 137. US Salinity Laboratory USDA, ARS., Riverside, California.

Tóth, J. (1963): A theoretical analysis of groundwater flow in small drainage basins. – J. Geophys. Res., 68(16), 4795–4812, doi:10.1029/JZ068i008p02354.

Tóth, J. (1999) Groundwater as a geologic agent: An overview of the causes, processes, and manifestations. – Hydrogeol. J., 7, 1–14.

Trček, B., Zojer, H. (2009): Recharge of springs. – In: Kresic and Stevanovic (eds.), Groundwater hydrology of springs, 87–127, Amsterdam (Elsevier).

Ufrecht, W. (2009): Schichtlagerung und Bruchtektonik im Einzugsgebiet des Blautopfs und dessen Umfeld (Mittlere Schwäbische Alb). – Laichinger Höhlenfreund, 44, 107–148.

Ufrecht, W. (2011): Karstgenese, Karstformenschatz und Karsthydrogeologie der Mittleren Schwäbischen Alb. – Jber. Mitt. Oberrhein. Geol. Ver., N.F. 93, 331–366.

Van Genuchten, M. Th., Šimůnek, J., Leij, F.J., Toride, N., Šejna, M. (2012): STANMOD: Model use, calibration and validation. – Trans. ASABE, 55, 1353–1366.

Vidal, H. (1953): Neue Ergebnisse zur Stratigraphie und Tektonik des nordwestlichen Wettersteingebirges und seines Vorlandes. – Geol. Bavarica München, (17), 56–88.

Villinger, E. (1978): Zur Karsthydrogeologie des Blautopfs und seines Einzugsgebietes (Schwäbische Alb). – Abh. Geol. Landesamt Baden-Württemberg, 8, 59–127.

Villinger, E. (1987): Der Blautopf bei Blaubeuren als Beispiel für die Entwicklung des Karstsystems im schwäbischen Malm. – Geol. Jb., C 49, 71–103.

Villinger, E., Ufrecht, W. (1989): Ergebnisse neuer Markierungsversuche im Einzugsgebiet des Blautopfs (mittlere Schwäbische Alb). – Mitt. Verb. Dt. Höhlen- u. Karstforscher, 35(1/2), 25–38.

Viviroli, D., Weingartner, R. (2004): The hydrological significance of mountains: from regional to global scale. – Hydrol. Earth Syst. Sci., 8(6), 1016–1029.

Viviroli, D., Weingartner, R. (2008): Water towers – A global view on the hydrological importance of mountains. – Adv. Glob. Change Res., 31, 15–20, doi:10.1007/978-1-4020-6748-8_2.

Wassmer, P., Schneider, J.L., Pollet, N., and Schmitter-Voirin, C. (2004): Effects of the internal structure of a rock–avalanche dam on the drainage mechanism of its impoundment, Flims sturzstrom and Ilanz paleo-lake, Swiss Alps. – Geomorph., 61, 3-17, doi: 10.1016/j.geomorph.2003.11.003.

Wetzel, K.-F. (2003): Runoff production processes in small alpine catchments within the unconsolidated Pleistocene sediments of the Lainbach area (upper Bavaria). – Hydrol. Process., 17, 2463–2483, doi:10.1002/hyp.1254.

Wetzel, K. (2004): On the hydrogeology of the Partnach area in the Wetterstein Mountains (Bavarian Alps). – Erdkunde, 58, 172–186.

White, W. B. (2003): Conceptual models for karstic aquifers. – Speleogenesis, 1, 1-6.

Winston, W. E., Criss, R.E. (2004): Dynamic hydrologic and geochemical response in a perennial karst spring. – Water Resour. Res., 40, W05106, doi:10.1029/2004WR003054.

Worthington, S. (2007): Groundwater residence times in unconfined carbonate aquifers. – J. Cave Karst Stud., 69 (1), 94–102.

Worthington, S. (2009): Diagnostic hydrogeologic characteristics of a karst aquifer (Kentucky, USA). – Hydrogeol J, 17 (7), 1665–1678, doi:10.1007/s10040-009-0489-0.

Worthington, S., Ford, D. (2009): Self-Organized Permeability in Carbonate Aquifers. – Ground Water, 47(3), 326–336, doi:10.1111/j.1745-6584.2009.00551.x.

Zillgens, B., Merz, B., Kirnbauer, R., Tilch, N. (2007): Analysis of the runoff response of an alpine catchment at different scales. – Hydrol. Earth Syst. Sci., 11, 1441–1454, doi:10.5194/hess-11-1441-2007.